ADDIS ABABA UNIVERSITY

ADDIS ABABA INSTITUTE OF TECHNOLOGY

SCHOOL OF CIVIL AND ENVIRONMENTAL ENGINEERING

Strengthening Torsion Critical Reinforced Concrete Beam by Externally Bonded Carbon Fiber Reinforced Polymer: Analytical to Experimental Investigation

A Thesis in Structural Engineering

By Mohammed Sirage

19/3/2018

Addis Ababa

Submitted in Partial Fulfillment of the Requirements for the Degree of Master of Science

ADDIS ABABA UNIVERSITY

ADDIS ABABA INSTITUTE OF TECHNOLOGY

SCHOOL OF CIVIL AND ENVIRONMENTAL ENGINEERING

"Strengthening Torsion Critical Reinforced Concrete Beam by Externally Bonded Carbon Fiber Reinforced Polymer: Analytical to Experimental Investigation"

By

Mohammed Sirage

Approved by the Board of Examiners:

Dr. Esayas G/Youhannes		
Advisor	**Signature**	**Date**
Dr.-Ing. Adil Zekaria		
Internal Examiner	**Signature**	**Date**
Dr.-Ing. Girma Zerayohannes		
External Examiner	**Signature**	**Date**
Dr. Agizew Nigussie		
Dean, SCEE	**Signature**	**Date**

Acknowledgment

My most grateful appreciation goes to my advisor Dr. Esayas G/Youhannes for his expert insight, continuous support, and guidance. I have felt a privilege to be his student and immensely enjoyed working with him. The thesis would not have been possible without his supervision and continuous encouragement.

I would like to express my deepest gratitude to my friend and colleague Yonas Solomon for his priceless and unconditional assistance throughout the thesis.

I express gratitude to Dr.-Ing. Adil Zekaria, Dr.-Ing. Girma Zerayohannes, Dr. Abrham Gebre and Firesenay Zerabruk for their helpful comments and suggestions.

Sincere thanks are extended to the staff of the Material Laboratory of AAIT for assisting me in the daunting tasks of the laboratory environment. The success of the experimental investigation was achieved with the priceless assistance of Binyam F., Demis, Fikru B., Masresha, Tezazu and Wubet A.

I would like to express gratitude to Abel S., Henok S., and Zetseate G., for their support during the laborious works during testing of the specimens.

I would like to thank my friends Leamlak and Balemlay for generously supplying me with reinforcement bars for the experimental specimens. I would like to extend my sincere gratitude to Mohammedjemal for the financial assistance during the experimental campaign and for providing me with the carbon fiber composites.

Last, but not least, I would like to express my deepest love and gratitude to my family; I wish to express my utmost gratitude to my mother, Rumana Saleh, for her love, constant support and encouragement.

Table of Contents

LIST OF TABLES

LIST OF FIGURES

LIST OF SYMBOL

The following symbols are used in this thesis:

1 = direction of applied principal tensile stress

$1f$ = direction of principal fiber direction

2 = direction of applied principal compressive stress

$2f$ = direction of principal fiber direction

A_c = solid cross-sectional area within the outer perimeter of concrete

A_e = effective confined area of concrete

A_f = Area of fiber

A_o = cross-sectional area within the center line of the shear flow

A_s = Area of steel

b = Width of a beam

b_o = distance between the centerline of the shear flow (perpendicular to the depth)

c = tension stiffening factor

E_2 = Softening/hardening modules for confined concrete

E_c = elastic modulus of concrete

E_f = elastic modulus of fiber

E_s = elastic modulus of bare steel bars

f_c = cylinder compressive strength of concrete

$f_{cc}^{'}$ = confined compressive strength of concrete

$f_{co}^{'}$ = cylinder compressive strength of concrete

f_{cr} = cracking tensile strength of concrete

f_f^- = smeared fiber stress

f_{fl} = smeared fiber stress in longitudinal direction direction

f_{flt} = smeared fiber stress

f_{ft} = smeared fiber stress in transverse direction

$f(FRP)$ = effect of FRP in compression softening

$f_f(x)$ = fiber stress as a function of x

f_l = smeared steel stress in longitudinal direction

f_s = smeared (average) stress in embedded steel bars

f_s^- = smeared steel stress

$f_s(x)$ = steel stress as a function of x

f_t = smeared steel stress in transverse direction

$f_y^{'}$ = smeared tensile steel stress at first yield

h = height of a beam

h_o = distance between the centerline of the shear flow (parallel to the depth)

k = torsion to moment ratio

K_c = Averaging factor for concrete in compression

$K_{f/s}$ = FRP/steel stiffness

K_t = Averaging factor for concrete in tension

K_w = effect of wrapping

l = longitudinal axis

L = total length

m = bending moment

n_f = ratio of fiber to steel stiffness

P = perimeter of the cross-section

p_c = perimeter of centerline of shear flow around a cross-section (jeng and Hsu,2009)

p_o = perimeter of centerline of shear flow around a cross-section

r = radius of chamfer

t = transverse axis

t_{wrap} = thickness of fiber (used in confined concrete)

T = *torsion*

t_f = thickness of fiber

$t_{d,i}$ = Thickness of the shear flow zone in panel i

$t_{d,13}$ = thickness of the shear flow zone in panel 1 and panel 3

$t_{d,2}$ = thickness of the shear flow zone in panel 2

$t_{d,4}$ = thickness of the shear flow zone in panel 4

α_1 = angle of applied principal tensile stress with respect to longitudinal axis

β = deviation angle

$\frac{\gamma_{12}}{2}$ = shear strain in1-2coordinate

γ_{lt} = shear strain in l-t

ε_1 = biaxial smeared strain in the 1-direction

ε_1^- = uniaxial smeared strain in the 1-direction

ε_{1f}^- = uniaxial smeared strain in the fiber 1-direction

ε_2 = biaxial smeared strain in the 2-direction

ε_2^- = uniaxial smeared strain in the 2-direction

ε_{2f}^- = uniaxial smeared strain in the fiber 2-direction

$\varepsilon_{2,i}$ = smeared strain in the 2-direction for panel i

ε_{2si} = smeared surface strain in the 2-direction for panel i

ε_{cr} = cracking strain of concrete

ε_{cu} = ultimate concrete strain in compression

ε_f^- = average strain in the fiber

$\varepsilon_{h,rup}$ = effective fiber rupture strain

ε_l = biaxial smeared strain in the l-direction

ε_{li} = strain in *l* direction in the *panel i*

ε_l^- = uniaxial smeared strain in the l-direction

ε_s = steel strain

ε_{sf} = maximum of the longitudinal and transverse steel stain

ε_s^- = average strain in the steel

ε_t = biaxial smeared strain in the t-direction

ε_t = peak strain for concrete in compression (Confined model)

ε_{ti} = strain in t direction in the panel i

ε_t^- = uniaxial smeared strain in the t-direction

ε_y = yield stain of bare bar

$\varepsilon_y^{'}$ = smeared tensile steel strain at first yield

ζ = softening coefficient

θ = angle of twist

ρ_e = effective reinforcement ratio

ρ_f = fiber reinforcement ratio

ρ_{fl} = longitudinal fiber ratio

ρ_{flt} = fiber ratio along l-t

ρ_{ft} = transverse fiber ratio

ρ_l = longitudinal steel ratio

ρ_t = transverse steel ratio

ρ_s = steel ratio

σ_1^c = smeared concrete stress in the 1-direction

σ_{1f} = smeared fiber stress in the 1-direction

σ_2^c = smeared concrete stress in the 2-direction

σ_{2f} = smeared fiber stress in the 2-direction

σ_c^- = average concrete stress

σ_{c1} = smeared tensile stress

$\sigma_c(x)$ = concrete stress as a function of x

σ_l = applied stress in the longitudinal direction

$\sigma_{l,2}$ = applied stress in the panel 2

$\sigma_{l,4}$ = applied stress in the panel 4

σ_t = applied stress in the transverse direction

$\tau_{12}{}^c$ = concrete shear stress in 1-2 coordinate

τ_{lt} = applied shear stress in l-t coordinate

υ_{12} = Stain increment in direction 1 due to change of strain in direction 2

υ_{21} = Stain increment in direction 2 due to change of strain 1 in direction

$\phi_{13,t}$ = curvature due to relative transverse straining of panel 1 and 3

$\phi_{13,l}$ = curvature due to relative longitudinal straining of panel 1 and 3

$\phi_{24,l}$ = curvature due to relative longitudinal straining of panel 2 and 4

$\phi_{24,t}$ = curvature due to relative transverse straining of panel 2 and 4

ψ_i = curvature in panel i

ABSTRACT

Although there is an enormous amount of knowledge on behavior, design and detailing of reinforced concrete (RC) members for torsion, many structural members are found to be torsion critical. If a structural member becomes torsion critical, the available mitigations are either to strengthen or to demolish the structural component. Considering its economic implications, demolishing the structure element might not be feasible; as a result, strengthening becomes the only option. One method of strengthening a torsion critical member is by using externally bonded carbon fiber reinforced polymers (CFRP). While there is a great deal of work conducted on strengthening torsion critical members, most of the studies are limited to the case of pure torsion. Often, along with torsional moment, most of the torsion critical beams are subjected to associated shear and flexural moment.

In this study, the effectiveness of the strengthening technique using CFRP is scrutinized by conducting experimental tests on specimens for the combined action of flexure and torsion. Furthermore, the thesis presented an analytical modeling of combined action using a proposed truss model (COMBINED-SMM-FRP).

In the thesis, an additional comprehensive analytical study was conducted using nonlinear finite element packages DuCOM-COM3 and VecTor3. Additionally, the capability of the proposed analytical model (COMBINED-SMM-FRP) in predicting the response of fiber wrapped RC members under the action of combined torsion and flexure was also examined.

The experimental, analytical and the nonlinear finite element studies showed the application of CFRP can substantially enhance the cracking and ultimate strength of torsion critical members. In the experimental investigation, an ultimate strength enhancement of more than 60 percent is observed for the strengthened specimen relative to their control specimens.

1 INTRODUCTION

1.1 General Background

Engineering structures are subjected to a variety of mechanical and environmental loading; as a result, structural members are forced to develop an internal resisting mechanism to counter the developed actions including shear force, bending moment and at times torsional moment.

The mechanism of reinforced concrete (RC) member's resistance to flexure is well understood. Although a tremendous amount of work has been carried out on shear, a unified rational theory still remains elusive. When reinforced concrete members are not properly designed and detailed for torsion, an undesirable brittle mode of failure will be imminent, yet relatively little focus has been given to this problem.

Torsional loadings can be separated into two basic categories: equilibrium torsion and compatibility torsion. When the torsional moment is required for the equilibrium of the structure, it is called equilibrium torsion. A balcony supported by plane frame could be an example of equilibrium torsion. When the torsional moment results from the compatibility of deformations between members meeting at a joint, it will be called compatibility torsion. Transverse beams supporting slabs with different spans might be exposed to compatibility torsion.

It is well known that the presence of properly unaccounted torsional moment reduces the load carrying capacity of RC members; resulting in a torsion critical member. RC members might be torsion critical due to different reasons. Some of the main reasons include:-

- Poor design or inappropriate detailing for torsion
- Change of design codes
- Change in the functionality of the structure
- Deterioration of concrete and corrosion of rebar
- Poor construction

The available mitigations for torsion critical structural members are either strengthening or demolishing the structural element. Often demolishing the members might not be feasible because of its economic repercussions, as a result, strengthening becomes the viable option.

Structural members could be strengthened using different materials and techniques. In this thesis, the behavior of torsion critical RC beams strengthened by using an externally applied epoxy-bonded carbon fiber reinforced polymers (CFRP) will be investigated. Although the material cost of the carbon fibers may be high, they are compensated by the lower cost of application and maintenance cost relative to the conventional strengthening schemes, such as member jacketing.

Carbon fibers are characterized by having very high tensile strength, large deformation capacity, immunity to corrosion and high strength to weight ratio. As a result of their low weight, carbon fiber strip application is easier to apply in confined space and eliminates the need for scaffolding resulting in a reduction of labor costs. The stiffness of the fibers can also be tailored to the design requirements. Fiber reinforced polymers are practically available in different sizes and FRP geometry and dimensions (fib bulletin 14).

It is infrequent to get RC beams that are subjected to pure torsion; there will be associated flexural moment and shear force. In addition to acting external mechanical forces, one source of shear force and flexural moment might be the dead load supported by the beam. Although those internal forces act as a unit rather than separately, it is customary to study each action separately by assuming no interaction and superimpose the individual effect to get the total action effect. By following this path there are numerous studies conducted on carbon fiber wrapped RC beams subjected pure torsion.

In this study, the effectiveness of the strengthening technique using carbon fibers is scrutinized by conducting experimental tests on specimens by subjecting them to the combined action of flexure and torsion. The strengthened beams, as well as the control beams, are tested for predetermined fixed ratio of torsion to flexural moment.

The thesis also incorporates an analytical modeling using truss model and a nonlinear finite element investigation. The experimental program is essential to study in depth about the behavior of torsion critical members and to verify the accuracy of the proposed analytical model and the finite element simulations.

1.2 Significance of the Study

The thesis will examine the behavior of strengthened RC beams tested under the combined action of torsion and flexural moment. Although there is a great deal of work done on the strengthening of RC beams, there are limited studies conducted on the torsional strengthening of beams subjected to combined loading. The experimental program results are expected to add-on the increasing database of reinforced concrete beams that are strengthened using CFRP and tested for torsion. The result of the experiment is expected to shed some light on the efficiency of the selected strengthening technique for members subjected to predominantly torsion and flexure. In practice, the investigation might play a role during a selection process of strengthening method for similar torsion critical RC beams.

1.3 Objective of the Study

1.3.1 General Objective

The general objective of the thesis is to investigate the torsional strengthening method of using CFRP for RC beams that are subjected to combined torsion and flexure.

1.3.2 Specific Objective

The specific objectives of the thesis include

- To investigate the effect of flexure on the torsional capacity of torsion critical beams.
- To investigate the effect of flexure on the torsional capacity of strengthened torsion critical beams.
- To investigate the failure mechanism of strengthened torsion critical beams.
- To propose an analytical model for RC members under the combined action of torsion and flexure.

1.4 Scope

The study will only include reinforced concrete beams subjected to flexure and torsion. The research doesn't incorporate the effect of shear force. Strengthening of severely damaged members due to previous loading histories is not covered in the study. The analytical work only covers RC beams that are subjected to Saint-Venant torsion and it doesn't cover warping torsion.

1.5 Methodology

The research is carried out in four phases. In the first phase, a review of relevant literature and the state of the art on strengthening using CFRP was covered. The second phase of the study includes the development of an analytical model by using previous works as a starting blueprint. Subsequent to the analytical work, a comprehensive experimental program was conducted to generate a reliable data. In the fourth and last phase of the study, analytical simulation using non-linear finite element software was conducted. The nonlinear finite element analysis tools DuCOM-COM3 and VecTor 3 were used.

1.6 Layout of Chapters

Chapter 2 provides a review of relevant literature. Much emphasis is given to cover the state of the art in the practice of using epoxy-bonded carbon fiber composites for the strengthening of flexure, shear, and torsion critical RC beams.

Chapter 3 covers the analytical study on the amendment of a previously developed model for RC membrane element to incorporate the effect of externally bonded carbon fiber and combined action of torsion-flexure. The chapter also gives separate solution algorithms for the prediction of loading history (Torsion Vs. Angle of Twist) of fiber wrapped RC beam subjected to pure torsion and combined torsion - flexure. Moreover, the chapter shows the applicability of the analytical model by coMParing the prediction of the developed model with results of selected experimental tests taken from journal publications.

Chapter 4 is devoted to the experimental program. The material used, specimen preparation, fabrication, the test set up and instrumentation are covered in the chapter.

Chapter 5 discusses the nonlinear finite element study using packages developed at University of Toronto and University of Tokyo.

Chapter 6 covers the discussion and coMParison of results from the analytical model, the finite element simulations, and the experiment.

Chapter 7 offers the conclusion of the study with recommendation for future works.

2 LITERATURE REVIEW

2.1 General Introduction

Although there is an enormous amount of knowledge on behavior, design and detailing of reinforced concrete members for torsion, many structural members are found to be torsion critical. If a structural member becomes torsion critical, the available mitigations are either to strengthen or to demolish the structural element. Considering its economic implications, demolishing the structural component might not be feasible; as a result, strengthening becomes the only option.

Structures might be torsion critical due to different reasons. Some of the main reasons include:-

- Inadequate design or detailing for torsion
- Change of design code
- Change in usage of the structure
- Deterioration and corrosion of rebar
- Poor construction

Structural members could be strengthened using different materials and techniques. One method of strengthening a torsion critical member is by using externally bonded carbon fiber reinforced polymers (ACI 440.2R-02; Fib bulletin 14).

Carbon fibers are characterized by very high tensile strength, large deformation capacity, immunity to corrosion and high strength to weight ratio. As a result of their low weight, carbon fiber strips application is easier in confined space and eliminates the need for scaffolding and consequently reduction in labor costs (Fib bulletin 14).

Carbon fiber composites for the strengthening of structures are available mainly in two forms. The first form is a thin unidirectional strip having a high uniaxial tensile strength and the second form is flexible sheets or fabrics made of fibers having a unidirectional or bi-directional strength and stiffness (Fib bulletin 14; ACI 440.2R-02).

Carbon fiber strips owing to their high tensile strength they are usually available with a thickness in the order of a fraction of 1 mm. To give insight into ultimate strength and behavior of carbon fiber, a comparison of carbon fiber composite and structural steel under short-term monotonic tensile test loading is forwarded by fib bulletin 14.

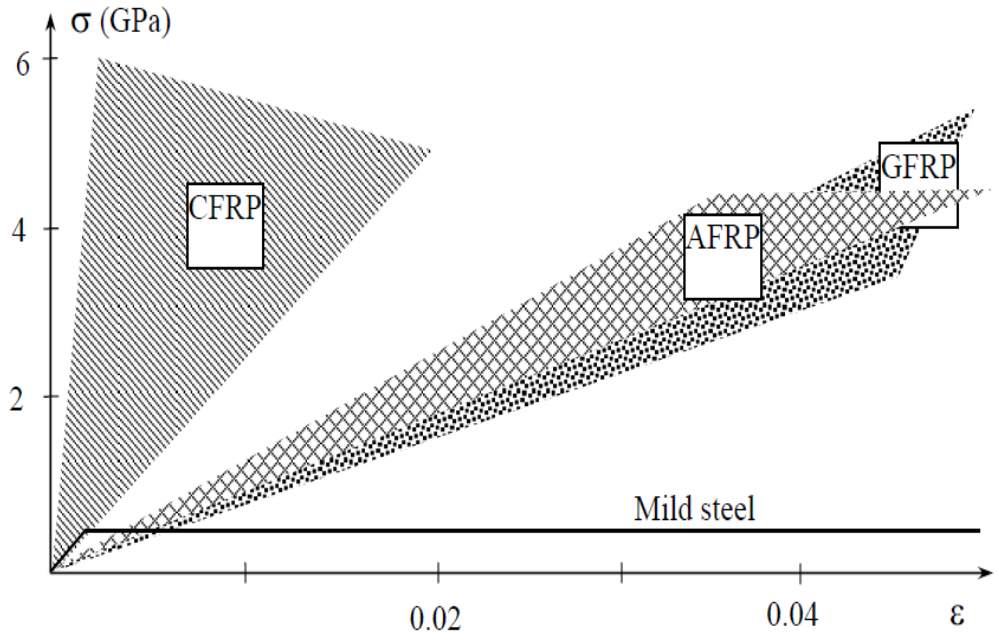

Figure 2-1- Uniaxial tension stress-strain diagrams for different unidirectional fiber reinforced polymer (FRP) and steel. CFRP = carbon FRP, AFRP = aramid FRP, GFRP = glass FRP. Adopted from fib bulletin 14

As it can be observed from the stress-strain diagrams shown in Figure 2-1, a typical unidirectional carbon fiber composites have a very high tensile strength (about 5 to 6 time of strength of structural steel), but contrary to steel which behaves in an elastoplastic manner carbon fiber strips, in general, are linear elastic to failure.

This chapter is dedicated to providing the state of the art in practice and application of carbon fiber composites for the strengthening of RC member's. Besides, much emphasis is given to the strengthening of torsion critical RC beams.

2.2 Recent Studies on the Strengthening of RC Members using CFRP

The behavior and use of CFRP for strengthening purpose have been studied thoroughly by different researchers. Due to a huge application of fiber composites, there is a technical specification for fiber reinforced polymer materials prepared by different institutes in different countries including ACI (ACI 440.2R-02), FIB (Fib bulletin 14), CSA (CSA-13 S806-12) and JCI (JCI TC952).

CFRP could be used to strengthen and increase the load carrying capacity of RC members. The applicability of the material for increasing the shear strength has been studied by different researchers (Chajes et al., 1995; Malvar et al., 1995; Norris et al., 1997; Ahmed Khalifa and Antonio Nanni, 1999; B. Taljsten and L. Elfgren, 1999; Kachlakev and McCurry, 2000; Zhang and Hsu, 2005; Michael A. Colalillo and Shamim A. Sheikh, 2014).

In recent years, the applicability of CFRP for strengthening the flexural capacity of RC members has been extensively studied (Meier and Kaiser, 1991; Ritchie et al., 1991; Sharif et al., 1994; Shahawy and Beitelman, 1996; Breña et al., 2003).

In the last two decade, the use of CFRP for enhancing torsional behavior has been investigated by different scholars. Most of the researchers conducted pure torsion tests on torsion critical beams (Ghobarah el al, 2002 ; Saravanan Panchacharam and Abdeldjelil Belarbi, 2002 ; Hamid R Ronagh and Peter F Dux, 2003 ; Ameli, M., Ronagh, H.R. and Dux, P.F, 2004; Salom et al, 2004 ; Abbas Abdel Majid Allawi, 2006 ; Hii and Al-Mahaidi, 2007 ; M.R.Mohammadizadeh and M.J. Fadaee, 2008).

Although there is a great deal of work conducted on strengthening torsion critical beams, there are very limited studies that considered and investigated strengthening torsional critical beams by conducted tests that allows shear, flexure, and torsion at the same time. Normally, along with torsional moment, most torsional critical beams are subjected to associated shear and flexural moment.

The subsequent sections will cover experimental and analytical works on the practice of carbon fiber strengthening. Experimental and analytical works on shear and flexural strengthening by different researchers will be discussed first. Later, review of experimental and analytical works on the torsional strengthening of RC beams will be covered.

2.3 Experimental and Analytical Studies on Flexural and Shear Strengthening

2.3.1 Experimental and Analytical Studies on Flexural Strengthening

Reinforced concrete beams may be strengthened for flexure through use of carbon fiber reinforced polymers with fiber directions oriented to the principal tensile stress direction.

According to studies (Meier and Kaiser, 1991; Ritchie et al., 1991; Sharif et al., 1994; Shahawy and Beitelman, 1996), flexural strength enhancement using FRPs to tension faces along the length of the beam can enhance the ultimate flexural strength. The increase in ultimate strength might range from 10 to 160 percent (ACI 440.2R-02).

Ritchie et al. (1991) conducted one of the earliest works in examining the effect of FRP for flexure. The authors tested 16 under reinforced beams to study the effect of externally bonded FRP for flexure. They used carbon, glass and kevlar fibers. The experimental test results showed that the provision of FRPs resulted in an increase of stiffness between 17-99 percent and an increase in ultimate strength of 40 to 97 percent. The authors also developed an iterative analytical model to predict the stiffness and ultimate strength of the strengthened member.

Sharif et al. (1994) experimentally and analytically investigated RC beams strengthened with fiberglass. A total of ten RC beams were tested. In the experimental program, the beam was loaded to 85 percent of the ultimate strength and then repaired with FRP plates. The results from the experiments generally indicate that the flexural strength of the repaired beams can substantially be enhanced by the provision of FRP.

Shahawy and Beitelman (1996) investigate the flexural behavior of structurally damaged pretension concrete slabs retrofitted with bonded carbon fiber reinforced plastic. The effect of CFRP on solid and voided slabs was investigated in terms of flexural strength, deflections, cracking behavior and failure modes. The experimental investigation showed a promising result with the CFRP restored the stiffness and strength of the damaged slab. The ultimate load increment for the retrofitted solid and voided slabs was found to be approximately 90% and 178% that of the pre-cracked slabs.

2.3.2 Experimental and Analytical Studies on Shear Strengthening

Carbon and other fiber reinforced polymers have been used to increase the shear carrying capacity of members. The brittle nature of shear failure necessitated for members to be strengthened so that a ductile flexural failure precede the brittle shear failure. The use of externally bonded fibers for enhancement of shear strength has been studied by many researchers (Chajes et al., 1995; Malvar et al., 1995; Norris et al., 1997; Ahmed Khalifa and Antonio Nanni, 1999; B. Taljsten and L. Elfgren, 1999; Kachlakev and McCurry, 2000; Zhang and Hsu, 2005; Michael A. Colalillo and Shamim A. Sheikh, 2014).

Although The mechanisms of shear resistance have been studied by different researchers, According to fib bulletin 14, detailed investigations on the shear strengthening of RC members is relatively limited and to a certain degree debatable. Most of the studies and researcher's assume that shear resistance mechanism by FRP is somehow similar to external placed reinforced bars (FIB bulletin 14). Due to its elastic behavior without any plasticity, most researchers fixed the shear capacity of fibers to be equal to the FRP effective ultimate strength corresponding to the effective strain and which is usually less than the uniaxial strength of the fibers.

According to ACI (ACI 440.2R-02)**,** the effective strain is the maximum strain that can be achieved in the FRP system at the ultimate load stage and it is governed by the failure mode of the FRP system and of the strengthened reinforced concrete member.

Triantafillou and Antonopoulos (2000) argued that it is very hard to accurately predict or quantify the FRP shear contribution. The reason is the shear resistance of FRPs is dependent on the mode of failure and the mode of failure is also dependent on various factors. The contribution of FRP to shear capacity is typically controlled by either the maximum effective strain or by debonding.

According to Triantafillou and Antonopoulos (Triantafillou and Antonopoulos, 2000)

"*the effectiveness of the external FRP shear reinforcement and its contribution to the shear capacity of RC members depends on the mode of failure, which may occur either by peeling off through the concrete near the concrete-FRP interface, or by FRP tensile fracture at a stress that may be lower than the FRP tensile strength (e.g., because of stress concentrations at debonded*

areas or at rounded corners). Whether peeling off or fracture will occur first depends on the bond conditions, available anchorage length, type of attachment at the FRP curtailment, FRP thickness, FRP elastic modulus, concrete strength, and other factors."

Studies on shear strength enhancement using carbon fiber reinforced polymers are still ongoing. Chajes et al. (1995) conducted an experimental investigation on twelve under-reinforced concrete T-beams at the University of Delaware. The RC beams were tested to study the effectiveness of using externally applied composite fabrics as a method of increasing a beam's shear capacity. In the experimental program they used aramid, E-glass, and graphite fiber reinforced fabrics. All the tested beams failed in shear and those with composite reinforcement displayed excellent bond characteristics. The experimental results show an increase in strength for individual beams ranged from 60 to 150 percent over that of the control beams.

Norris et al. (1997) studied the behavior of damaged or understrength concrete beams retrofitted with thin carbon fiber reinforced plastic sheets. Nineteen beams were fabricated, loaded beyond concrete cracking strength, and retrofitted with three different CFRP systems. The beams were subsequently loaded up to failure. The experimental result showed that CFRP sheets can provide an increase in strength and stiffness to existing concrete beams when bonded to the web and tension face.

Kachlakev and McCurry (2000) conducted an experimental investigation on four beams to simulate scenarios from the existing bridge (Horsetail Creek bridge beams), unless mitigated the bridge beams would have been shear critical for the projected traffic load. The authors provided CFRP to enhance the flexural strength and uniaxial GFRP to enhance the shear capacity. Results from the experiments show that the use of fiber reinforced polymers composites for structural strengthening provides increases in capacity of approximately 150% when compared to the unstrengthened section.

Ahmed Khalifa and Antonio Nanni (1999) studied the shear performance of reinforced concrete T-section beams with different configurations of externally bonded carbon fiber polymer sheets. The experimental program consisted of six full-scale, simply supported beams. One beam was used as a benchmark and five beams were strengthened using different configurations of CFRP.

The experimental results show that externally bonded CFRP increased the shear capacity of the beam ranging from 35 to 145 percent.

B. Taljsten and L. Elfgren (1999) studied different methods and application of carbon fiber reinforced plastic (CFRP). The aim of the study was to investigate the shear strength of beams after strengthening with CFRP and to examine different ways of applying the fiber composite. The experiment showed an increase in strength of almost 300 percent. The authors presented the possibility of reaching a strengthening effect of 100% with completely fractured beams.

Zhang and Hsu (2005) conducted an experimental and analytical study on the strengthening of RC beams using CFRP. To investigate the shear behavior and contribution of CFRP shear reinforcement, 11 RC beams without shear reinforcement was cast. All the beams were designed to be shear critical. The result shows the feasibility of using an externally applied CFRP system to restore or increase the shear capacity of RC beams. Although the effect of anchorage not considered, the authors proposed design approach with an acceptable prediction.

Recently Michael A. Colalillo and Shamim A. Sheikh (2014) have studied the behavior of shear-critical reinforced concrete beams strengthened with Fiber-Reinforced Polymer. In 2016 shear performance of reinforced concrete beams with corroded stirrups strengthened with CFRP has been investigated by Hongming Li, Jin Wu, and Zhe Wang. In the same year, Waleed et al. (2016) studied the effect of longitudinal CFRP Plates on shear strength of RC Beams.

2.4 Experimental and Analytical Studies on Torsional Strengthening

When RC members are subjected to torsion, shear stress will develop throughout the section resulting in diagonal spiral cracks. The difference between the diagonal shear and spiral torsional cracks is illustrated in Figure 2-2.

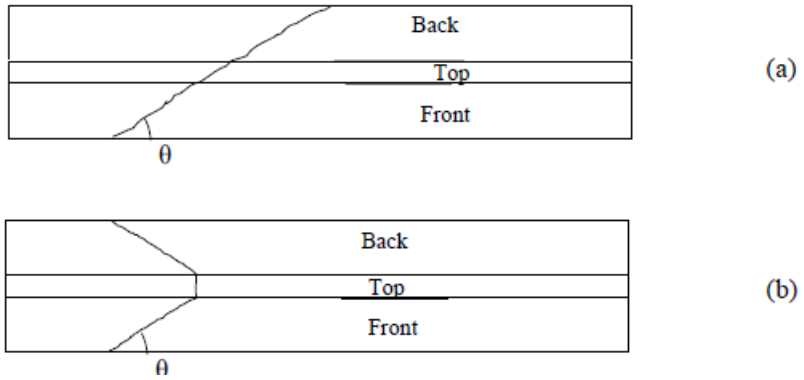

Figure 2-2 - (a) Torsional and (b) shear cracking (adopted from Fib bulletin 14)

Comparing with flexural and shear strengthening, according to Panchacharam and Belarbi (2002), studies related to the strengthening of torsional members with FRP composites is very limited and insufficient data or design guidelines are available in the literature.

Even though it recognized the limited amount of research and testing on FRP-strengthened concrete elements in torsion**,** According to fib bulletin 14, design procedures for torsional strengthening can follow a similar approach to that of shear strengthening with minor alteration.

Although Fib bulletin 14 provisions for torsion demanded an externally bonded FRP jacket to be provided in full wrapping around the element's cross-section to contribute to torsional capacity, researchers showed with adequate anchorage, it is possible to have more than 20 percent increase in ultimate strength with three side wrapping (Saravanan Panchacharam and Abdeldjelil Belarbi, 2002; Hamid R Ronagh and Peter F Dux, 2003).

The feasibility of CFRP for the strengthening of torsional behavior has been investigated by many researchers and most of the studies are conducted in the last two decade.

Ghobarah et al (2002) performed torsional tests on 11 reinforced concrete beams strengthened with CFRP and GFRP in different configurations. The experimental result showed that wrapping the beams has in general improved the torsional capacity by up to 72%.

Saravanan Panchacharam and Abdeldjelil Belarbi (2002) conducted analytical and experimental work on torsional strengthening of RC members. They considered different variables including the glass fiber Orientation, the number of beam faces strengthened (three or four), the effect of the number of FRP plies used, and the influence of anchors in their study. Their investigation showed a very promising result on the feasibility of using FRP for torsion critical members.

In 2003 Hamid R Ronagh and Peter F Dux (2003) experimentally investigated three RC concrete beams. The RC beams were intentionally designed to be torsion critical. Two of the three beams were reinforced with CFRP. The pure torsion test shows that the torsional strength of beams strengthened with fibers was almost twice than that of the control beam.

In 2004 Ameli, M., Ronagh, H.R. and Dux, P.F (2004) conducted pure torsion test on 12 reinforced concrete beams wrapped by carbon and glass fibers. Different configurations were used for the FRPs and the torque-twist angle paths of the beams were recorded to failure. The experimental result showed a significant enhancement in the ultimate torque with 87 and 143 percent increase for one and two layers of carbon fiber wrapping respectively.

In 2004 Salom et al (2004) experimentally and analytically studied six identical spandrel beams. The beams were tested with pure torsion. The specimens include two baseline specimens with four retrofitted sample for comparison. The variables considered in the study include fiber orientation and effects of a laminate anchoring system. The experiments showed that the CFRP could increase the torsional capacity of concrete beams by more than 70%.

Abbas Abdel Majid Allawi (2006) conducted an experimental and analytical investigation by testing twelve prototype beams with solid and hollow sections under pure torsion. Nine of these beams were strengthened with CFRP laminates in different strengthening systems. The experimental results show that the bonding of CFRP laminates to beams provides an increase as much as 90% in the ultimate torsional capacity as compared to the corresponding reference beams.

Hii and Al-Mahaidi (2007) conducted experimental work on six CFRP strengthened medium-scale thin-walled box-section and solid RC beams. Photogrammetry was used to measure the displacement field. From the tests, an increase in both cracking and ultimate strengths of up to 40 and 78% was observed and due to the carbon fiber strengthening, it was found that the crack widths were reduced and aggregate interlocking action was improved.

In 2008 torsional behavior of high strength concrete beams strengthened using CFRP Sheets was investigated by M.R.Mohammadizadeh and M.J. Fadaee. The experimental results showed an increase in ultimate strength of 50 and 90 percent for one and two layer wrapping respectively.

Even though there is a surge of research on strengthening RC members for torsion, most of the studies focus on experimental tests on torsion critical beams for the case of pure torsion only. Although most torsion critical beams are subjected to combined loading, there are very limited studies that considered and investigated strengthened torsional critical beams by conducted tests that allow shear, flexure, and torsion at the same time.

The inadequate volume of work on ultimate strength, serviceability, and long-term creep rapture can be observed from the limited provisions and guidelines forwarded by prominent codes. From the known institutes, only fib bulletin forwarded guideline for torsional strengthening design and none of the institutes including FIB and ACI offered comprehensive rules for detailing of torsional strengthening.

3 ANALYTICAL MODEL (COMBINED–SMM-FRP)

3.1 Historical Background on the Analytical Model

The first theory for torsion of elastic homogeneous circular members was developed by Claude-Louis Navier. Navier's work also includes linear theory for flexure (ACI 445.1R-12) and his work guided the development of various torsion theories. Three decades later, Navier's work on circular elastic members was followed by Saint-Venant's solution for rectangular homogeneous and elastic members subjected to torsion. Saint-Venant developed a semi-inverse method to solve the torsional problem and his torsional constant considers wrapping of the cross-section due to torsion. According to Saint-Venant, the most efficient section to resist torsion is a thin tube.

Following Saint-Venant theory in 1896, Bredt (1896) was able to derive a simple equation for thin tubes. His formulation is also used to model reinforced concrete members subjected to torsion in modern truss based models for torsion. His work becomes a base for modern theories of torsion for reinforced concrete members. In his derivation, the shear flow around the perimeter has a constant value and equals to torsional moment divided by twice the area enclosed by the shear flow zone.

After the development of reinforced concrete in 1867, theories and design guidelines for RC members subjected to flexure, shear, and torsion turn out to be a major research focus area. Generally speaking, reinforced concrete theories are difficult to develop due to the nonlinearity of concrete and anisotropic behavior arising from cracking of the concrete. In terms of shear and torsion, Ritter (1899) and Mörsch (1902) developed truss model. Extending the 2D truss model to 3D, Rausch (1929) developed a theory for torsion of RC members. His space truss model was made up of 45 degree oriented diagonal struts, longitudinal and transverse ties connected at the joint by a hinge and torsion is resisted by compression in the diagonal struts and tension in ties and longitudinal reinforcements. Moreover, in the model concrete tensile strength is ignored.

After 1950s torsional theories for RC follows two distinct paths in skew bending theory (Lessig, 1959; Walsh et.al, 1966; Collins et al, 1968; Elfgren et al., 1974) and formulations based membrane element truss model. The skew bending theory only used equilibrium equations and assumed all transverse and longitudinal bars to be yielded. While the modern truss model-based

theories such as Compression field theory (Mitchell and Collins, 1974), Softened Truss Model (Hsu and Mo, 1985) and Softened Membrane Model for Torsion (Jeng and Hsu, 2009) incorporates the three Navier's principle of mechanics.

In this chapter analytical model for carbon fiber wrapped RC beam subjected to combined torsion and flexure will be presented. The analytical model will use softened membrane model for torsion by Jeng and Hsu (2009) as a basic framework.

3.2 Basics on Softened Membrane Model for Shear and Torsion (SMMT)

Softened membrane model for torsion (SMMT) is developed by Jeng and Hsu (2009). The model is an extension of softened membrane model (SMM) for shear by Hsu and Zhu (2002). SMM is a fixed angle smeared truss model and in addition to Navier's principle of mechanics, it incorporated poisons effect for concrete subjected to biaxial stress condition. The Poisson ratios are also known as Hsu/Zhu ratios. The provision of poisons effect makes the model powerful in its ability to predict loading history through cracking to peak and post peak phases. In addition to compatibility equations appropriate for torsion, Jeng and Hsu incorporated two modifications to the constitutive relationships of concrete suggested by SMM.

The first modification address the tensile relationship of concrete, the pre-cracking stiffness and the strain at peak stress are increased by 45%. Second, the Hsu/Zhu ratio for torsion is taken as 80% of the Hsu/Zhu ratio for shear. The above two modification are incorporated due to curvature of membrane element produced by the torsion.

SMMT model can predict the entire load history curve, including the ranges before and after cracking, as well as the ascending and descending branches. The solution algorithm and comparison with more than 70 experimental tests can be referred from the original technical paper (Jeng and Hsu, 2009).

3.3 Analytical Model Formulation

3.3.1 Members Subjected to Torsion and Flexure

Engineering structures are exposed to a variety of mechanical and environmental loading; as a result, structural members are forced to develop an internal resisting mechanism to counter the developed actions. As it can be seen from Figure 3-1, a structural member may be subjected to a maximum of six internal actions in biaxial bending, biaxial shear, normal stress, and torsion.

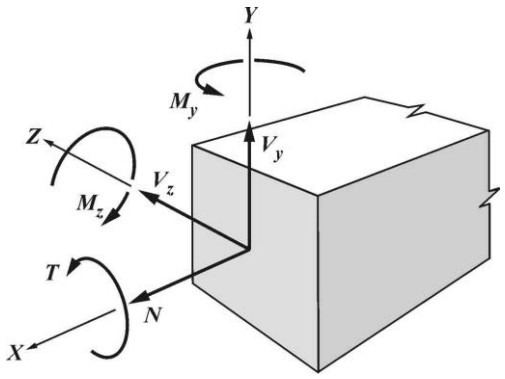

Figure 3-1- Internal forces and longitudinal and transverse directions for panels (Rahal and Collins (1995))

On the other hand, RC beams in frame structures are commonly subjected to uniaxial bending, shear, and at times torsional moment. In the following sections, by narrowing our attention to flexure and torsion, a truss model-based analytical model for RC beams wrapped with CFRP will be forwarded. The forwarded analytical model is expected to predict the response of RC members that are predominantly subjected to combined torsion and flexure.

Torsion in a rectangular section will induce shear stresses that flow around the member and the torsion will cause warping of the wall panels. After cracking of the member, the torsion is resisted by an equivalent hollow section having a constant thickness (Mitchell and Collins, 1974; Hsu and Mo, 1985). According to Bredt (1896), the shear flow in each wall are equal, as a result of this constant shear flow, the pure torsional behavior of members could be predicted by careful analysis of membrane element from one of the panel.

When considering a uniaxial bending in addition to torsion, the equivalent hollow section that was responsible for resisting the torsion will be subjected to compressive and tensile normal stress. As it can be seen from Figure 3-2, it may be presumed that the membrane element at the

top is subjected to additional compressive normal stress, while the bottom panel will be subjected to tensile stress and the side panels are subjected to shearing stress due to torsion. To simplify the idealization, the normal stresses in the side panels are intentionally ignored in the model.

Because of these different boundary conditions, in predicting the behavior of the member, we have to consider each membrane elements (Panel 1, panel 2, panel 3 and panel 4). The resulting problem will be somehow difficult relative to predicting the behavior of pure torsion.

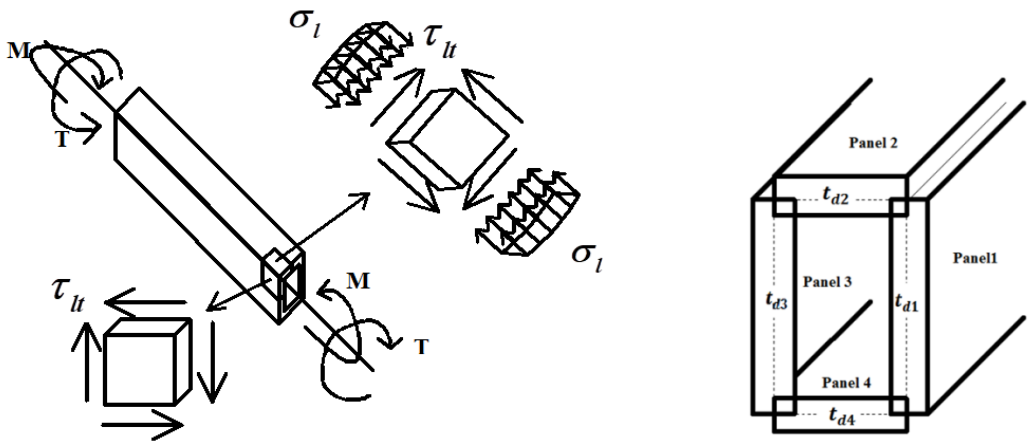

Figure 3-2 - Member subjected to combined torsion and flexure

The positive direction of longitudinal and transverse axis for each panel is shown in Figure 3-3 and these directions will be used in the subsequent formulations for each of the membrane elements.

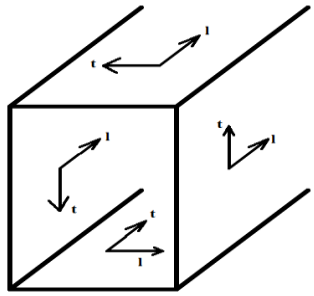

Figure 3-3- Longitudinal and transverse direction of panels

The formulations for the prediction of RC member's response to the action of combined torsion and flexure must satisfy two conditions.

A) At panel level, they must satisfy Navier principles of mechanics (Equilibrium, compatibility and material law).

B) At member level, strain compatibility among the wall panels must be satisfied.

In satisfying the first condition, the proposed model will incorporate part of the equilibrium and compatibility equations used in the softened membrane model for torsion by Jeng and Hsu (2009). The appropriate material constitutive models will be adopted from different research works and detail discussion will be given in the following sections.

In the following sections explanation of the proposed model will be provided first by discussing the equilibrium, compatibility and material law at the panel level. After satisfying the panel level analysis, member level analysis will follow by describing a method of satisfying strain compatibility in the wall panels.

The method of solution for the proposed model allows predicting load-deformation response to specified ratios of torsional to bending moment. The solution algorithms for the case of pure torsion and torsion with bending will be separately provided. Validation of the model for the case of pure torsion and combined torsion-flexure will be given by comparing the prediction of the developed model with experimental results from selected studies by other researchers.

3.3.2 Combined Softened Membrane Model for Torsion (COMBINED–SMM-FRP)

The model adopted parts of the softened membrane model's (SMM) equilibrium and compatibility requirements. SMM is a fixed angle smeared truss model and in addition to satisfying Navier's principle of mechanics, it incorporated poisons effect for concrete subjected to a biaxial stress condition. Analogous to SMM, the proposed model assumes the direction of cracks to be perpendicular to the applied principal tensile stresses, as a result, all the equilibrium, compatibility equations are formulated between the applied principal stress coordinate system $1-2$ and the stationary coordinate system $l-t$.

3.3.2.1 Equilibrium Equation

The in-plane equilibrium of membrane element, according to the SMM satisfies three algebraic equation and they can be derived by using concept transformation of stress.

A portion of Fiber wrapped RC membrane element can be idealized as composed of concrete, reinforcement and fiber strip as shown in Figure 3-4.

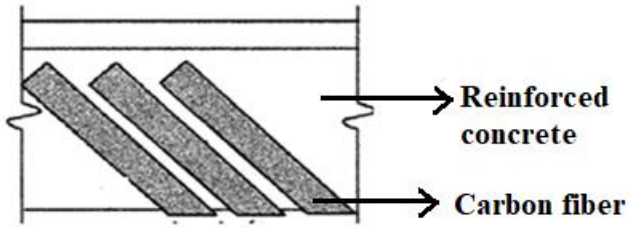

Figure 3-4 - RC membrane element wrapped with fiber

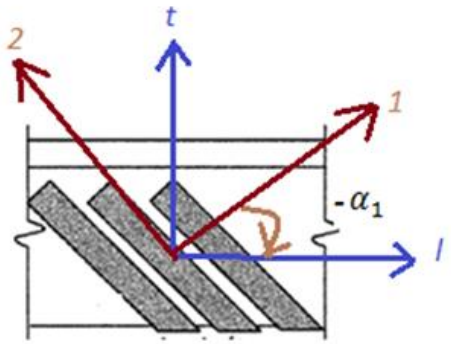

Figure 3-5 - Applied principal stress and longitudinal -transversal axis

Using transformation matrix, stress along l and t direction can be expressed as a function of stress in the applied principal directions *1* and *2* of the concrete, reinforcement stress and carbon fibers stress along *l* and *t* direction (see equation 3.2, 3.3 & 3.4).

$$\begin{bmatrix} \sigma_l & \tau_{lt} \\ \tau_{tl} & \sigma_t \end{bmatrix} = \begin{bmatrix} \cos(-\alpha_1) & \sin(-\alpha_1) \\ -\sin(-\alpha_1) & \cos(-\alpha_1) \end{bmatrix} \begin{bmatrix} \sigma_1^c & \tau_{12}^c \\ \tau_{21}^c & \sigma_2^c \end{bmatrix} \begin{bmatrix} \cos(-\alpha_1) & \sin(-\alpha_1) \\ -\sin(-\alpha_1) & \cos(-\alpha_1) \end{bmatrix}^T + \begin{bmatrix} \rho_l f_l & 0 \\ 0 & \rho_t f_t \end{bmatrix} + \begin{bmatrix} \rho_{fl} f_{fl} & \rho_{ftl} f_{flt} \\ \rho_{ftl} f_{flt} & \rho_{ft} f_{ft} \end{bmatrix} \quad (3.1)$$

Where:

1 = direction of applied principal tensile stress
2 = direction of applied principal compressive stress
l = longitudinal axis
t = transverse axis
f_{fl} = smeared fiber stress in longitudinal direction direction
f_{flt} = smeared fiber stress
f_{ft} = smeared fiber stress in transverse direction
f_l = smeared steel stress in longitudinal direction
f_t = smeared steel stress in transverse direction
α_1 = angle of applied principal tensile stress with respect to longitudinal axis
ρ_{fl} = longitudinal fiber ratio
ρ_{flt} = fiber ratio along l-t
ρ_{ft} = transverse fiber ratio
ρ_l = longitudinal steel ratio
ρ_t = transverse steel ratio
σ_1^c = smeared concrete stress in the 1-direction
σ_2^c = smeared concrete stress in the 2-direction
σ_l = applied stress in the longitudinal direction
σ_t = applied stress in the transverse direction
τ_{lt} = applied shear stress in l-t coordinate

Solving the above formulation

$$\sigma_l = \sigma_1^c cos^2\alpha_1 + \sigma_2^c sin^2\alpha_1 - \tau_{12}{}^c 2\sin\alpha_1 cos\alpha_1 + \rho_l f_l + \rho_{fl} f_{fl} \qquad (3.2)$$

$$\sigma_t = \sigma_1^c sin^2\alpha_1 + \sigma_2^c cos^2\alpha_1 + \tau_{12}{}^c 2\sin\alpha_1 cos\alpha_1 + \rho_t f_t + \rho_{ft} f_{ft} \qquad (3.3)$$

$$\tau_{lt} = \left(\sigma_1^c - \sigma_2^c\right) sin\alpha_1 cos\alpha_1 + \tau_{12}{}^c \left(cos^2\alpha_1 - sin^2\alpha_1\right) + \rho_{flt} f_{flt} \qquad (3.4)$$

The Fixed angle α_1 in softened membrane model can be expressed as a function of applied stress as:

$$\cot 2\alpha_1 = \frac{\sigma_l - \sigma_t}{2\tau_{lt}} \qquad (3.5)$$

Carbon fiber strips could be provided with their main fiber direction perpendicular, parallel or at some inclination from the longitudinal axis (see Figure 3-6), using transformation matrix the

carbon fiber contribution in the different direction can be equated. The stress transformation along the longitudinal and transverse direction can be expressed using equation 3.8, 3.9 and 3.10.

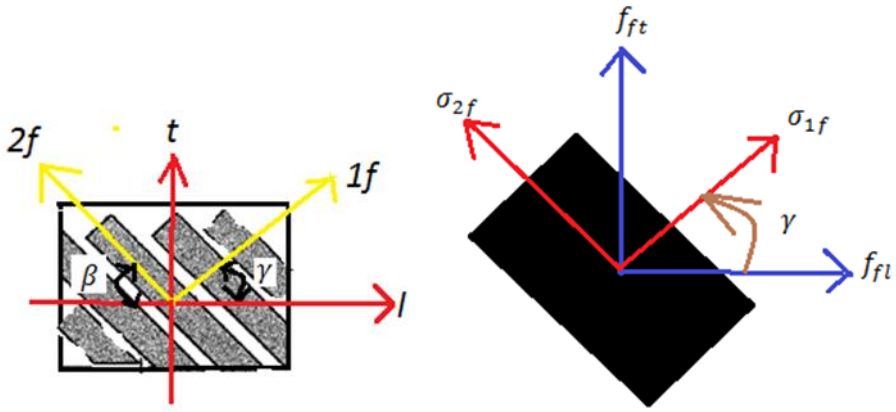

Figure 3-6 - The principal direction of the fiber

Transformation matrix $$T = \begin{bmatrix} \cos\gamma & -\sin\gamma \\ \sin\gamma & \cos\gamma \end{bmatrix} \quad (3.6)$$

$$\begin{bmatrix} f_{fl} & f_{flt} \\ f_{ltl} & f_{ft} \end{bmatrix} = [T]\begin{bmatrix} \sigma_{1f} & 0 \\ 0 & \sigma_{2f} \end{bmatrix}[T]^T \quad (3.7)$$

Where:

$1f$ = direction of principal fiber direction
$2f$ = direction of principal fiber direction

σ_{1f} = smeared fiber stress in the 1-direction
σ_{2f} = smeared fiber stress in the 2-direction

Solving the formulation,

$$f_{fl} = \sigma_{1f}cos^2\gamma + \sigma_{2f}sin^2\gamma \quad (3.8)$$

$$f_{ft} = \sigma_{1f}sin^2\gamma + \sigma_{2f}cos^2\gamma \quad (3.9)$$

$$f_{flt} = \left(\sigma_{1f} - \sigma_{2f}\right)sin\gamma cos\gamma \quad (3.10)$$

3.3.2.2 Compatibility Equations

The three strain components in the applied principal stress coordinate system are $\varepsilon_1, \varepsilon_2$ and γ_{12}. the relationship between the fixed coordinate system strains $\varepsilon_1, \varepsilon_2$ and γ_{12} and the stationary strain components $\varepsilon_l, \varepsilon_t$ and γ_{lt} can be derived by using strain transformation**.** Using a transformation matrix, the compatibility equations can obtained as shown below.

$$\begin{bmatrix} \varepsilon_l & \frac{\gamma_{lt}}{2} \\ \frac{\gamma_{lt}}{2} & \varepsilon_t \end{bmatrix} = \begin{bmatrix} \cos(-\alpha_1) & \sin(-\alpha_1) \\ -\sin(-\alpha_1) & \cos(-\alpha_1) \end{bmatrix} \begin{bmatrix} \varepsilon_1 & \frac{\gamma_{12}}{2} \\ \frac{\gamma_{21}}{2} & \varepsilon_2 \end{bmatrix} \begin{bmatrix} \cos(-\alpha_1) & \sin(-\alpha_1) \\ -\sin(-\alpha_1) & \cos(-\alpha_1) \end{bmatrix}^T \tag{3.11}$$

Where:

$\varepsilon_1 =$ biaxial smeared strain in the 1-direction
$\varepsilon_2 =$ biaxial smeared strain in the 2-direction
$\varepsilon_l =$ biaxial smeared strain in the l-direction
$\varepsilon_t =$ biaxial smeared strain in the t-direction

$$\varepsilon_l = \varepsilon_1 cos^2\alpha_1 + \varepsilon_2 sin^2\alpha_1 - \frac{\gamma_{12}}{2} 2\sin\alpha_1 cos\alpha_1 \tag{3.12}$$

$$\varepsilon_t = \varepsilon_1 sin^2\alpha_1 + \varepsilon_2 cos^2\alpha_1 + \frac{\gamma_{12}}{2} 2\sin\alpha_1 cos\alpha_1 \tag{3.13}$$

$$\frac{\gamma_{lt}}{2} = (\varepsilon_1 - \varepsilon_2) sin\alpha_1 cos\alpha_1 + \frac{\gamma_{12}}{2}\left(cos^2\alpha_1 - sin^2\alpha_1\right) \tag{3.14}$$

3.3.2.3 Poisson Effect

Poisson ratio describes strain change in one direction due to change of strain in the perpendicular direction. Considering crack in reinforced concrete as material property rather than discontinuity i.e. smeared crack approach, a reinforced concrete member can be described as continuous material. In their Softened membrane model by utilizing this approach Hsu and Zhu (2002) proposed two Hsu-Zhu Poisson ratios for reinforced concrete membrane element.

$$\begin{aligned}
&\upsilon_{12} = 0.2 + 850\varepsilon_{sf} \quad \varepsilon_{sf} < \varepsilon_y \\
&\upsilon_{12} = 1.9 \quad \varepsilon_{sf} > \varepsilon_y \\
&\upsilon_{21} = 0 \ \textit{after crack} \quad \upsilon_{21} = 0.2 \ \textit{before crack} \\
&\varepsilon_{sf} = \max(\varepsilon_t \ or \ \varepsilon_l) \\
&\textit{where} \\
&\upsilon_{12} = \text{Stain increment in direction 1 due to change of strain in direction 2} \\
&\upsilon_{21} = \text{Stain increment in direction 2 due to change of strain in direction 1}
\end{aligned} \tag{3.15}$$

Recently a study was conducted on Poisson ratio by Yang et al. (2017) using RC membrane elements wrapped with external carbon fibers. The study showed that the fibers have a stiffening effect and the original model by Hsu and Zhu (2002) was found to be overestimating the strain increment in tensile direction due to compressive strain for fiber-wrapped members. Due to this finding and by incorporating FRP stiffness, the researcher's proposed a similar and modified Poisson ratio for RC members wrapped with carbon fiber strips. In this thesis, the Hsu-Zhu ratios proposed by Yang et al (2017) are adopted.

$$\begin{aligned}
&\upsilon_{12} = 0.2 + k\varepsilon_{sf} \qquad \varepsilon_{sf} < \varepsilon_y \qquad k = \frac{1.7 - 0.00058\rho_f E_f}{\varepsilon_y} \\
&\upsilon_{12} = 1.9 - 0.00058\rho_f E_f \qquad \varepsilon_{sf} > \varepsilon_y \\
&\upsilon_{21} = 0 \ \textit{after crack} \qquad \upsilon_{21} = 0.2 \ \textit{before crack} \\
&\varepsilon_{sf} = \max(\varepsilon_t \ or \ \varepsilon_l)
\end{aligned} \tag{3.16}$$

3.3.2.4 Relationship between Biaxial and Uniaxial Strain

When reinforced concrete membrane modeled in smeared or average approach, RC members are essentially assumed to be a continuum with anisotropic behavior. When a 2-D continuum RC element defined in the $1-2$ coordinate is subjected to stresses and if Hsu/Zhu ratios ($v12$ and $v21$) are considered, the uniaxial strains ε_1^- and ε_2^- can be expressed as a function of the biaxial strains ε_1 and ε_2 as follows

$$\varepsilon_1^- = \frac{1}{1-\upsilon_{12}\upsilon_{21}}\varepsilon_1 + \frac{\upsilon_{12}}{1-\upsilon_{12}\upsilon_{21}}\varepsilon_2 \tag{3.17}$$

$$\varepsilon_2^- = \frac{\upsilon_{21}}{1-\upsilon_{12}\upsilon_{21}}\varepsilon_1 + \frac{1}{1-\upsilon_{12}\upsilon_{21}}\varepsilon_2 \tag{3.18}$$

Once the uniaxial strains in principal axis are obtained, using transformation matrix the uniaxial strains along longitudinal and transverse direction can found as follows

$$\varepsilon_l^- = \varepsilon_1^- cos^2\alpha_1 + \varepsilon_2^- sin^2\alpha_1 - \frac{\gamma_{12}}{2} 2 sin\ \alpha_1 cos\ \alpha_1 \tag{3.19}$$

$$\varepsilon_t^- = \varepsilon_1^- sin^2\alpha_1 + \varepsilon_2^- cos^2\alpha_1 + \frac{\gamma_{12}}{2} 2 sin\ \alpha_1 cos\ \alpha_1 \tag{3.20}$$

Where

ε_l^- = uniaxial smeared strain in the l-direction

ε_t^- = uniaxial smeared strain in the t-direction

Similarly, the uniaxial strain in the fibers can also be derived using a transformation matrix. Referring to the different axis in Figure 3-7, the final equation can be derived as shown below.

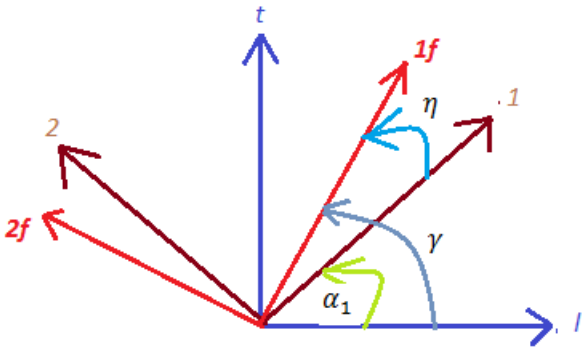

Figure 3-7 – Applied principal axis, the principal axis of the fiber and stationary axis

$$\text{Tranformation matrix } T = \begin{bmatrix} \cos\eta & \sin\eta \\ -\sin\eta & \cos\eta \end{bmatrix}$$

$$\begin{bmatrix} \bar{\varepsilon}_{1f} \\ \bar{\varepsilon}_{2f} \\ \bar{\gamma}_{12f} \end{bmatrix} = [T] \begin{bmatrix} \bar{\varepsilon}_1 & \frac{\gamma_{12}}{2} \\ \frac{\gamma_{12}}{2} & \bar{\varepsilon}_2 \end{bmatrix} [T]^T \tag{3.21}$$

$$\bar{\varepsilon}_{1f} = \bar{\varepsilon}_1 cos^2\eta + \bar{\varepsilon}_2 sin^2\eta + \frac{\gamma_{12}}{2} 2 \sin\eta \cos\eta \tag{3.22}$$

$$\bar{\varepsilon}_{2f} = \bar{\varepsilon}_1 sin^2\eta + \bar{\varepsilon}_2 cos^2\eta - \frac{\gamma_{12}}{2} 2 \sin\eta \cos\eta \tag{3.23}$$

$$\eta = \gamma - \alpha_1$$

Where:

$\bar{\varepsilon}_{1f}$ = uniaxial smeared strain in the fiber 1-direction

$\bar{\varepsilon}_{2f}$ = uniaxial smeared strain in the fiber 2-direction

η is the angle between the principal fiber direction $1f$ and applied principal stress

3.3.2.5 Constitutive Models

3.3.2.5.1 Constitutive Model for Carbon Fiber Strips

Carbon fibers are essentially elastic material showing little or no plastic deformation and their behavior is modeled using the following simple relation.

$$\sigma_f = E_f \varepsilon_f \quad for\ 0 < \varepsilon_f < \varepsilon_{rup} \tag{3.24}$$

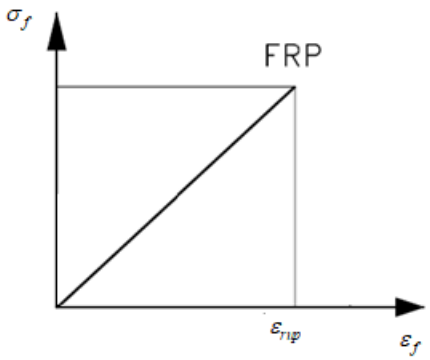

Figure 3-8 – Constitutive model for Carbon fiber

3.3.2.5.2 Constitutive Model for Concrete in Tension

In a smeared constitutive law for concrete in tension, before cracking the stress-strain relationship is essentially linear. After cracking, due to bond stress, concrete resist tension with relatively small strength results in descending branch of a curve.

The relationship between the smeared tensile stress of the concrete and smeared strain for fiber-wrapped RC prism (see Figure 3-9) can be established using the following procedure. In the formulation, the subsequent assumption shall be made:

- Perfect bond between the fiber and the underlying concrete substrate
- No bond slip

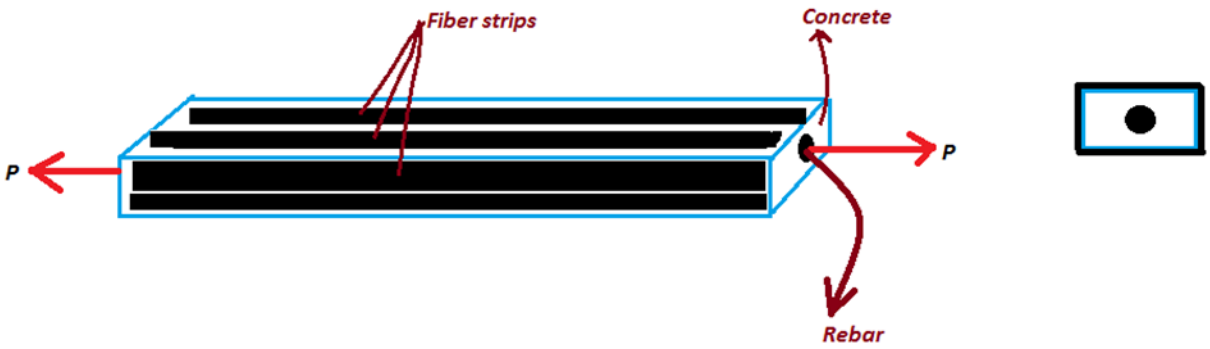

Figure 3-9 - RC prism wrapped with CFRP

1. The equilibrium between an external load and internal resistance by rebar, fiber, and concrete in tension should be maintained throughout the length of the prism.

$$P = A_s f_s(x) + A_f f_f(x) + A_c \sigma_c(x) \tag{3.25}$$

Where:

P = Applied load
$f_s(x)$ = steel stress as a function of x
A_s = Area of steel
$f_f(x)$ = fiber stress as a function of x
$\sigma_c(x)$ = concrete stress as a function of x

2. Formulate expression for average tensile stress in concrete, rebar and carbon fiber strip

$$f_s^- = \frac{1}{L}\int f_s(x)dx = \frac{1}{L}\int E_s \varepsilon_s(x)dx = E_s \varepsilon_s^- \tag{3.26}$$

$$f_f^- = \frac{1}{L}\int f_f(x)dx = \frac{1}{L}\int E_f \varepsilon_f(x)dx = E_f \varepsilon_f^- \tag{3.27}$$

$$\sigma_c^- = \frac{1}{L}\int \sigma_c(x)dx \tag{3.28}$$

Where:

f_s^- = smeared steel stress f_f^- = smeared fiber stress σ_c^- = average concrete stress

3. formulate equilibrium equation in terms of average or smeared stress

$$\frac{P}{A_c} = \rho_s \frac{1}{L}\int f_s(x)\,dx + \rho_f \frac{1}{L}\int f_f(x)\,dx + \frac{1}{L}\int \sigma_c(x)\,dx \tag{3.29}$$

$$\frac{P}{A_c} = \rho_s E_s \bar{\varepsilon_s} + \rho_f E_f \bar{\varepsilon_f} + \bar{\sigma_c} \tag{3.30}$$

$$\bar{\varepsilon_s} = \bar{\varepsilon_f} = \bar{\varepsilon_1} \tag{3.31}$$

Where:

$\bar{\varepsilon_s}$ = average strain in the steel

$\bar{\varepsilon_f}$ = average strain in the fiber

$\bar{\varepsilon_1}$ = average strain in the fiber

ρ_f = fiber reinforcement ratio

ρ_s = steel ratio

4. express the smeared tensile stress as a function of steel stress, fiber stress and externally applied load

$$\bar{\sigma_c} = \frac{P}{A_c} - \rho_s E_s \bar{\varepsilon_1} + \rho_f E_f \bar{\varepsilon_1} \tag{3.32}$$

By conducting a uniaxial tensile test on concrete prism wrapped with carbon fiber and using the above equation one can plot the smeared tensile stress-strain relationship in tension. Using the above method Yang et al. (2015) proposed a constitutive model for concrete in tension. Their constitutive model is adopted in this model.

The smeared tensile stress-strain relationship is expressed by equation 3.33 and comparison between smeared tensile stress-strain for RC prism and fiber wrapped RC prism is shown in Figure 3-10.

$$\sigma_{c1} = E_c \varepsilon_1^- \quad when\ \varepsilon_1^- < \varepsilon_{cr}$$

$$\sigma_{c1} = f_{cr}\left(\frac{\varepsilon_{cr}}{\varepsilon_1^-}\right)^C \quad when\ \varepsilon_1^- > \varepsilon_{cr}$$

$$C = K_w * K_{f/s} \qquad \varepsilon_{cr} = 0.00008 \qquad f_{cr} = 0.31\sqrt{f_c}$$

$$K_w = effect\ of\ wrapping \begin{cases} 1\ for\ full\ wrapping \\ 1.6\ for\ side\ wrapping \end{cases}$$

$$K_{f/s} = FRP/steel\ stiffness = 0.25\left(\frac{\rho_f E_f}{\rho_s E_s}\right) + 0.15 \tag{3.33}$$

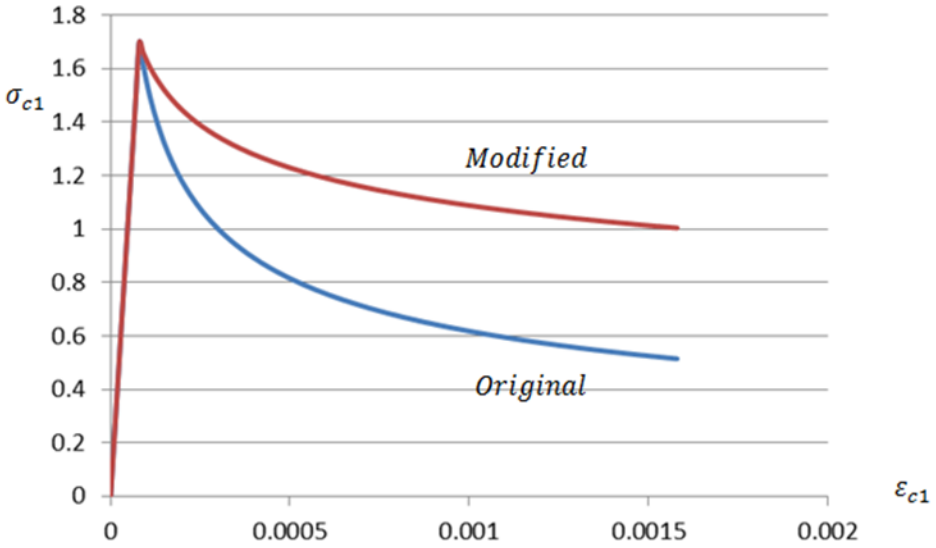

Figure 3-10 - Comparison between the modified and original constitutive model for concrete in tension

3.3.2.5.3 Constitutive Model for Shear Stress-Strain Relationships of Concrete $\tau_{12}{}^c\, v_s\, \gamma_{12}$

There are numerous analytical and empirical shear stress-strain relationships of concrete. Due to its efficiency in solution and the accuracy of prediction, the shear transfer model of Zhu et al (2001) is adopted in the proposed model**.**

$$\tau_{12}{}^c = \frac{\sigma_1^c - \sigma_2^c}{2(\varepsilon_1 - \varepsilon_2)}\gamma_{12} \tag{3.34}$$

3.3.2.5.4 Constitutive Model for Embedded Steel

Recently the effect of carbon fiber strips on the behavior of embedded steel was studied by Yang et al. (2017). The researchers proposed an equation that is similar to the equation proposed by Belarbi and Hsu (1994) by changing only the reinforcement ratio to account the effect of carbon fiber. The proposed equation by the researchers agrees well with experimental results.

The bilinear equations proposed by Yang et al. (2017) is expressed by equation 3.35 and comparison between the constitutive model for FRP wrapped embedded steel with unstrengthened embedded steel is shown in Figure 3-11.

$$
\begin{aligned}
&f_s = E_s\varepsilon_s && \varepsilon_s < \varepsilon_y^{'}\\
&f_s = (0.91-2B)\,f_y + (0.02+0.25B)\,E_s\varepsilon_s && \varepsilon_s > \varepsilon_y^{'}\\
&\varepsilon_y^{'} = \frac{f_y^{'}}{E_s} \qquad f_y^{'} = (0.93-2B)\,f_y\\
&B = \frac{1}{\rho_e}\left(\frac{f_{cr}}{f_y}\right)^{1.5} \qquad f_{cr} = 0.31\sqrt{f_c}\\
&\rho_e = \rho_s + n_f\rho_f \qquad n_f = \frac{E_f}{E_s}
\end{aligned}
\tag{3.35}
$$

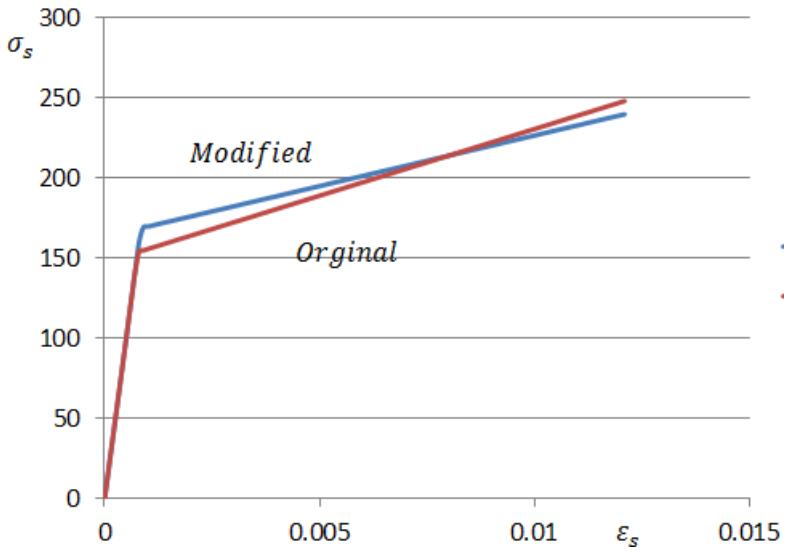

Figure 3-11 - Comparison between the modified and original constitutive model for embedded steel

In the model f_s will be used as f_l or f_t along the longitudinal and transverse directions.

3.3.2.5.5 Constitutive Model for Concrete Wrapped with Carbon Fiber

The stress-strain response of carbon fiber wrapped concrete in compression is different from conventional concrete without fiber strip. The constitutive model for CFRP wrapped concrete is adapted from a recent study by Hany et al (2015). The developed model prediction closely resembles test from different researchers. Some of the strong advantages of using this model include its simplicity and its ability in predicting the ascending or the descending curve after the peak unconfined stress of concrete ($\varepsilon_c = 0.2\%$) (see Figure 3-12). The model is also suitable for numerical analysis.

In the model, the post unconfined peak strength curve of fiber wrapped concrete depends on the number of FRP wraps. For a small amount of wrapping the post-peak behavior will be descending curve whereas for a large amount of wrapping the behavior will be a linear ascending curve.

The equations proposed by Hany et al (2015) are expressed by equation 3.36.

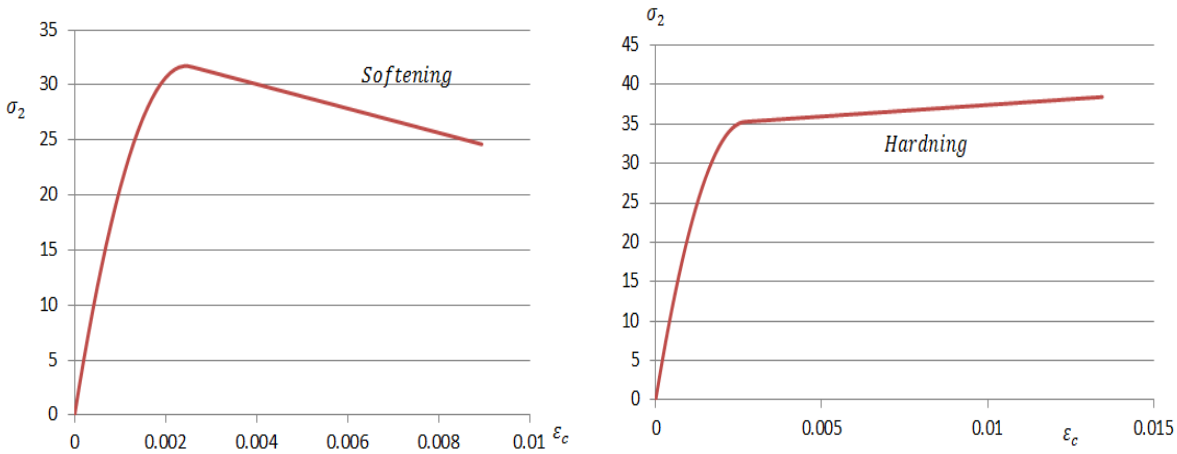

Figure 3-12 - A Constitutive model for concrete wrapped with carbon fiber (Softening and hardening)

$$\sigma_c = E_c\varepsilon_c - \frac{\left(E_c - E_2\right)^2}{4.6 * f_{co}^{'}}\left(\varepsilon_c\right)^2 \quad for\, 0 < \varepsilon_c < \varepsilon_t$$

$$\sigma_c = 1.15 f_{co}^{'} + E_2\varepsilon_c \quad for\ \varepsilon_t < \varepsilon_c < \varepsilon_{cu}$$

$$\text{Where } \varepsilon_t = \frac{2.3 f_{co}^{'}}{E_c - E_2} \qquad E_c = 4730\sqrt{f_{co}^{'}} \qquad E_2 = \frac{\left(f_{cc}^{'} - 1.15 f_{co}^{'}\right)}{\varepsilon_{cu}}$$

$$\frac{f_{cc}^{'}}{f_{co}^{'}} = 0.7 + 4.62\left(\frac{A_e}{A_c}\right)\left(\frac{b}{h}\right)^{0.92}\left(\frac{f_l}{f_{co}^{'}}\right) \qquad \frac{\varepsilon_{cu}}{\varepsilon_o} = 3.89 + 14.76\left(\frac{A_e}{A_c}\right)\left(\frac{b}{h}\right)^{0.94}\left(\frac{f_l}{f_{co}^{'}}\right) \qquad (3.36)$$

$$f_l = \left(\frac{\rho_f E_f}{2}\right)\varepsilon_{h,rup} \qquad \varepsilon_{h,rup} = 0.6\varepsilon_{fu} \qquad \rho_f = \frac{4 * t_{wrap}}{D} \qquad D = \sqrt{b^2 + h^2}$$

$$\frac{A_e}{A_c} = 1 - \frac{\left(\frac{b}{h}\right)\left(h - 2r\right)^2 + \left(\frac{h}{b}\right)\left(b - 2r\right)^2}{3A_c}$$

3.3.2.5.6 Concrete Softening

Reinforced concrete element subjected to shear stress is actually subjected to biaxial stresses (biaxial tension-compression). Due to this biaxial stress condition, it was observed that the compressive strength of concrete in the direction of principal compression was reduced by cracking due to principal tension in the perpendicular direction. This softening effect is quantified by different researchers (Vecchio and Collins, 1986; Hsu, Belarbi, and Pang, 1995; Belarbi and Hsu, 1995; pang and Hsu, 1995).

The softening coefficient for CFRP wrapped membrane elements was recently studied by Moslehy (2010) by testing eight full-sized FRP-strengthened RC panels under biaxial tension-compression loading.

In 2017 by incorporating Moslehy's test results further study on softening of CFRP reinforced RC membrane conducted by Yang et al (2017).The research resulted in a simplified factor for the contribution of FRP on softening.

$$\zeta = \left(\frac{5.8}{\sqrt{f_c^{'}}} < 0.9\right)\left(\frac{1}{\sqrt{1 + 250\varepsilon_1^{-}}}\right)\left(1 - \frac{|\beta|}{24}\right) f\left(FRP\right) \qquad (3.37)$$

$$f\left(FRP\right)=\left(1+\frac{16.785*E_f\left(mpa\right)*\varepsilon_1^-*T_{frp(mm)}^{2/3}}{10^6}\right)\left(1.12-16\varepsilon_1^-\right)\ \ Moslehy\ \left(2010\right) \tag{3.38}$$

$$f\left(FRP\right)=\left(1+0.0076\sqrt{\rho_f E_f}\right)\qquad Yang\ et\ al\ \left(2017\right) \tag{3.39}$$

$$\beta=\frac{1}{2}tan^{-1}\left(\frac{\gamma_{12}}{\varepsilon_1-\varepsilon_2}\right) \tag{3.40}$$

Where:

$\beta=$deviation angle

$\zeta=$softening coefficient

In this thesis, the softening coefficient by Yang et al. (2017) is adapted due to excellent agreement between the prediction of the proposed equation and the experimental results.

3.3.2.6 Additional Equations for Torsion

Bredt (Bredt (1896)) was able to derive a simple equation for thin tubes. His formulation is also used to model reinforced concrete members subjected to torsion in modern truss based models for torsion. In his derivation, the shear flow around the perimeter has a constant value and equals to torsional moment divided by twice the area enclosed by the shear flow zone.

$$\tau_{lt}=\frac{T}{2A_o t_d} \tag{3.41}$$

Where:

$A_o=$cross-sectional area within the center line of the shear flow

$T=torsion$

$t_d=$Thickness of the shear flow zone

When RC members are subjected to torsion, the angle of twist θ produces warping in the wall of the member, which in turn, causes bending in the concrete struts. In another word, the concrete struts are not only subjected to compression due to the circulatory shear but also subjected to bending due to the warping of the wall (see Figure 3-13). For combined load cases where bending exist with torsion, an additional curvature will be induced to the diagonal struts due to curvature caused by the difference in relative longitudinal and transverse straining of neighboring membranes. The expressions of curvature for combined loading were first derived by Onsongo (1978) using analogy similar to stress transformation. The derived expressions are directly adapted to the proposed model.

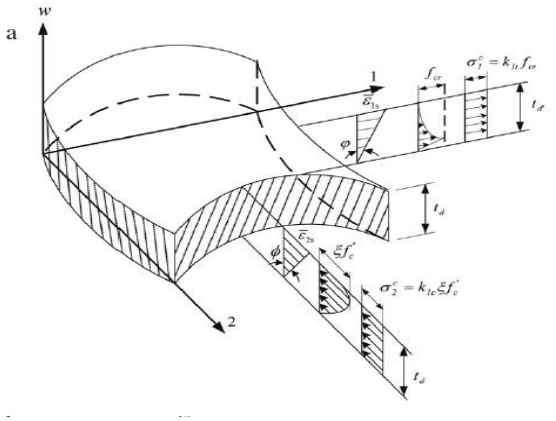

Figure 3-13 - A Nonlinear variation of tensile and compressive stress due to bending of wall (courtesy of Jeng and Hsu (2009))

The expression of curvature for each panel subjected to combined loading adopted from Onsongo (1978) is given as

$$\psi_1 = \theta \sin 2\alpha_1 + \phi_{13,t} \cos^2 \alpha_1 + \phi_{13,l} \sin^2 \alpha_1 \tag{3.42}$$

$$\psi_2 = \theta \sin 2\alpha_2 + \phi_{24,t} \cos^2 \alpha_2 + \phi_{24,l} \sin^2 \alpha_2 \tag{3.43}$$

$$\psi_3 = \theta \sin 2\alpha_3 - \phi_{13,t} \cos^2 \alpha_3 - \phi_{13,l} \sin^2 \alpha_3 \tag{3.44}$$

$$\psi_4 = \theta \sin 2\alpha_4 - \phi_{24,t} \cos^2 \alpha_4 - \phi_{24,l} \sin^2 \alpha_4 \tag{3.45}$$

Where:

α_1 = angle of applied principal tensile stress with respect to longitudinal axis in panel i

θ = angle of twist

ψ_i = curvature in panel i

$\phi_{13,t}$ = curvature due to relative transverse straining of panel 1 and 3

$\phi_{13,l}$ = curvature due to relative longitudinal straining of panel 1 and 3

$\phi_{24,l}$ = curvature due to relative longitudinal straining of panel 2 and 4

$\phi_{24,t}$ = curvature due to relative transverse straining of panel 2 and 4

In the above expression θ is the angle of twist and $\phi_{ij,t}$ and $\phi_{ij,l}$ are curvatures due to relative longitudinal and transverse stain of opposite panels (see Figure 3-14). For combined torsion and flexure, the angle of twist is dependent on shearing strain and thickness of shear flow zone .the expression for the angle of twist is given by equation 3.46.

$$\theta = \frac{((\gamma_{lt1} + \gamma_{lt3})h_o + (\gamma_{lt2} + \gamma_{lt4})b_o)}{2A_o} \tag{3.46}$$

The curvature due to relative longitudinal and transverse strain of opposite panels $\phi_{ij,t}$ and $\phi_{ij,l}$ is given by the following formulas.

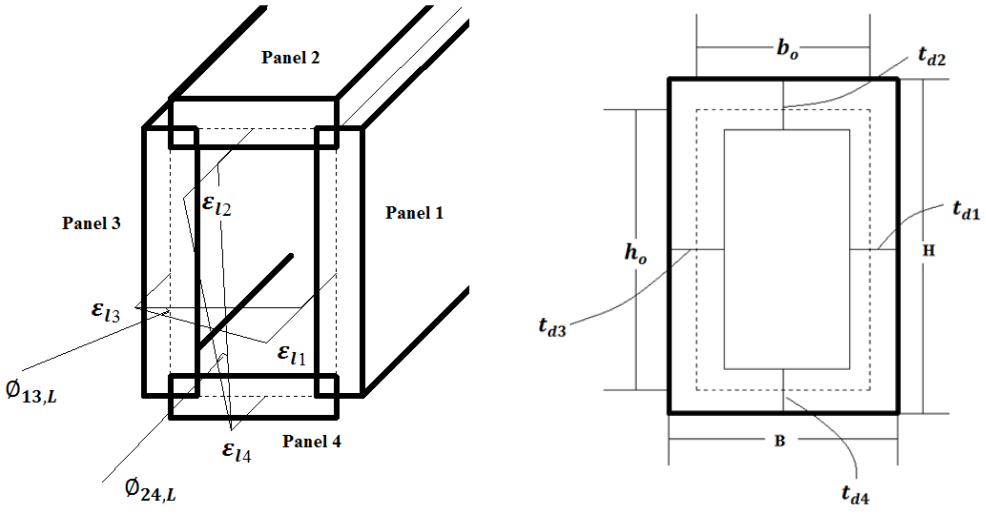

Figure 3-14 – Curvature due to longitudinal strains in the walls

$$\phi_{13,l} = \frac{\varepsilon_{l1} - \varepsilon_{l3}}{b_o} \qquad \phi_{13,t} = \frac{\varepsilon_{lt} - \varepsilon_{lt}}{b_o}$$
$$\phi_{24,l} = \frac{\varepsilon_{l2} - \varepsilon_{l4}}{h_o} \qquad \phi_{24,t} = \frac{\varepsilon_{2t} - \varepsilon_{4t}}{h_o} \tag{3.47}$$

Where:

ε_{li} = strain in l direction in the *panel i*

ε_{ti} = strain in t direction in the *panel i*

b_o = distance between the centerline of the shear flow (perpendicular to the depth)

The curvature derived in the above equations will produce a non-uniform strain distribution in the concrete struts. Taking a unit width of a concrete strut with a wall thickness h and neglecting the effect of tension, the thickness of the shear flow zone can be established. The area in the outer portion that is in compression is considered to be effective to resist the shear flow (see Figure 3-15).

The strain distribution is assumed to be linear along the depth of the wall. The thickness t_d can be related to the curvature ψ_i and the maximum strain at the surface ε_{2si} by the simple relationship as

$$t_{d,i} = \frac{\varepsilon_{2si}}{\psi_i} \tag{3.48}$$

The maximum strain at the surface ε_{2si} is related to the average strain $\varepsilon_{2,i}$ by the simple relationship given by equation 3.49.

$$\varepsilon_{2,i} = \frac{\varepsilon_{2s,i}}{2} \tag{3.49}$$

The curvature will induce a nonlinear stress distribution (see Figure 3-15), and it is preferable to replace the resulting nonlinear stress by equivalent uniform stress so that it becomes easier to relate the smeared strain with the smeared stress. In the following sections, to satisfy the above aim, averaging factor in compression as well as in tension will be derived.

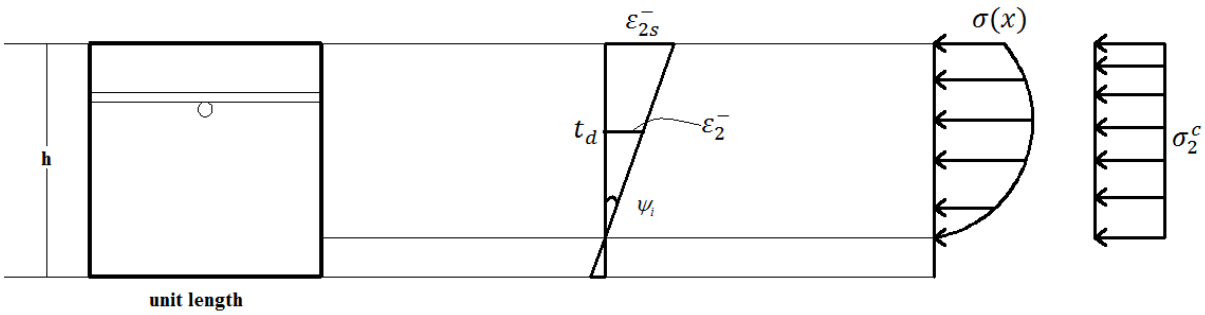

Figure 3-15 - Curvature induced nonlinear stress distribution

3.3.3 Averaging Factor K_t , k_c for Solving σ_1^c and σ_2^c

3.3.3.1 Averaging Factor for Concrete in Compression k_c

In the following formulation, it is assumed that softening of concrete only affect the stress, not the strains. First, let's derive the averaging factor for strain in the outer fiber of concrete k_c from $0 < \varepsilon_{2s}^{-} < \varepsilon_t$. Later, the expression of the averaging factor for $\varepsilon_t < \varepsilon_{2s}^{-} < \varepsilon_{cu}$ will be derived.

$$k_c \text{ for } 0 < \varepsilon_{2s}^{-} < \varepsilon_t$$

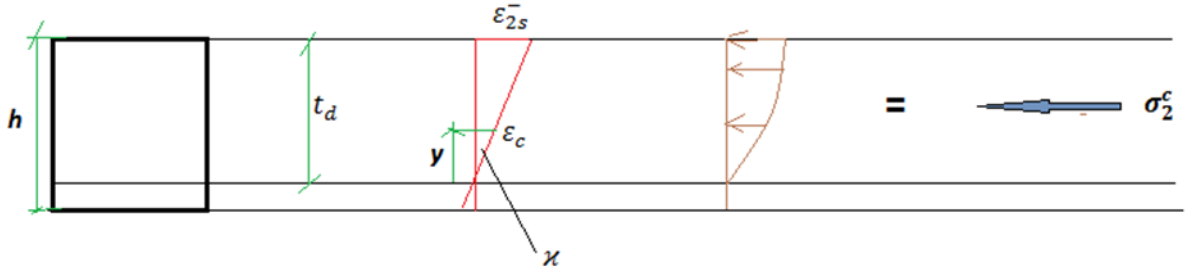

$$\sigma_2^c = K_c \zeta f_{co}^{'} = \frac{1}{1^* t_d} \int_0^{t_d} \sigma_c dy \qquad for\, 0 < \varepsilon_{2s}^{-} < \varepsilon_t \quad \sigma_c = \zeta \left(E_c \varepsilon_c - \frac{(E_c - E_2)^2}{4.6^* f_{co}^{'}} (\varepsilon_c)^2 \right) \tag{3.50}$$

First express ε as a function of distance from the neutral axis y

$\varepsilon_c = \frac{\bar{\varepsilon}_{2s} y}{t_d}$ substituting in the above equation $\sigma_c = \zeta\left(E_c\left(\frac{\bar{\varepsilon}_{2s} y}{t_d}\right) - \frac{(E_c - E_2)^2}{4.6 * f_{co}^{'}}\left(\frac{\bar{\varepsilon}_{2s} y}{t_d}\right)^2\right)$

$$\sigma_2^c = K_c \zeta f_{co}^{'} = \frac{1}{1 * t_d}\int_0^{t_d} \zeta\left(E_c\left(\frac{\bar{\varepsilon}_{2s} y}{t_d}\right) - \frac{(E_c - E_2)^2}{4.6 * f_{co}^{'}}\left(\frac{\bar{\varepsilon}_{2s} y}{t_d}\right)^2\right) dy \quad \text{by taking } \bar{\varepsilon}_2 = \frac{\bar{\varepsilon}_{2s}}{2} \tag{3.51}$$

And manipulating the above integration, one can express the averaging factor K_c as shown below.

$$K_c = \left(E_c \bar{\varepsilon}_2 - \frac{(E_c - E_2)^2 \bar{\varepsilon}_2^{-2}}{3.45 * f_{co}^{'}}\right)\frac{1}{f_{co}^{'}} \quad for\, 0 < \bar{\varepsilon}_{2s} < \varepsilon_t \tag{3.52}$$

k_c for $\varepsilon_t < \bar{\varepsilon}_{2s} < \varepsilon_{cu}$

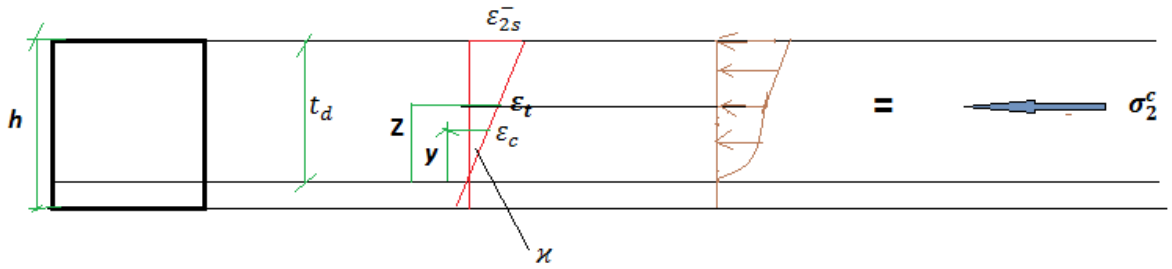

$z = \frac{\varepsilon_t t_d}{\bar{\varepsilon}_{2s}}$ $\varepsilon_c = \frac{\bar{\varepsilon}_{2s} y}{t_d}$ $\bar{\varepsilon}_2 = \frac{\bar{\varepsilon}_{2s}}{2}$

$$\sigma_2^c = K_c \zeta f_{co}^{'} = \frac{1}{1 * t_d}\int_0^{t_d} \sigma_c dy = \int_0^{z} \zeta\left(E_c\left(\frac{\bar{\varepsilon}_{2s} y}{t_d}\right) - \frac{(E_c - E_2)^2}{4.6 * f_{co}^{'}}\left(\frac{\bar{\varepsilon}_{2s} y}{t_d}\right)^2\right) dy + \int_z^{t_d} \zeta\left(1.15 f_{co}^{'} + E_2 \varepsilon_c\right) dy$$

$$\int_0^{t_d} \sigma_c dy = \int_0^{z} \zeta\left(E_c\left(\frac{\bar{\varepsilon}_{2s} y}{t_d}\right) - \frac{(E_c - E_2)^2}{4.6 * f_{co}^{'}}\left(\frac{\bar{\varepsilon}_{2s} y}{t_d}\right)^2\right) dy + \int_z^{t_d} \zeta\left(1.15 f_{co}^{'} + E_2 \varepsilon_c\right) dy$$

$$\int_0^{t_d} \sigma_c dy = \int_0^{\frac{\varepsilon_t t_d}{2\bar{\varepsilon}_2}} \zeta\left(E_c\left(\frac{2\bar{\varepsilon}_2 y}{t_d}\right) - \frac{(E_c - E_2)^2}{4.6 * f_{co}^{'}}\left(\frac{2\bar{\varepsilon}_2 y}{t_d}\right)^2\right) dy + \int_{\frac{\varepsilon_t t_d}{2\bar{\varepsilon}_2}}^{t_d} \zeta\left(1.15 f_{co}^{'} + E_2 \frac{2\bar{\varepsilon}_2 y}{t_d}\right) dy$$

After manipulating the above integration one can express the averaging factor K_c as showed below.

$$K_c = \left[\frac{E_c \varepsilon_t^2}{4\bar{\varepsilon}_2} - \frac{(E_c - E_2)^2 \varepsilon_t^3}{27.6 \bar{\varepsilon}_2 f_{co}^{'}} + 1.15 f_{co}^{'}\left[\frac{2\bar{\varepsilon}_2 - \varepsilon_t}{2\bar{\varepsilon}_2}\right] + E_2 \bar{\varepsilon}_2\left(\frac{4\bar{\varepsilon}_2^{-2} - \varepsilon_t^2}{4\bar{\varepsilon}_2^{-2}}\right)\right]\frac{1}{f_{co}^{'}} \quad for\, \varepsilon_t < \bar{\varepsilon}_{2s} < \varepsilon_{cu}$$

(3.53)

Therefore, the stress averaging factor for concrete in compression can be summarized as

$$K_c = \begin{cases} \left(E_c\varepsilon_2^- - \dfrac{\left(E_c - E_2\right)^2 \varepsilon_2^{-2}}{3.45^* f_{co}^{'}} \right) \dfrac{1}{f_{co}^{'}} & for\ 0 < \varepsilon_{2s}^- < \varepsilon_t \\ \left[\dfrac{E_c\varepsilon_t^{\,2}}{4\varepsilon_2^-} - \dfrac{\left(E_c - E_2\right)^2 \varepsilon_t^{\,3}}{27.6\varepsilon_2^- f_{co}^{'}} + 1.15 f_{co}^{'} \left[\dfrac{2\varepsilon_2^- - \varepsilon_t}{2\varepsilon_2^-} \right] + E_2\varepsilon_2^- \left(\dfrac{4\varepsilon_2^{-2} - \varepsilon_t^{\,2}}{4\varepsilon_2^{-2}} \right) \right] \dfrac{1}{f_{co}^{'}} & for\ \varepsilon_t < \varepsilon_{2s}^- < \varepsilon_{cu} \end{cases}$$

(3.54)

3.3.3.2 Averaging Factor for Concrete in Tension k_t

$$k_t \ for\ 0 < \varepsilon_{1s}^- < \varepsilon_{cr}$$

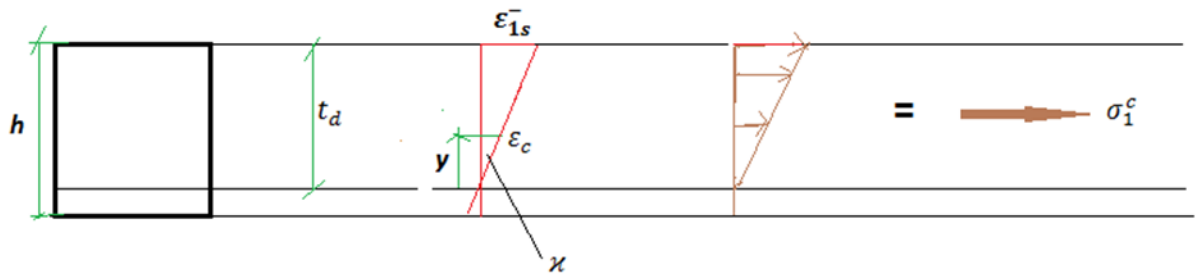

$$for\ 0 < \varepsilon_{1s}^- < \varepsilon_{cr} \qquad \varepsilon_{1s}^- = 2\varepsilon_1^-$$

$$\sigma_1^c = K_t f_{cr} = \frac{1}{1^* t_d} \int_0^{\varepsilon_{1s}^-} E_c \varepsilon_{c1}\, d\varepsilon \qquad \varepsilon_{c1} = \frac{\varepsilon_{1s}^- y}{t_d}$$

$$\sigma_1^c = K_t f_{cr} = \frac{1}{1^* t_d} \int_0^{t_d} E_c \frac{\varepsilon_{1s}^- y}{t_d} dy$$

After manipulating the above integration one can express the averaging factor K_t as showed below

$$K_t = \frac{E_c\varepsilon_1^-}{f_{cr}} \qquad for \quad 0 < \varepsilon_{1s}^- < \varepsilon_{cr}$$

(3.55)

$$k_t \ for \quad \varepsilon_{cr} < \varepsilon_{1s}^- < \varepsilon_{ult1}$$

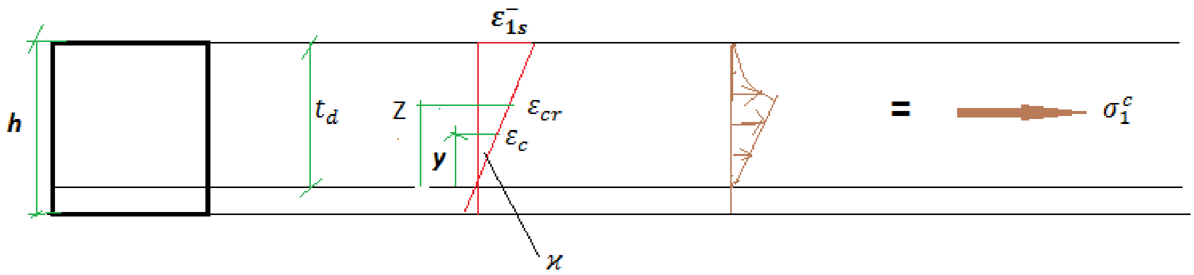

$$z = \frac{\varepsilon_{cr} t_d}{\varepsilon_{1s}^-} \qquad \varepsilon_{c1} = \frac{\varepsilon_{1s}^- y}{t_d}$$

$$\sigma_1^c = K_t f_{cr} = \frac{1}{1 * t_d}\left[\int_0^z E_c\left(\frac{\varepsilon_{1s}^- y}{t_d}\right)dy + \int_z^{t_d} f_{cr}\left(\frac{\varepsilon_{cr} t_d}{\varepsilon_{1s}^- y}\right)^C dy\right]$$

$$\sigma_1^c = K_t f_{cr} = \frac{1}{1 * t_d}\left[\int_0^{\frac{\varepsilon_{cr} t_d}{\varepsilon_{1s}^-}} E_c\left(\frac{\varepsilon_{1s}^- y}{t_d}\right)dy + \int_{\frac{\varepsilon_{cr} t_d}{\varepsilon_{1s}^-}}^{t_d} f_{cr}\left(\frac{\varepsilon_{cr} t_d}{\varepsilon_{1s}^- y}\right)^C dy\right] \tag{3.56}$$

After substituting $\varepsilon_{1s}^- = 2\varepsilon_1^-$ and manipulating the above integration one can express the averaging factor K_t as shown below.

$$K_t = \frac{E_c \varepsilon_{cr}{}^2 t_d}{4\varepsilon_1^- f_{cr}} + \left(\frac{\varepsilon_{cr} t_d}{2\varepsilon_1^-}\right)^c \left(\frac{1}{1-c}\right)\left[t_d{}^{(1-c)} - \frac{\varepsilon_{cr} t_d}{2\varepsilon_1^-}{}^{(1-c)}\right]\frac{1}{t_d} \qquad for \quad \varepsilon_{cr} < \varepsilon_{1s}^- < \varepsilon_{ult1} \tag{3.57}$$

Therefore the stress averaging factor for concrete in tension can be summarized as

$$K_t = \begin{Bmatrix} \dfrac{E_c \varepsilon_1^-}{f_{cr}} & for \quad 0 < \varepsilon_{1s}^- < \varepsilon_{cr} \\ \dfrac{E_c \varepsilon_{cr}{}^2 t_d}{4\varepsilon_1^- f_{cr}} + \left(\dfrac{\varepsilon_{cr} t_d}{2\varepsilon_1^-}\right)^c \left(\dfrac{1}{1-c}\right)\left[t_d{}^{(1-c)} - \dfrac{\varepsilon_{cr} t_d}{2\varepsilon_1^-}{}^{(1-c)}\right]\dfrac{1}{t_d} & for \quad \varepsilon_{cr} < \varepsilon_{1s}^- < \varepsilon_{ult1} \end{Bmatrix} \tag{3.58}$$

3.3.4 Geometric Cross sections and Reinforcement Ratios

The thickness t_d can be calculated using the curvature ψ_i and the maximum strain at the surface ε_{2si} .After equating the thickness of the shear flow zone on each panel, the other geometric properties and mechanical steel ratios can be calculated as follows

$$t_{d,i} = \frac{\varepsilon_{2si}}{\psi_i} \qquad b_o = b - \left(\frac{t_{d1}}{2}\right) - \left(\frac{t_{d3}}{2}\right) \qquad h_o = h - \left(\frac{t_{d2}}{2}\right) - \left(\frac{t_{d4}}{2}\right)$$
$$A_o = b_o h_o \qquad P_o = 2b_o + 2h_o$$
$$\rho_{li} = \frac{A_l}{P_o t_{di}} \qquad \rho_{ti} = \frac{A_{t1}}{St_{di}} \qquad \rho_{fli} = \frac{A_{lf}}{P_o t_{di}} \qquad \rho_{fti} = \frac{A_{tf1}}{St_{di}} \text{ for Continuous wrapping } \rho_{ft} = \frac{t_f}{t_{di}} \tag{3.59}$$

3.3.5 Boundary Conditions for Combined Torsion and Uniaxial Bending

Torsion in rectangular sections will induce shear stresses that flow around the member. When considering a uniaxial bending moment in addition to torsion, the equivalent hollow section that was responsible for resisting the torsion will be subjected to additional compressive and tensile normal stress (see Figure 3-16).

In the proposed model the following three assumptions will be used regarding the distribution of shear and normal stresses due to combined loading.

- The applied torsion and uniaxial bending can be distributed to the four wall panels as uniform normal and shear stresses.
- The four wall panels will be subjected to a uniform shear stress due to the applied torsion.
- Two opposite panels will be subjected to uniform compressive and tensile stress due to the applied uniaxial bending.

The applied shear flow due to torsion is constant for all the panels and its formulation is straightforward. However for the case of uniaxial bending the formulation of equivalent stresses will be somehow difficult due to its dependence on the thickness of the shear flow depth. The applied compressive and tensile stress due to uniaxial bending can be calculated by using the above assumptions and force equilibrium. The application of the force equilibrium will follow the following two steps (see Figure 3-16).

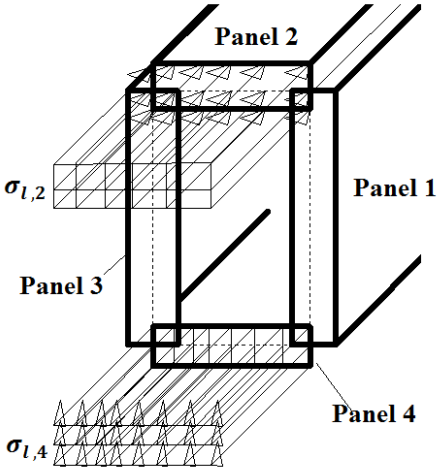

Figure 3-16 - Membrane elements subjected to uniaxial bending

1. Horizontal force equilibrium should be satisfied.

$$\sum F_x = 0 \quad \sigma_{l,4} t_{d,4} b_o + \sigma_{l,2} t_{d,2} b_o = 0$$

2. Rotational equilibrium should be satisfied, by equating the moment about the geometric center of the cross-section, the applied stresses due to uniaxial bending m are expressed as below.

$$m = \sigma_{l,4} t_{d,4} b_o \frac{h_o}{2} + \sigma_{l,2} t_{d,2} b_o \frac{h_o}{2}$$

$$\sigma_{l,4} = \frac{m}{t_{d,4} b_o h_o} \qquad \sigma_{l,2} = \frac{-m}{t_{d,2} b_o h_o} \tag{3.60}$$

3.4 Solution Algorithm

To facilitate the solution algorithm, two control equilibrium conditions will provided. The first one is derived by adding equation (3.2) and equation(3.3). The second control equation is derived by subtracting equation (3.3) from(3.2). The two control equations are given by equation 3.61 and 3.62.

$$\sigma_l + \sigma_t = \sigma_1^c + \sigma_2^c + \rho_l f_l + \rho_{fl} f_{fl} + \rho_t f_t + \rho_{ft} f_{ft} \tag{3.61}$$

$$\sigma_l - \sigma_t = \sigma_1^c \left(cos^2\alpha_1 - sin^2\alpha_1\right) + \sigma_2^c \left(sin^2\alpha_1 - cos^2\alpha_1\right) - 2\tau_{12}{}^c 2\sin\alpha_1 cos\alpha_1 + \left(\rho_l f_l + \rho_{fl} f_{fl}\right) - \left(\rho_t f_t + \rho_{ft} f_{ft}\right)$$
(3.62)

When members are subjected to torsion, all four panels will be exposed to equal shear flow. Due to this uniform stress condition on each of the panels, observation of a single panel element will be sufficient to understand the behavior of the structural member as a whole, as a result of this, a separate simplified solution algorithm will be provided for the case of pure torsion.

In the following section, two separate solution algorithms will be proposed for the case of pure torsion and for the case of combine action due to uniaxial bending and torsion.

3.4.1 Solution Algorithm for Pure Torsion

The solution algorithm for pure torsion is simpler than that of combined torsion and flexure. The calculation of the thickness of the shear flow, perimeter and area can be done without iteration. The thickness of the shear flow can be calculated as a function of perimeter, area and assumed principal strains. The formula for the thickness of shear flow zone is given below and detail derivation can be referred from the original paper by Jeng and Hsu (2009).

$$t_d = \frac{\left(\frac{HP_c}{2} + P_c\right) - \sqrt{\left(\frac{HP_c}{2} + P_c\right)^2 - 4HA_c\left(H+4\right)}}{2\left(H+4\right)} \qquad H = \frac{4\varepsilon_2^-}{\left(\gamma_{lt}\right) sin2\alpha_1} \tag{3.63}$$

$$p_o = p_c - 4t_d \tag{3.64}$$

$$A_o = A_c + t_d{}^2 - \left(\frac{p_c}{2}\right)t_d \tag{3.65}$$

The uniform shear stress and strain in panels leads to modification of the curvature and angle of twist as given below

$$\psi = \theta \sin 2\alpha_1 \tag{3.66}$$

$$\theta = \left(\frac{p_o}{2A_o}\right)\left(\gamma_{lt}\right) \tag{3.67}$$

The solution algorithm for members subjected to pure torsion is given in the following flowchart.

Solution Algorithm for Pure Torsion

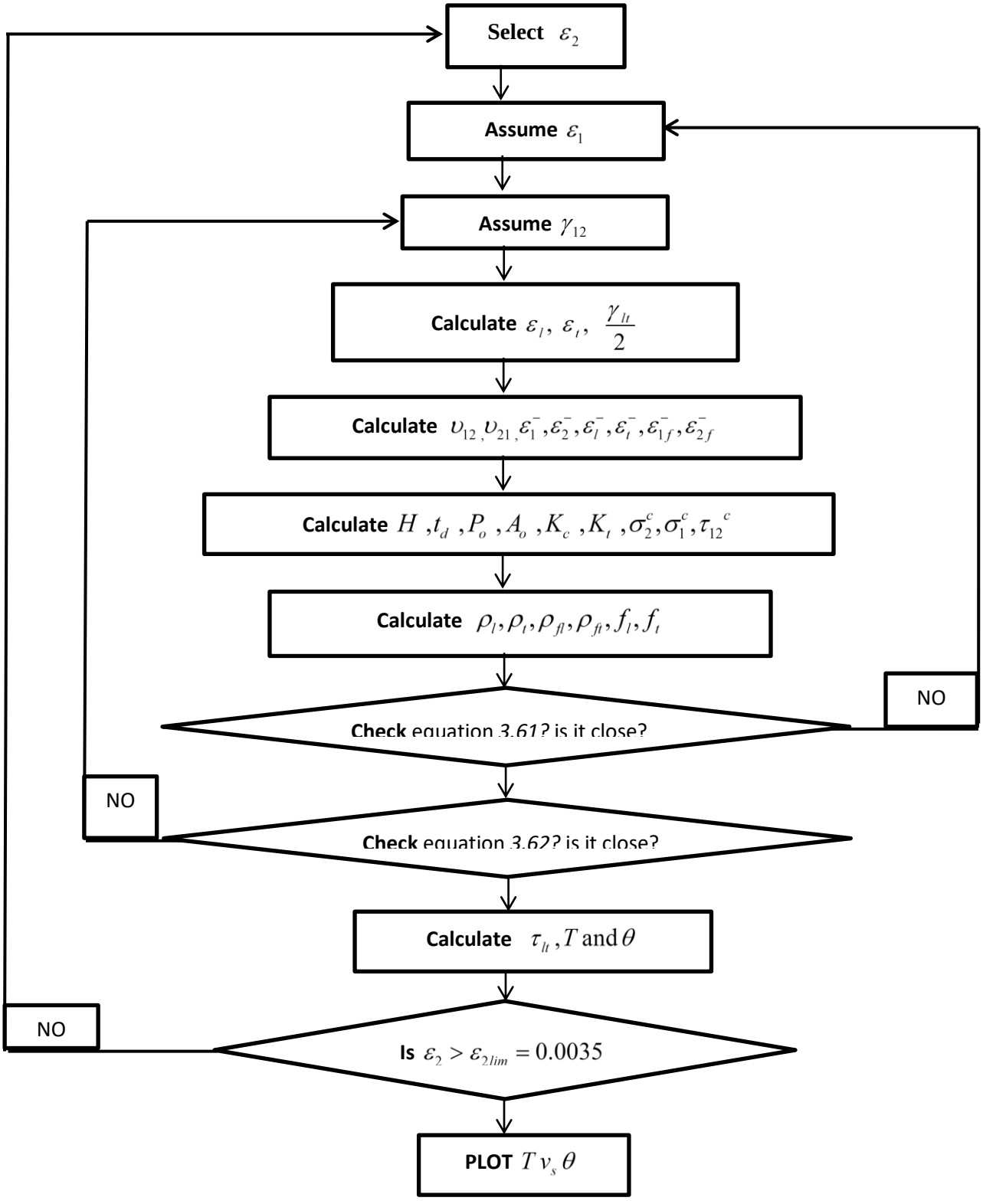

Figure 3-17 - Solution algorithm for pure torsion

3.4.2 Solution Algorithm for Combined Torsion and Uniaxial Bending

The solution for combined action is somehow more difficult than that of pure torsion. The number of variables that are assumed to plot a single point on torsion – angle of twist coordinate is four times larger than the pure torsions algorithm. To reduce the number of assumed variables, a careful observation on the behavior of each panel due to combined loading has to be made.

When a rectangular member is subjected to combined torsion and uniaxial bending, the side panels will be subjected to similar shear flow, as a result, both panel 1 and panel 3 will have equal longitudinal and transverse strain. The consequence of this equal strain will be no additional curvature on these two panels due to opposite panel i.e. $\phi_{13,l} = 0$ $\phi_{13,t} = 0$.Due to the similar boundary condition, these two panels (Panel 1 and Panel 3) will have a similar initial assumption.

The second observation is the method of determination of the fixed angles α_1. When members are subjected to pure shear α_1 is always 45°, as a result, panel 1 and panel 3 will have a fixed angle of 45°.

For the cases of panel 2 and panel 4, when these members are subjected to combined load increasing in a proportional manner, the applied principal axis angles can be predetermined using torsion to bending moment ratio. The angles determination can be done in the following manner.

The fixed angle α_1 , the shear stress τ_{lt}, and the normal stress σ_l are related to each other. Their relationship can be reduced to a constant dependent on the proportional constant of bending to torsion as follows.

$$\tan 2\alpha_1 = \frac{2\tau_{lt}}{\sigma_l - \sigma_t} \tag{3.68}$$

$$\sigma_l = \frac{m}{t_d A_o} \tag{3.69}$$

$$\tau_{lt} = \frac{T}{2A_o t_d} = \frac{km}{2A_o t_d} \tag{3.70}$$

where k is proportional factor between Torsion and moment $k = \frac{T}{m}$.

$$\tan 2\alpha_1 = \frac{2\tau_{lt}}{\sigma_l - \sigma_t} \qquad \tan 2\alpha_1 = \frac{2\left(\frac{km}{2A_o t_d}\right)}{\frac{m}{t_d A_o}} \tag{3.71}$$

$$\tan 2\alpha_1 = k$$

Therefore, for different ratio of torsion to flexure, the fixed angle can be calculated using equation 3.71. For demonstration, some results are given in Table 3-1.

Table 3-1-Values for fixed angle as a function of proportionality ratio

$k = \frac{T}{m}$	α_1
∞	45
2	31.71
1	22.5
0	0

When the normal stress, σ_l, is in compression, the computed values will be the negative of the above-tabulated values.

Solution Algorithm for Torsion and Uniaxial Bending

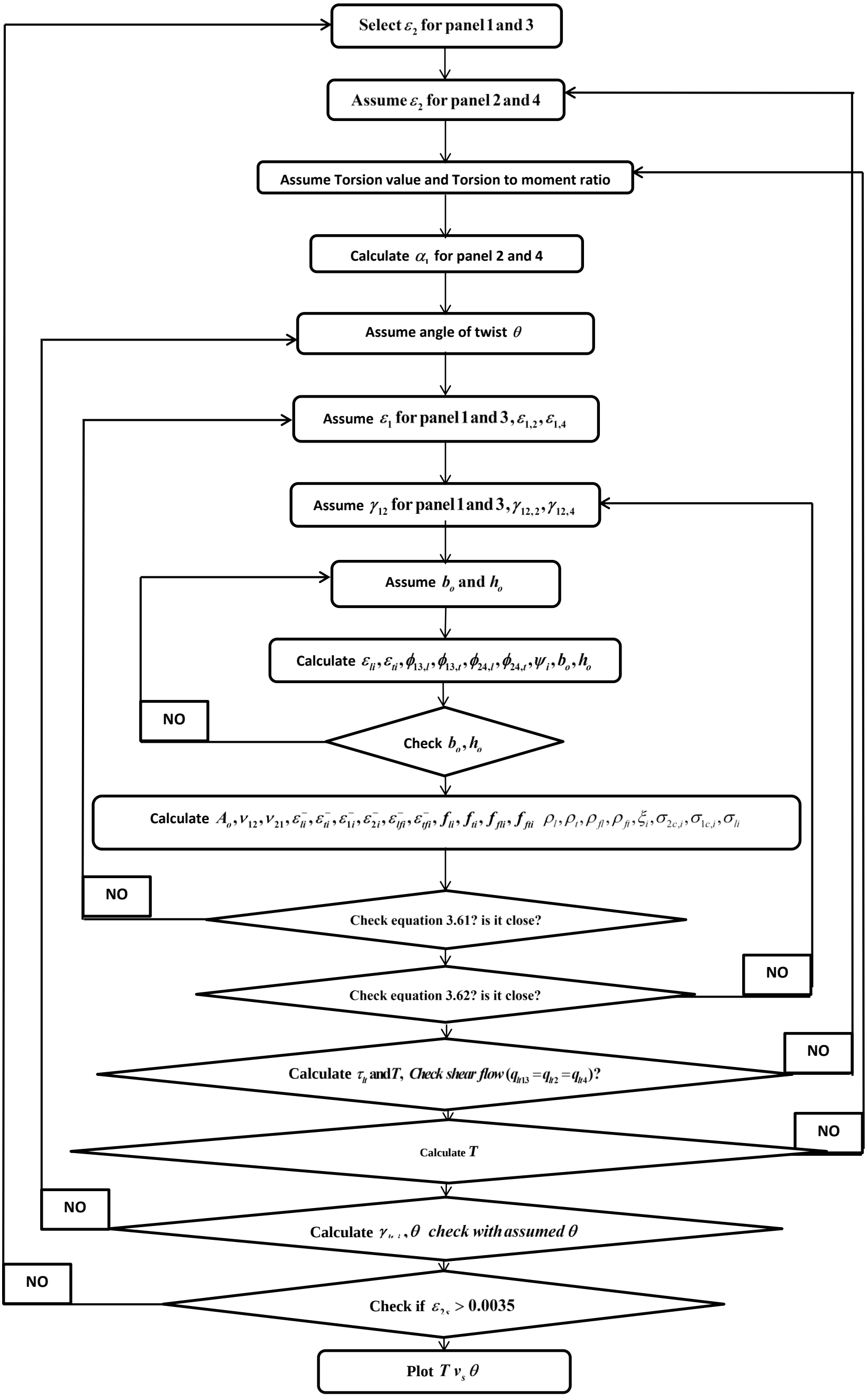

Figure 3-18-Flowchart for combined torsion and flexure

3.5 Analytical Model Applicability

3.5.1 RC Beams Wrapped with Carbon Fiber Subjected to Pure Torsion

The applicability of the proposed model will be demonstrated by comparing the prediction of the proposed model with experimental results of four RC members selected from the literature. The selected specimens from the literature are tested under pure torsion and they include specimens wrapped with continuous carbon fiber strips throughout the members, member strengthened using discrete carbon fiber strips wrapped transversely at some spacing and conventional RC members without carbon fiber strip.

3.5.1.1 M.R.Mohammadizadeh and M.J. Fadaee (2008) beams

The authors conducted a pure torsional test on seven rectangular beam specimens having a width of 150 and a depth of 350 mm. The length of the beams was 2000 mm. The specimens were reinforced with four 14 mm diameter longitudinal bars located at four corners and transverse reinforcements of diameter 8 mm spaced at 80 mm.

Continues CFRP was provided vertically with respect to the longitudinal beam axis. CW1 was wrapped with one layer of CFRP around the perimeter of the section and Beam CW2 was wrapped by two layers of CFRP. Three reference beams without carbon fiber strips were also tested for pure torsion (REF1, REF2, and REF3).

High strength concrete was used and the cylinder compressive strength of the concrete for CW1 and CW2 was 79.12 and 74.95 MPa respectively. The cylinder compressive strength of the reference beams REF1, REF2, REF3 was 78.94, 77.82 and 79.34 MPa respectively.

The yield strengths of the transverse and longitudinal reinforced bars were 397 MPa and 480 MPa respectively. The mechanical properties of the carbon fiber used are given in Table 3-2.

Table 3-2- Mechanical properties of the fiber

Modulus	240,000 MPa
Design Thickness	0.176 mm
Design Tensile Strength	3800 MPa
Ultimate Tensile Elongation	1.55%

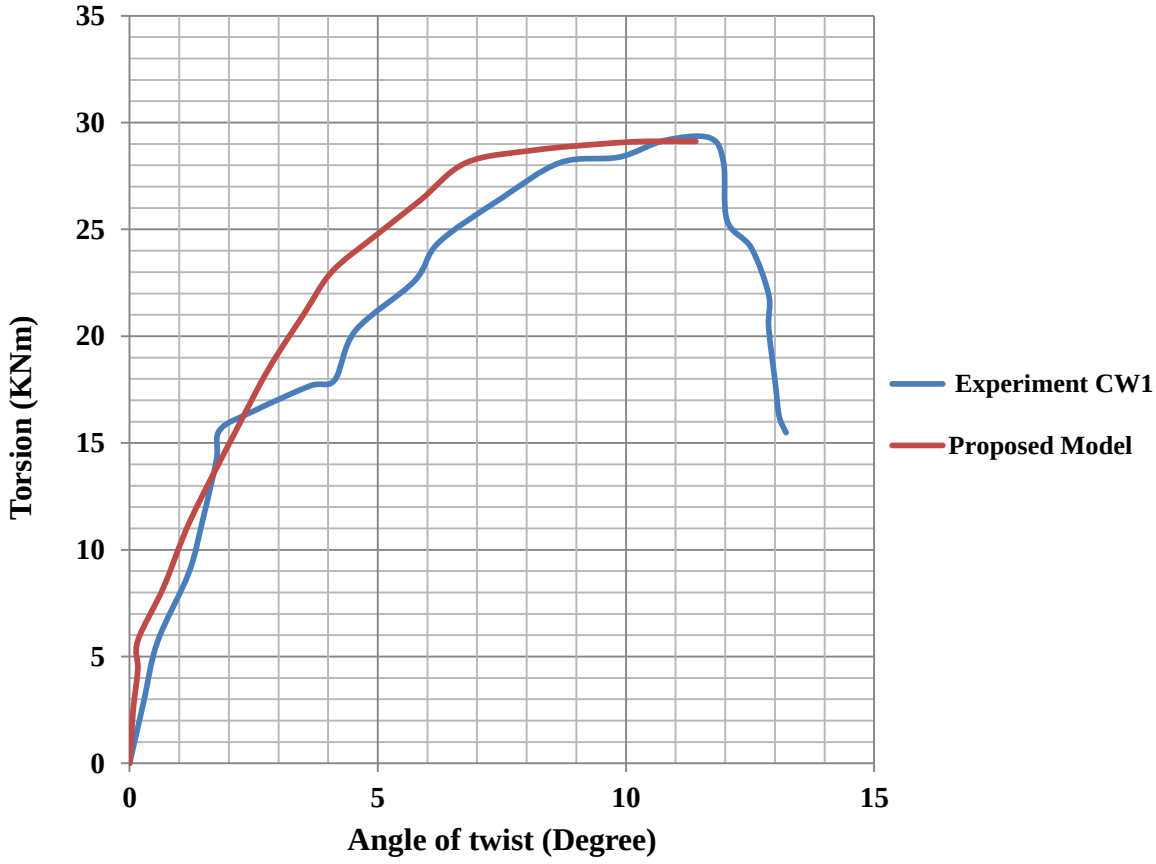

Figure 3-19- Proposed model and experimental result for specimen wrapped with continuous carbon fiber strips (CW1)

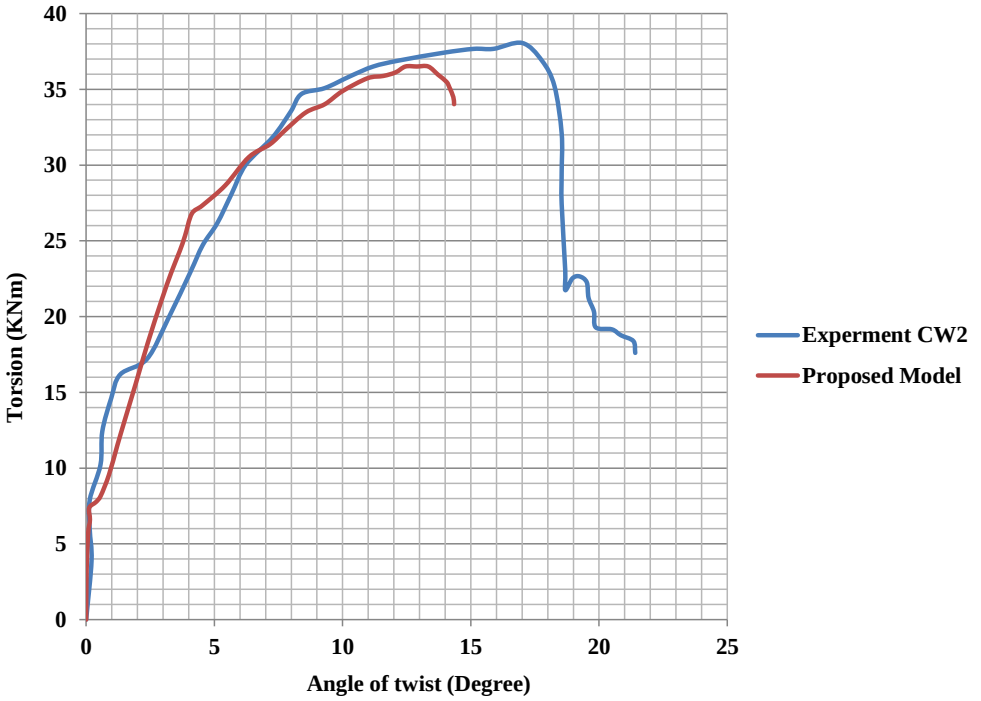

Figure 3-20-Proposed model and experimental result for specimen wrapped with continuous carbon fiber strips (CW2)

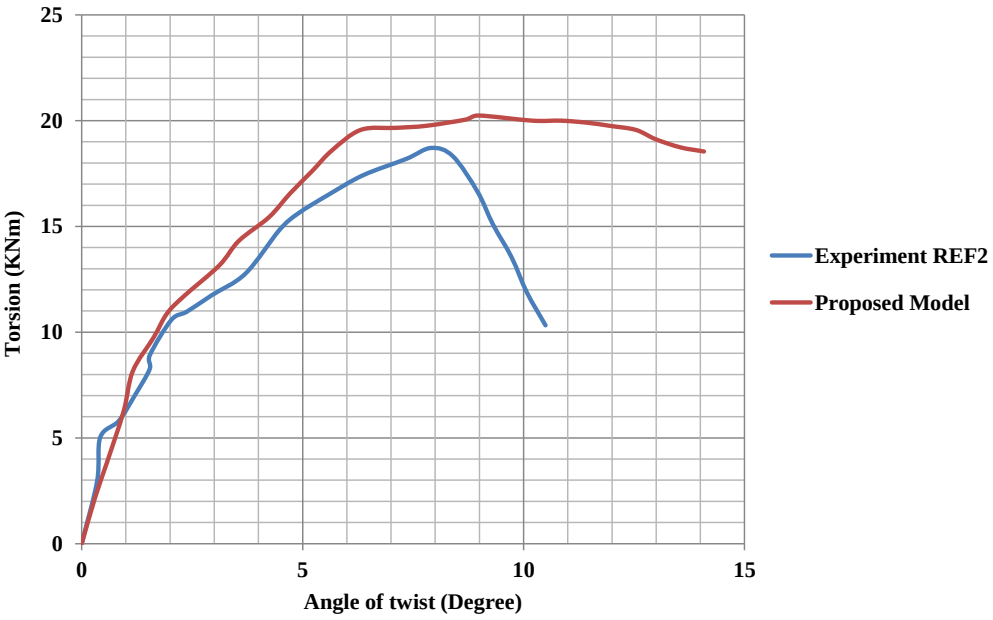

Figure 3-21- Proposed model and experimental result for reference RC beam without carbon fiber strips (REF2)

The experimental results and the prediction of the analytical model are shown in Figure 3-19, Figure 3-20 and Figure 3-21. The proposed model closely predicts the ultimate capacity of specimens wrapped with one and two layers of carbon fiber. However, the proposed model slightly overestimates the capacity of the reference RC beam.

3.5.1.2 Hii1 and Al-Mahaidi (2006) beams

The authors tested six RC beams with a width of 500 mm and depth of 350 mm. The length of the specimens was 2.5 m. Two specimens were solid sections (CS1, FS050D2). FS050D2 was wrapped with two layers of carbon fiber strips with a width of 50 mm placed perpendicular to the longitudinal axis with a spacing of 150 mm. The RC beams were reinforced with 6 mm diameter and 426 MPa yield strength closed stirrups at a spacing of 125 mm. Fourteen 10 mm diameter bars with yield strength of 398 MPa were used for longitudinal reinforcement. The compressive strength of the concrete was 56.4 MPa. The mechanical properties of the carbon fiber used are given in Table 3-3.

Table 3-3-Mechanical properties of the fiber

Modulus	240,000 MPa
Design Thickness	0.176 mm
Design Tensile Strength	3800 MPa
Ultimate Tensile Elongation	1.55%

The experimental results and the prediction of the analytical model are shown in Figure 3-22. The proposed model closely predicts the ultimate capacity but the prediction of pre-cracking loads and stiffness somehow deviates from the experiment behavior. This deviation might be due to the relatively larger width and shallower depth of the tested specimen.

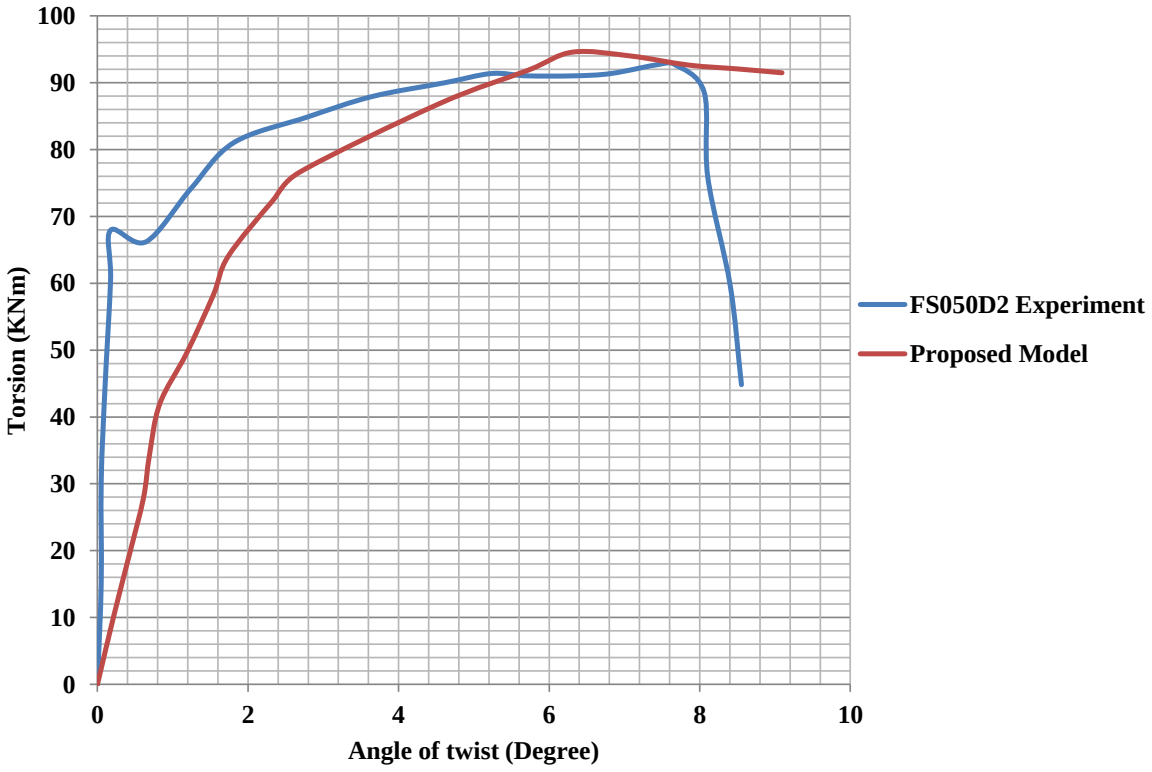

Figure 3-22- Proposed and experimental result for RC beam wrapped transversely at some spacing with discrete carbon fiber strips (FS050D2)

As it has been demonstrated in the above comparisons, the proposed model can be used to predict the behavior RC beams with fibers wrapped continuously or with spacing. Moreover, the proposed model can also be used to predict the behavior RC beams without carbon fiber wrapping.

3.5.2 RC Beams Subjected to Combined Torsion and Flexure

The model's applicability for combined action will be verified by comparing the prediction of the model with experimental results of Onsongo (1978) and McMullen and Warwaruk (1970). The specimens were tested with wide ranges of torsion to moment combination. Most of the beams that are used for verifications were unsymmetrically reinforced with a larger portion of the total longitudinal rebar provided in the flexural tension zone. The detail descriptions of the specimens are given in Table 3-4, Table 3-5, and Figure 3-23.

Table 3-4-McMullen and Warwaruk beams

	Longitudinal rebar		Transverse rebar							
Beam No	Top	Bottom	Size (mm)	Spacing (mm)	Width (mm)	Height (mm)	f_c (MPa)	f_y*	f_y#	T/M
1-3	2ϕ10	2ϕ20	10	82.55	152	304	34.9	379	365	2
1-4	2ϕ10	2ϕ20	10	82.55	152	304	34.3	379	365	1
2-2	2ϕ20	2ϕ20	10	82.55	152	304	34.6	370	365	2
2-3	2ϕ20	2ϕ20	10	82.55	152	304	37.9	370	365	1

**Transverse reinforcement (MPa)* *# longitudinal reinforcement (MPa)*

T/M= *Torsion to flexure ratio*

Table 3-5-Onsongo test beam

	Transverse rebar							
Beam	Size (mm)	Spacing (mm)	f_c (MPa)	f_y*	f_y# (ϕ10)	f_y# (ϕ12.7)	f_y# (ϕ25.4)	T/M
TBS2	12.5	76	36.5	443	406	433	436	1.28
TBS4	12.5	76	15.5	443	406	433	436	1.28

**Transverse reinforcement (MPa)* *# longitudinal reinforcement (MPa)*

T/M= *Torsion to flexure ratio*

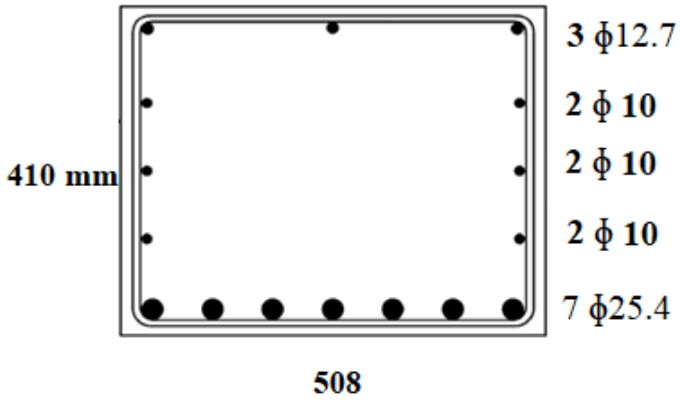

Figure 3-23-Onsongo beams cross-section (TBS2 and TBS4)

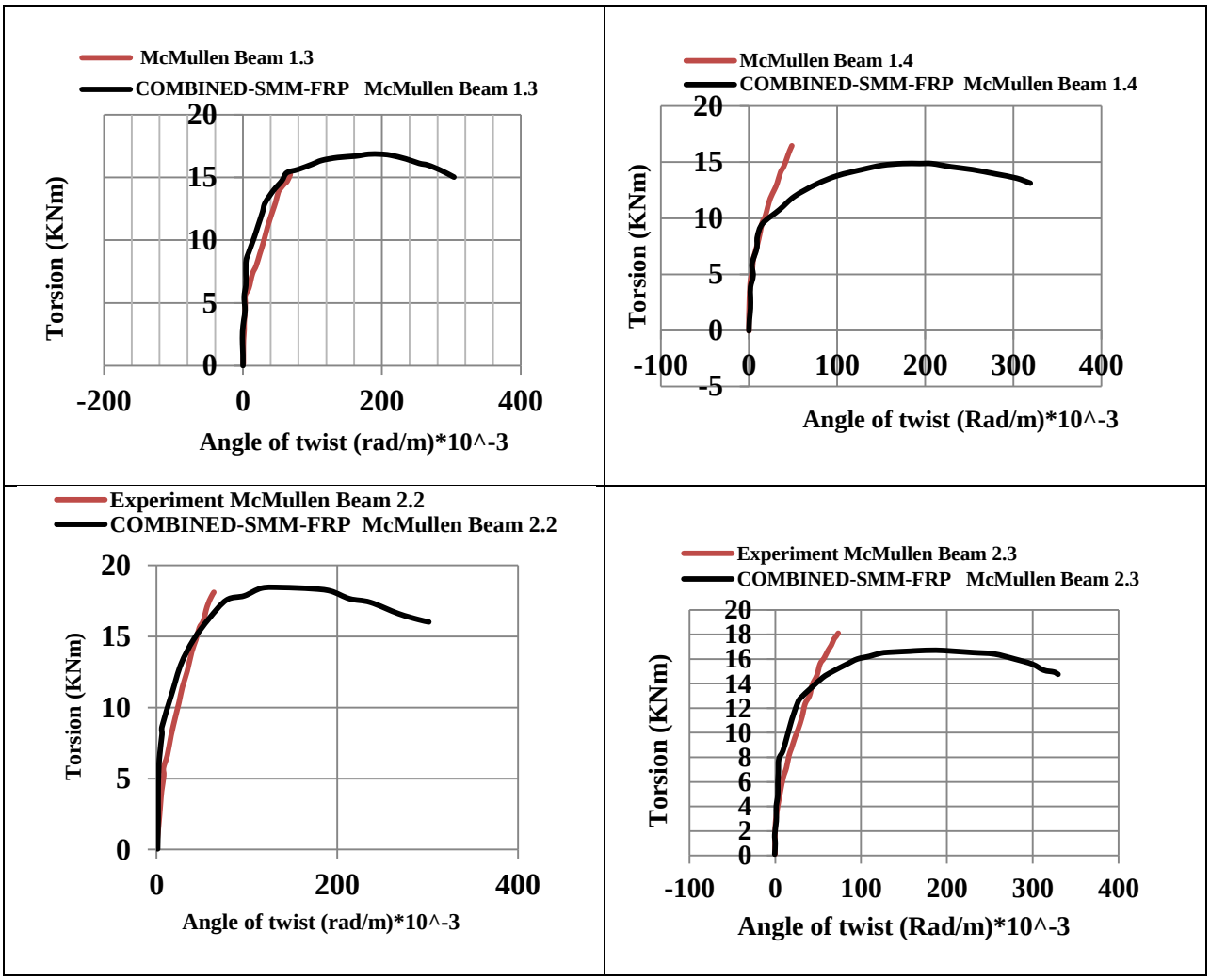

Figure 3-24-Proposed model and experimental result of McMullen and Warwaruk beams

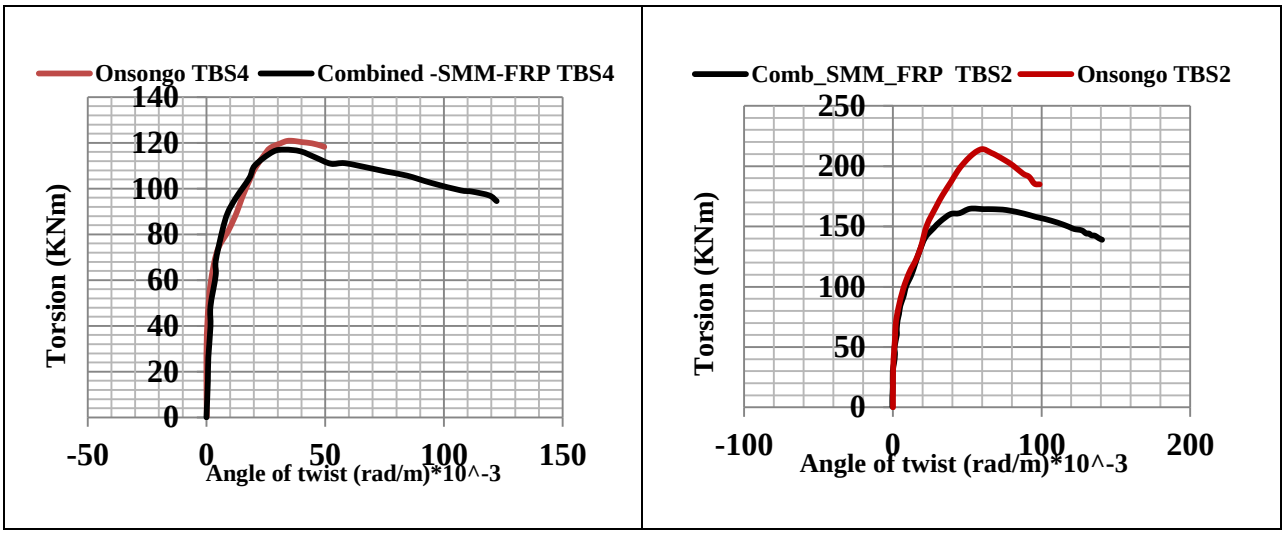

Figure 3-25-proposed model and experimental result of Onsongo beams

The experimental investigations conducted by Onsongo (1978) were displacement controlled which resulted in plots with ascending and descending branches whereas tests by McMullen and Warwaruk (1970) were that of force based. Consequently, the experimental plots of McMullen and Warwaruk beams were limited up to the peak strength.

As it has been validated in the above comparisons (see Figure 3-25), the proposed model can be used to predict the behavior RC beams subjected to combined torsion and flexure.

4 EXPERIMENTAL PROGRAM

This chapter will describe the experimental work conducted at the Materials Laboratory of Addis Ababa Institute of Technology (AAiT). The experimental work is aimed to study the behavior of torsion critical beams subjected to combined torsion and uniaxial bending.

In the experimental program, four reinforced concrete beams in two groups were cast. The main variables were the spacing of transverse reinforcement and the application of members strengthening using carbon fiber. All four rectangular beam specimens have a width of 150 mm and depth of 200mm. The total length of the specimens was 2.2 m and the critical region where a uniform torsion and flexure acts have a length of 1m.

Prior to the experimental program, analytical simulation using VecTor 3, a nonlinear finite element software developed at University of Toronto, has been conducted to avoid premature failures.

In the following sections testing setup, test specimens, materials used, specimen fabrication, specimen preparation, and instrumentation will be discussed.

4.1 Test Setup for Torsion with Uniaxial Bending

The test specimens are designed in such a manner to create combined flexure and torsion with zero shear force in the central region of the section (critical section). The ratio of the torsional to flexural moment can greatly affect the outcome of the experimental program. As it can be seen from Figure 4-1, a four-point loading is modified to apply a constant torsion and flexure on the critical region. The test specimens are constructed with semicircular supports to allow end rotation (twist). A constant ratio of flexural to torsional moment will be maintained throughout the experimental program. The ratio of bending to the torsional moment in the critical region can be maintained by adjusting the lever arm of the loading point from the longitudinal centerline of the beam (see Figure 4-1).

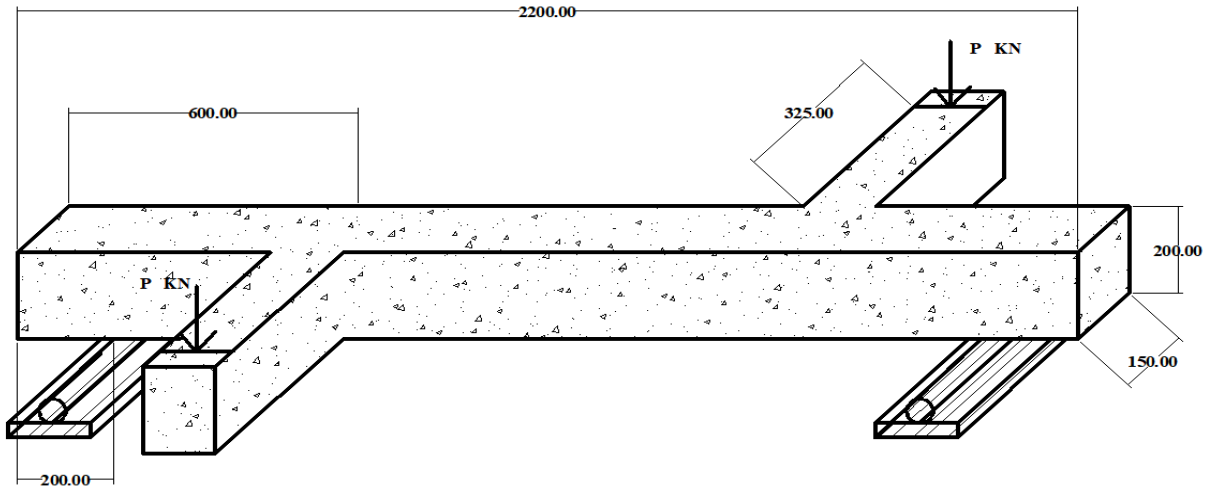

Figure 4-1-Test set up (all dimensions are in mm)

Considering the extreme scenarios, providing a very small lever arm means essentially testing for flexure with a very small torsional moment. If the lever arm is large then the torsional moment will be the dominant action. As it can be seen from Table 4-1, by fixing other dimensions of the proposed test beam, for different flexure to torsional moment ratios the required length of the lever arm will vary considerably.

Table 4-1– Required length of the lever arm for different flexure to torsional moment ratios

Flexure to Torsion ratio	Eccentricity (m)*	Length of the overhang (m)+
0.25	1.6	1.575
0.5	0.8	0.775
0.75	0.533	0.508
1	0.4	0.375
1.25	0.32	0.295
1.5	0.266	0.2416

* *Eccentricity is measured between the loading point and the center line of the beam.*

+*Length of the overhang is measured between the junction and end of the arm* (see Figure 4-1).

Using Table 4-1, one can observe that as flexure to torsion ratio gets smaller the needed lever arm (eccentricity) will be large and the test specimen will basically be subjected to higher torsional moment with a small bending moment. On the other extreme, when the ratio gets larger, it results in a large bending moment with a small twist; as a result, the required eccentricity will be small.

In this thesis by giving consideration to the objective of the study and physical limitation of the laboratory testing set up, the adopted flexure to torsional moment ratio is one.

4.2 Specimens

There will be two groups of specimens. Each group will have two RC beams. The second group will be provided with relatively close transverse reinforcement than the first group.

Both groups will have one control beam tested via combined action of torsion and flexure. After strengthening of the members using carbon fiber strips, the remaining specimen from each group will be tested for combined action of flexure and torsion. The full cross-sectional wrapping scheme with a lap of 200 mm will be used for both beams.

The detail of each test specimen in the two groups with their designations, wrapping schemes and other properties are given in Table 4-2, Figure 4-2 and Figure 4-3.

Table 4-2 - Details of test specimens

Group	Specimen designation	Longitudinal reinforcement	Transverse reinforcement	Wrapping scheme	Number of layers
1	T100,1	$2\phi 8$ top $2\phi 10$ bottom	$\phi 8c/c100mm$	–	–
	T100,2	$2\phi 8$ top $2\phi 10$ bottom	$\phi 8c/c100mm$	FULL	2
2	T50,1	$2\phi 8$ top $2\phi 10$ bottom	$\phi 8c/c50mm$	–	–
	T50,2	$2\phi 8$ top $2\phi 10$ bottom	$\phi 8c/c50mm$	FULL	2

T=Torsion with flexure $100/50 = spacing\ of\ transverse\ rebars$ $1/2 = Test\ beam$

- *To force the failure on the specimen into the control region, a closely spaced transverse reinforcement is used near the supports* $(\phi 8c/c50mm)$.

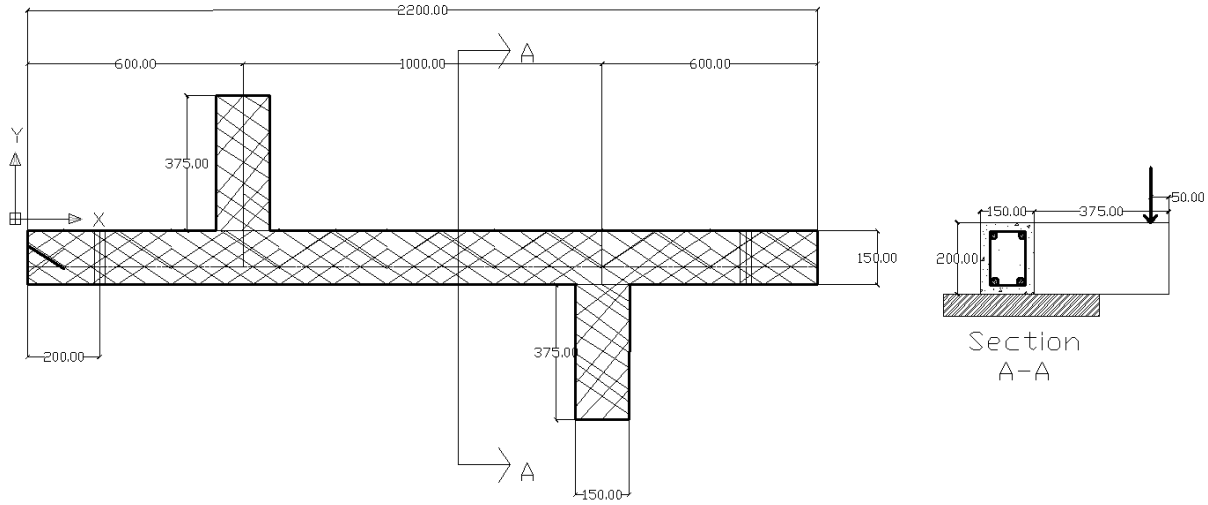

Figure 4-2 - Top view of test specimens

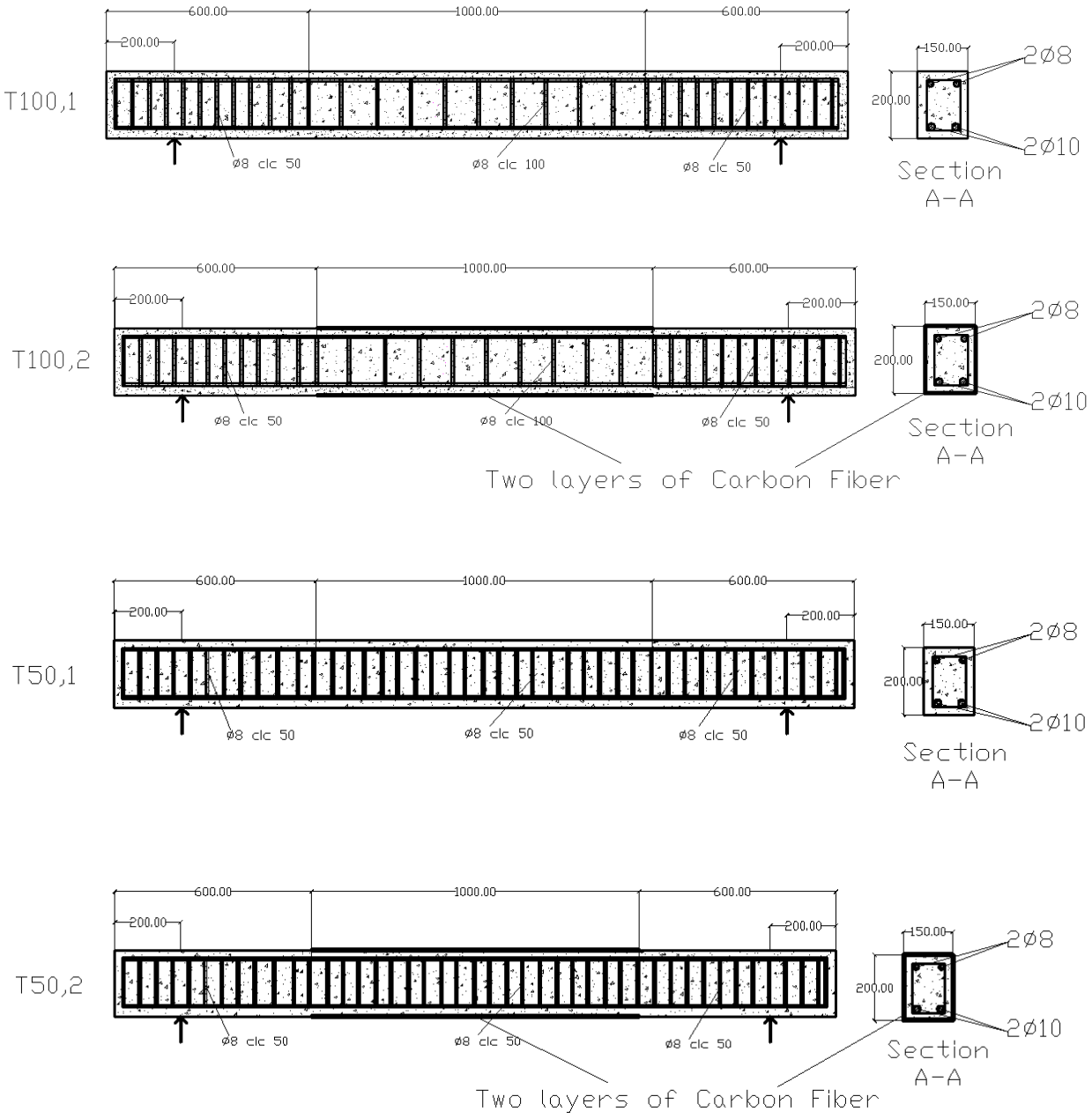

Figure 4-3 -Longitudinal and transverse reinforcement detailing for specimens

4.3 Materials

4.3.1 Concrete

A mix design for the target cylindrical strength of 30 MPa was planned using ACI mix design. An ordinary portland cement, aggregate with a maximum size of 25 mm and 75-100 mm of slump were specified as shown in Table 4-3.

Table 4-3-Mix Design before adjustment

Target compressive strength (cylindrical) (MPa)	30
Cement type	Ordinary Portland Cement
Maximum aggregate size (mm)	25
Mixing water (Kg/m^3)	193
Cement (Kg/m^3)	331.48
Fine aggregate (Kg/m^3)	822.6
Course aggregate (Kg/m^3)	1047

Prior to mixing of the ingredients, a thorough material preparation of fine and coarse aggregate was conducted. Course and fine aggregate were washed with water to remove any impurities and then, the aggregates were weighted and packed using plastic bags to preserve and avoid a fluctuation of moisture content (see Figure 4-4a). The moisture and silt contents of the aggregates were tested before sealing of the bags (see Figure 4-4 (b), (c)) and the results from the tests were carefully documented.

(a)

(b)

(c)

Figure 4-4- (a) Packed aggregates (b) Moisture containt test (C) Silt content test

The test specimens were cast using three mixes. The mixing of the concrete constituents was preceded by adjustment of the mixing water for the excess moisture on the aggregates using the previously documented data. For each mix, two cubes (150*150*150mm) and one cylinder (150*300) sample were taken. During concreting work, the slump was continuously checked to avoid erratic mixes within a casted specimen (see Figure 4-5). On the test day of the beam specimens, the mechanical properties of the representative samples were acquired by conducting compression and splitting tensile tests (see Figure 4-6). The compressive and tensile strength of the samples with their designation is given in Table 4-4 and Table 4-5.

Figure 4-6- Compressive strength test

Figure 4-5-Concrete slump test

Table 4-4-Compressive strength of the samples

Beam sample	Cube Designations	Mass (Kg)	Compressive Strength (MPa)	Mean Strength	Standard deviation	Coefficient of Variation (%)
T100,1	T100,1A	7.737	34.23	43.32	9.4	21.7
	T100,1B	7.897	38.49			
	T100,1C	7.823	36.92			
	T100,1D	8.005	-			
	T100,1E	7.761	53.34			
	T100,1F	7.947	53.63			
T100,2	T100,2A	7780	52.72	53.35	1.68	3.16
	T100,2B	7737	54.66			
	T100,2C	7959	52.22			
	T100,2D	7866	53.55			
	T100,2E	7918	51.16			
	T100,2F	7771	55.80			
T50,2	T50,1A	7.696	47.61	47.38	1.44	3.03
	T50,1B	7.660	47.19			
	T50,1C	7.670	47.39			
	T50,1D	7.830	-			
	T50,1E	7.693	49.39			
	T50,1F	7.690	45.34			
T50,1	T50,2A	7.823	47.83	45.88	3.02	6.58
	T50,2B	8.001	-			
	T50,2C	8.126	41.39			
	T50,2D	7.705	47.42			
	T50,2E	7.922	46.89			
	T50,2F	7.977	-			

- *Premature edge failure*

Table 4-5- Tensile strength of samples

Beam sample	Sample Designations	Tensile strength(MPa)	Mean strength	Standard deviations	Coefficient of variation (%)
T100,1	T100,1G	2.86	2.46	0.35	14.36
	T100,1H	2.35			
	T100,1I	2.18			
T100,2	T100,2J	3.05	3.1	0.06	2.07
	T100,2K	3.17			
	T100,2L	3.07			
T50,2	T50,1G	1.66	1.83	0.22	12.08
	T50,1H	2.08			
	T50,1I	1.75			
T50,1	T50,2G	4.37	3.8	1.25	32.9
	T50,2H	4.66			
	T50,2I	2.37			

4.3.2 Steel

In the experimental program, deformed bars with diameter 8 and 10 mm of longitudinal, diameter 8mm of transverse and in the overhang regions, diameter 14 mm of longitudinal reinforcement bars were used.

A uniaxial tension test was conducted on sample reinforcements to determine the mechanical properties. The mechanical properties of the reinforcements are given in Table 4-6.

Figure 4-7-Tensile strength testing machine

Table 4-6- Mechanical properties of reinforcements

Diameter	ϕ8 Longitudinal	ϕ8 Transverse	ϕ10 Longitudinal	ϕ14 Longitudinal
Modules of elasticity GPa	200*	200*	200*	200*
Yield strength MPa	547.2	547.2	486.4	480
Ultimate strength MPa	622.6	622.6	563.14	561.1
Ultimate strain (milli strain)	100	100	55	75

** Assumed value*

4.3.3 Carbon Fiber Strips

In the experimental program, a high strength carbon fiber was used to strengthen the specimens. The essential mechanical properties are directly obtained from the manufacturer manual and they are provided in Table 4-7.

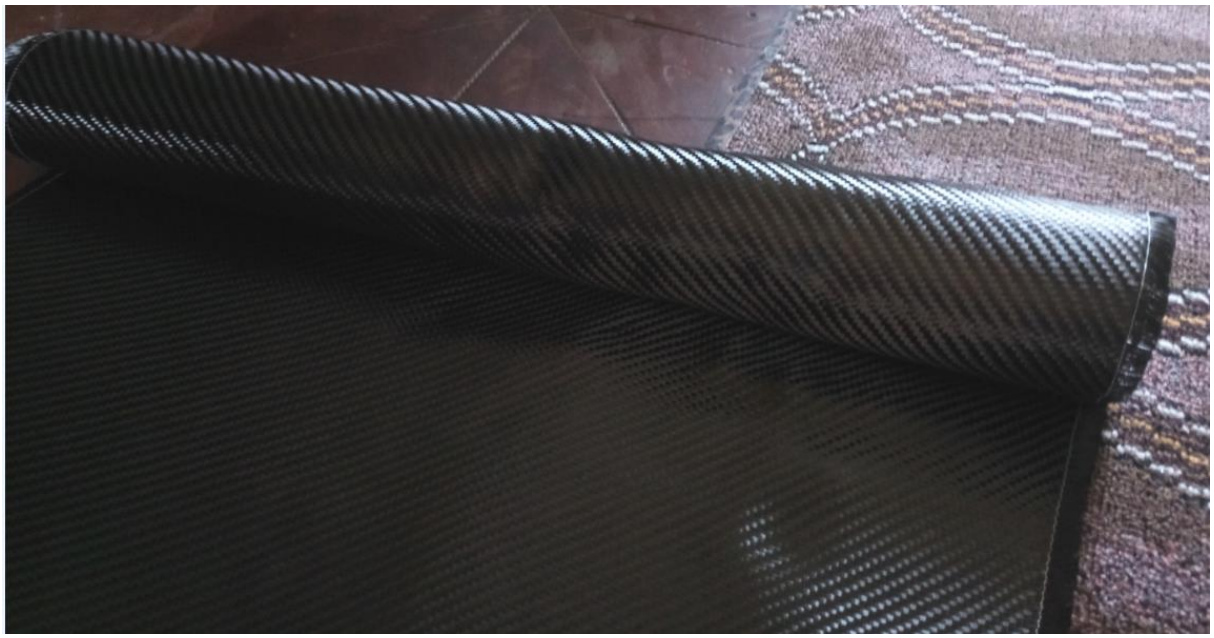

Figure 4-8-Carbon fiber strip

Table 4-7 - Properties of the Carbon Fiber

Density	1.7 kg/m3
Modulus of elasticity	240,000 MPa
Design Thickness	0.111 mm
Design Tensile Strength	4380 MPa
Ultimate Tensile Elongation	Elongation 1.9 %

4.4 Specimen Fabrication

The test specimens were cast in two stages.

- In the first stage, using a steel formwork the RC specimens without their semicircular support was cast (see Figure 4-10).
- In the second stage, the casted specimens were cured for seven days until they develop adequate strength to withstand the stress during lifting. After carefully lifting and preparing the surface, a semicircular support was cast (see Figure 4-11).

The test specimens were cast using a steel formwork constructed in the Mechanical laboratory of AAIT.

Figure 4-9 - Rebar cages (T50, 1)

Figure 4-10 - Formwork with rebar (first stage)

Figure 4-11 - Semicircular support formwork and second stage casting

During the casting of the specimens, the reinforcement cages were assembled by strictly following the design. Prior to specimen casting, the formwork was adequately restrained and then a release agent was applied to the surfaces. The reinforcement cages were then placed inside the formwork after maintaining a concrete cover of 25mm.

The specimens were cast outside the laboratory and a 28mm diameter electric vibrator was used to consolidate the mix. The casted concrete was cured by covering with wet cotton. The cotton was constantly saturated and covered by plastic sheets to avoid water loss due to evaporation.

4.5 Specimen Preparation

The surfaces of the control specimens, T50, 1 and T100, 1, was coated with a white paint to aid the visibility of the cracking process during testing. The remaining specimens, T50, 2 and T100, 2, are used to study the effect of carbon fiber on torsional capacity RC beams; as a result, they needed a comprehensive plan on the course of bonding of the fiber strips to the concrete substrate.

Specimen preparation process for the application of carbon fibers was initiated by preparing the concrete surface. To avoid the premature failure of fibers due to sharp edges and to enhance the bond strength, the edges were rounded and the specimen surface was roughened by using a hand operated grinder (see Figure 4-12).

Figure 4-12- Specimen surface preparation

Once the surface has been properly roughened, all the dust particles were cleaned from the specimens using a wet towel. Following the surface preparation, to enhance the bond between the substrate and the fiber matrix, as it recommended by the manufacturer, a surface primer was coated (see Figure 4-13). A wet lay-up system using epoxy was used to impregnate the fibers and form a composite matrix. The mixing of the epoxy components was conducted according to the manufacturer specification.

Figure 4-13-Primer on the substrate

Prior to the application of the fiber to the concrete beams, the carbon fibers strips were cut to the required dimensions by strictly following the experimental plan. The application of the fiber to the surface was done initially by coating the epoxy resin to the previously prepared surface and then, the prepared carbon fiber strips were applied to the coated surface. The subsequent layer

was bonded by coating the epoxy resin on the preceding fiber surface. A hand roller was used during the application of the fibers to squeeze out any excess epoxy and to remove air bubbles.

Figure 4-14- Specimen after the application of externally bonded carbon fibers

4.6 Instrumentation

The instrumentation was mainly designed to capture the Torsion – Angle of twist behavior of the test specimens. Displacement measurement transducers were systematically used to capture the angle of twist. The angle of twist due to the combined loading was measured at the two ends of the test specimens as shown in Figure 4-15. Furthermore, Strain gauges were assembled to measure the axial straining of selected transverse reinforcements.

Figure 4-15-Angle of twist measurement using displacement transducer

A concentrated load was applied to the spreader beam using a hydraulic jack and continues monitoring of the applied load was done through the use of a load cell (see Figure 4-18). The load cell, the displacement transducers, and the strain gauges were connected to a data logger. The experimental data were recorded in excel format by the data logger and accessed through USB flash disk.

Figure 4-16-Datalogger

Figure 4-17-Load Cell

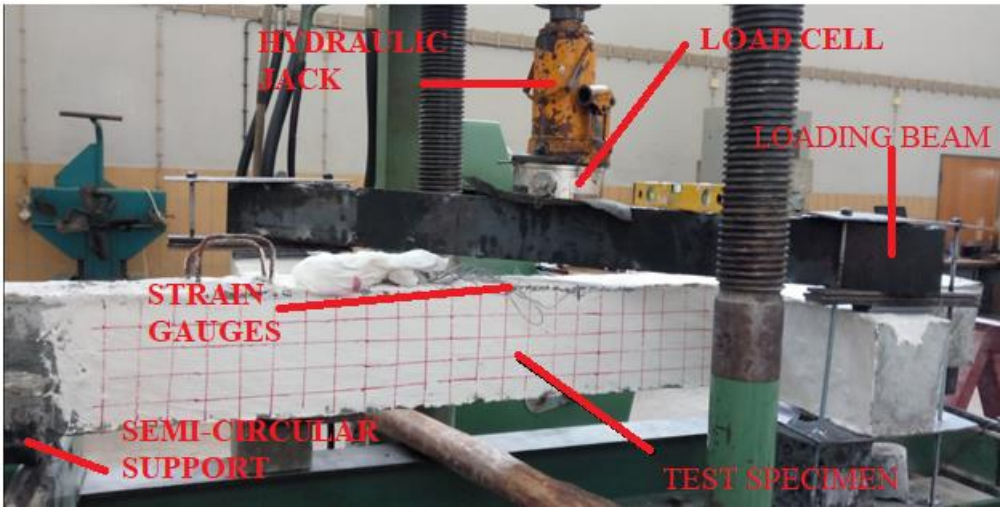

Figure 4-18- Test set up

5 NONLINEAR FINITE ELEMENTS ANALYSIS

5.1 Introduction

In this chapter, a nonlinear finite element modeling of RC beams subjected to combined torsion and flexure will be described. The nonlinear finite element analysis tools DuCOM-COM3 and VECTOR 3 will be used.

In the modeling of RC element for shear as well as torsion, two research directions have been taken in smeared modeling by researchers. In the assessment of direction, gradual formation, rotation of cracks, two types of theories have been developed, namely, the rotating and the fixed angle theories.

The Modified compression field theory is a rotating angle truss model developed at University of Toronto by Vecchio and Collins (1986). In the following years, Vecchio and his colleagues at the University of Toronto incorporated the theory into a nonlinear finite analysis tool for reinforced concrete elements. The original version was called TRIX and later by incorporating different tools specialized for different modeling problem called VecTor suits.

The principal works in fixed angle theories include the works of Hsu and his colleagues at the University of Houston and the two and four-way fixed angle model of Maekawa and his coworkers. DuCOM-COM3 is a computer program developed at the University of Tokyo by incorporating the four-way fixed angle model.

VecTor suits and DuCOM-COM3 have been used to model and predict the behaviors of RC members and for most cases with very good results. In this chapter, a nonlinear finite element simulation will be conducted using both tools to investigate their capability of modeling and predicting the behavior of carbon fiber wrapped RC members subjected to combined torsion and flexural loading.

5.2 NLFEA using VecTor Suits

VecTor suits are computer programs for a nonlinear finite element analysis of reinforced concrete. The VecTor suits include VecTor2, VecTor3, VecTor4, VecTor5, and VecTor6. These programs have been developed at the University of Toronto and each program is dedicated for different modeling problems including 2D structures (VecTor2), 3D structures (VecTor3), shell structure (VecTor4), plane frame (VecTor5) and axis symmetric solid (VecTor6). These programs allow more accurate assessments of structural strength, post-peak behavior, failure mode, deflections and cracking.

The theoretical bases of VecTor suits are the Modified Compression Field Theory (Vecchio and Collins, 1986) and the Disturbed Stress Field Model (Vecchio, 2000). The vector suits use a preprocessor Formworks-Plus and postprocessor Janus and Augustus. Formworks-Plus is a universal pre-processor for the entire VecTor software suite, including VecTor2, VecTor3, VecTor4, VecTor5, and VecTor6. A post-processor Janus is used for extracting and graphically displaying the results of the structural analysis.

The input of VecTor3 is in the form of ASCII text files. There are five main input files that are required for any analysis job.

1. 'VECTOR.JOB' is used for defining the analysis job parameters.
2. 'VT3.AUX', is used for defining additional parameters that are specific to special types of structures.
3. 'VT3T.AUX', is used for defining the main parameters, properties, and structural mechanics models that control heat transfer analysis.
4. 'S3R' is the structural input file and it is used for defining the geometry and materials of the structure to be analyzed.
5. 'L3R' is the load file and it is used for defining the load of the structural model.

5.2.1 Specimens

VecTor 3 is used to conduct a three-dimensional static nonlinear analysis. The specimens that are used in the simulation are identical with the specimens used in the experimental program. The specimen's designation with their properties is provided in Table 5-1.

Table 5-1- Specimen designation and their properties

Group	Specimen designation	Longitudinal reinforcement	Transverse reinforcement	Wrapping scheme	Number of layers
1	VT100,1	$2\phi 8$ top $2\phi 10$ bottom	$\phi 8c/c100mm$	_	_
	VT100,2	$2\phi 8$ top $2\phi 10$ bottom	$\phi 8c/c100mm$	FULL	2
2	VT50,1	$2\phi 8$ top $2\phi 10$ bottom	$\phi 8c/c50mm$	_	_
	VT50,2	$2\phi 8$ top $2\phi 10$ bottom	$\phi 8c/c50mm$	FULL	2

T=Torsion with flexure $100/50 = spacing\ of\ transverse\ rebars$ $1/2 = Test\ beam$

V = VecTor Simulation

5.2.2 Materials

The compressive and tensile strength of the concrete for each specimen were directly taken from the experimental program. The mechanical behavior of longitudinal and transverse reinforcements was also taken from the tests conducted in the material testing laboratory of AAiT. The mechanical property of the carbon fiber strips was directly taken from the manufacturer manual. The modulus of elasticity and other properties were left as the default values in the VecTor 3 program; the program calculates appropriate values using the following formulas.

- Initial Tangent Modulus, Ec $Ec = 5500\sqrt{f\,c}$ MPa
- Cylinder Strain at peak strength, e_o $\varepsilon o = 1.8 + 0.0075\,f'c$ millistrain
- Poisson's Ratio 0.15
- Thermal Expansion Coefficient, Cc 10x10-6 /°C
- Density 2400 kg/m3

The mechanical properties used in the nonlinear finite element modeling for the concrete, steel and carbon fiber strips are presented in Table 5-2, Table 5-3, and Table 5-4.

Table 5-2-Mechanical properties of concrete used in the VecTor 3 model

Beam sample	Cubic compressive strength (MPa)	Tensile strength (MPa)
VT100,1	43.32	2.46
VT100,2	53.35	3.10
VT50,2	47.38	1.83
VT50,1	45.88	4.52

T=Torsion with flexure $100/50 = spacing\ of\ transverse\ rebars$ $1/2 = Test\ beam$

V = VecTor Simulation

Table 5-3- Mechanical properties of the steel bars

Diameter	ϕ8 Longitudinal	ϕ8 Transverse	ϕ10 Longitudinal	ϕ14 Longitudinal
Modules of elasticity GPa	200*	200*	200*	200*
Yield strength MPa	547.2	547.2	486.4	480
Ultimate strength MPa	622.6	622.6	563.14	561.1
Ultimate strain (milli strain)	100	100	55	75

**assumed value*

Table 5-4-Mechanical properties of fibers

Density	1.7 kg/m3
Modulus	240,000 MPa
Design Thickness	0.111 mm
Design Tensile Strength	4380 MPa
Ultimate Tensile Elongation	Elongation 1.9 %

5.2.3 Modeling

The stiffness matrix in VecTor suits is constructed from the determined values of the stress and the strain from the selected models. This necessitates an appropriate selection of constitutive models, particularly for the concrete.

The nonlinear uniaxial stress-strain response of concrete in compression is modeled using two segments, namely, the compression pre-peak and the compression post peak segment.

Models suitable for normal strength concrete were carefully chosen. Thus, the pre-peak and post-peak segments were modeled using the Hognestad parabola and the modified Park-Kent model respectively.

The tension stiffening response of concrete is modeled using the modified Bentz (2003) model. Furthermore, the tension softening behavior is assumed to have a descending linear softening.

The compression softening due to transverse cracking was modeled using Vecchio 1992-A model. In the model, both the peak strength and peak strains are softened due to the transverse cracking. The confined concrete strength, dilation, and cracking criterion are modeled using Kupfer /Richart model**,** Variable-Kupfer model, and Mohr-Coulomb criterion respectively.

In VecTor suits, it is possible to model reinforcements in discrete as well as smeared manner. Both approaches were used for modeling of longitudinal and transverse rebar. Moreover, the carbon fiber strips were modeled as a discrete externally provided tension only rebar. The area of fibers in the tributary area was used as the area of the tension-only reinforcement.

Even though the debonding phenomenon of the fiber strips on concrete substrate necessitates appropriate modeling of bond-slip relationship, a perfect bond between the fiber and the underlining concrete was assumed. The reason for using this approach is due to the incapability of modeling bond-slip in three-dimensional models. Although the freely available version is not capable of modeling bond-slip in 3D, it is possible to model the behavior of slipping for two-dimensional problems.

5.2.4 Loading and Support Condition

The beam specimens are subjected to combined torsion and flexure. To allow end rotation of the beams and to mimic the semicircular supports of the experimental test specimens, steel elastic bearings was used at the mid-point of the support axis. Furthermore, the translation movement in the three principal directions of the steel bearings was restrained. To avoid restraining of axial elongation, only the vertical and transverse directions were restrained at the other end.

The experimental programs were planned to have a loading scenario controlled by displacement. As a result, to capture the post-peak behavior and to properly compare the results, a displacement controlled loading of 0.5 mm per load step is applied in the finite element simulation. The displacement control loading was applied at nodes situated at loading wings positioned 400mm away from the centerline of the main beam.

By incorporating the above materials, models, and support mechanism, the finite element models of the specimens were created using the graphical preprocessor Formworks. The three dimensional, longitudinal and sectional views of the specimens are shown in Figure 5-1 and Figure 5-2.

VT50,1 and VT100,1

Three-dimensional view	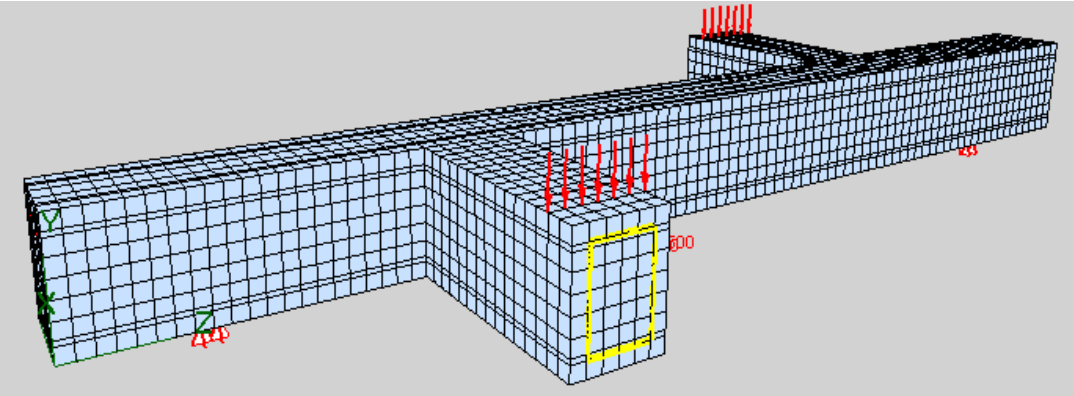
Longitudinal sections+ *(VT50,1)* *(VT100,1)*	*(a)* 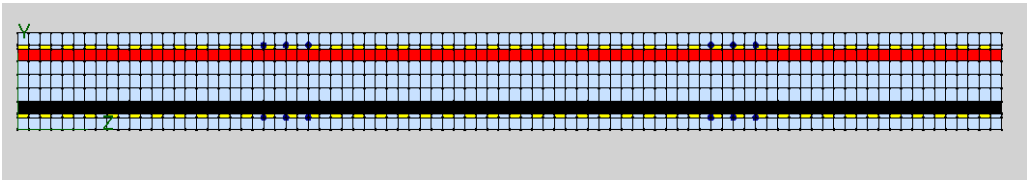 *(b)* 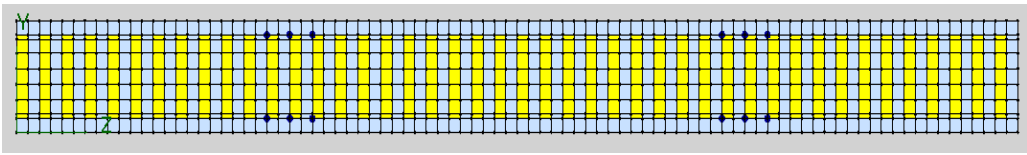 *(c)* 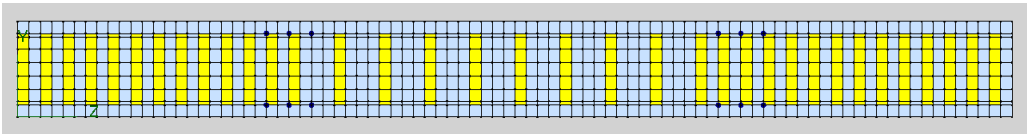
*Sectional view**	*(a)* 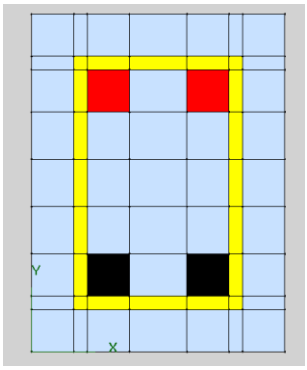 *(b)* 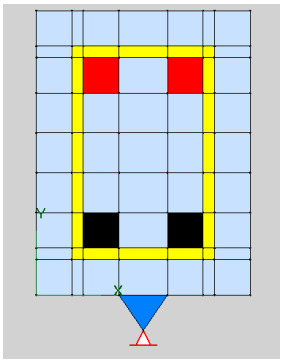

Figure 5-1- Sectional view for specimen VT50, 1 and VT100, 1

RED= diameter 8 reinforcement (Smeared) *BLACK= diameter 10 reinforcement (Smeared)*

YELLOW= diameter 8 transverse reinforcement (Smeared on the main beam and discrete on the overhung)

\+ *(a) At the center (b) &(c) near cover* * *(a) at mid span (b) at support*

VT50,2 and VT100,2

Three-dimensional view	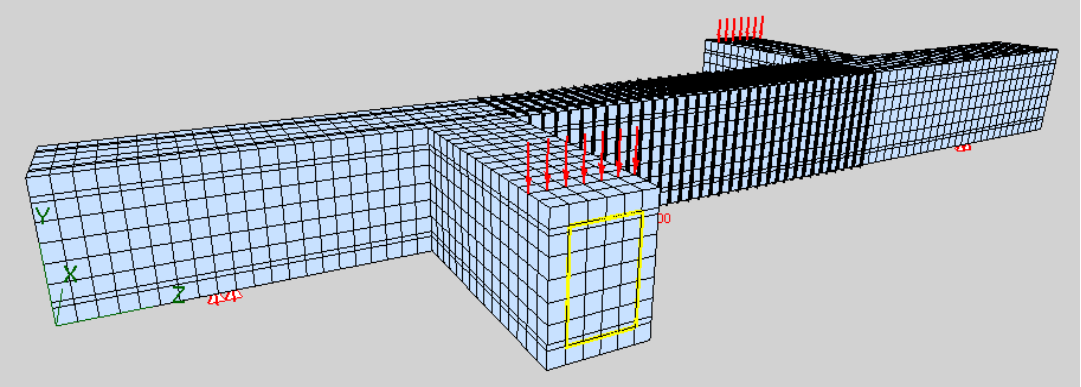
Longitudinal sections+ *(VT50,2)* *(VT100,2)*	*(a)* 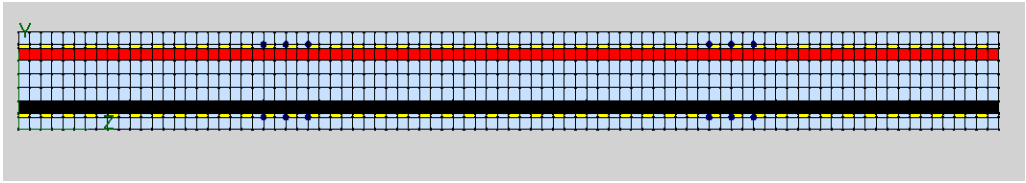 *(b)* 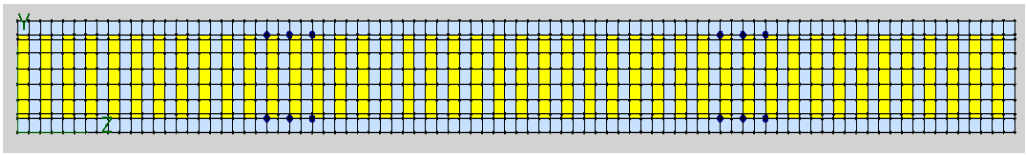 *(c)* 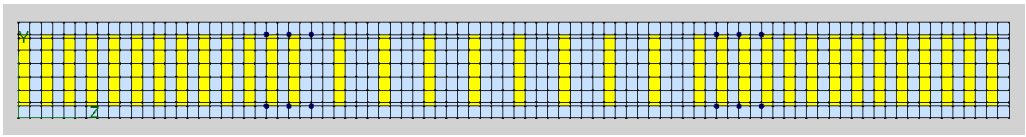
Sectional view*	*(a)* 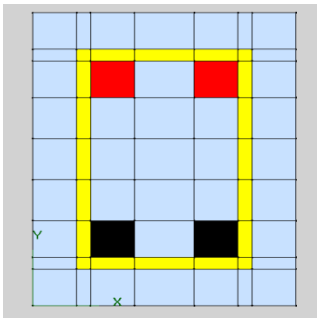 *(b)* 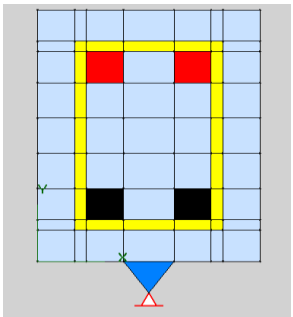

Figure 5-2-Sectional view for specimen VT50, 2 and VT100, 2

RED= diameter 8 reinforcement (Smeared) *BLACK= diameter 10 reinforcement (Smeared)*

YELLOW= diameter 8 transverse reinforcement (Smeared on the main beam and discrete on the overhung)

+ *(a) At the center (b) &(c) near cover* * *(a) at mid-span (b) at support*

5.3 NLFEA using DUCOM-COM3

DuCOM-COM3 is a computer program which developed at the University of Tokyo. The program is a multi-scale analysis code that links the thermo-chemo-physics platforms DuCOM and COM3. DuCOM is an integrated thermo-hygro analysis code that includes cement hydration in the concrete mixture, micro-pore structure formation, and mass transport models for concrete ranging from 10-3 to 10-9 meter scales of micro-voids, while COM3 is a 3D finite-element analysis platform for structural concrete with and without cracks. For modeling of cracks in RC structures, COM3 uses the four-way fixed angle model.

DuCOM-COM3 is equipped with a graphical pre and post processor. The pre-processor is used for defining the analysis job parameters, geometry, load and material whereas the post-processor is used for extracting and graphically displaying the results of the structural analysis.

5.3.1 Specimens

The specimens that are used in the DuCOM-COM3 are similar to the specimens used in the VecTor 3 simulation and the experimental program. The specimen's designation with their properties is provided in Table 5-5.

Table 5-5- Specimen designation and their properties

Group	Specimen designation	Longitudinal reinforcement	Transverse reinforcement	Wrapping scheme	Number of layers
1	DT100,1	$2\phi 8$ top $2\phi 10$ bottom	$\phi 8c/c100mm$	_	_
	DT100,2	$2\phi 8$ top $2\phi 10$ bottom	$\phi 8c/c100mm$	FULL	2
2	DT50,1	$2\phi 8$ top $2\phi 10$ bottom	$\phi 8c/c50mm$	_	_
	DT50,2	$2\phi 8$ top $2\phi 10$ bottom	$\phi 8c/c50mm$	FULL	2

$T = Torsion\ with\ flexure \quad 100/50 = spacing\ of\ transverse\ rebars \quad 1/2 = Test\ beam$

$D = DUCOM - COM3\ Simulation$

5.3.2 Materials

The appropriate mechanical properties of the concrete for each specimen were directly taken from the experimental program. Similar to the VecTor3 modeling, the mechanical behavior of longitudinal and transverse reinforcements was taken from the experimental tests. The material properties of the carbon fiber strip were directly taken from the manufacturer manual. The mechanical properties used in the DuCOM-COM3 are identical to their respective materials in the VecTor 3 model and they are previously presented in Table 5-2, Table 5-3, and Table 5-4.

5.3.3 Modeling

During modeling, only material nonlinearity was considered and from the default parameters, only the parameter of time-dependent constitutive models was changed. The concrete compression softening was accounted using the default model of the tool and time-dependent constitutive models for concrete in compression, tension and shear were used. The pre and post-peak response of the concrete in compression are modeled using Elastoplastic and Fracture (EPF) model (Maekawa, 2003). The tension stiffening behavior of concrete in tension was modeled using the coefficient 0.4 whereas the tension softening was modeled using coefficients by considering element size and the fracture energy of plain concrete in tension. The concrete shear stress transfer was modeled using the contact density model (Li et.al, 1987). In the DuCOM-COM3 modeling, the reinforcements are modeled in a smeared manner. Moreover, the carbon fiber strip was modeled as externally provided plate element.

5.3.4 Loading and Support Condition

Similar to the VecTor 3 model, to allow end rotation of the beams and to model the semicircular supports of the experimental test specimens, steel elastic bearings were used at the mid-point of the support axis. In addition, the translation movement in the three principal directions of the steel bearings was restrained at one end.To avoid restraining of axial elongation, only the vertical and transverse directions were restrained at the other end. To capture the post-peak behavior and to properly compare the results, a displacement controlled loading of 0.1 mm per load step is applied in the finite element simulation. By incorporating the above materials, models, and support mechanism, the finite element models of the specimens were created. The three dimensional, longitudinal and sectional views of the specimens are shown in Figure 5-3 and Figure 5-4.

	DT50,1 and DT100,1
Three-dimensional view	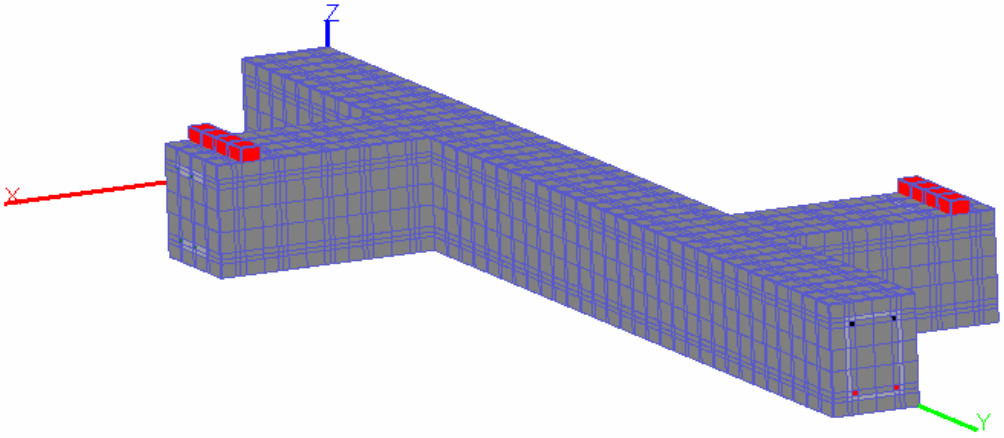
Longitudinal sections+ *(DT50,1) (DT100,1)*	*a)*  *b)* 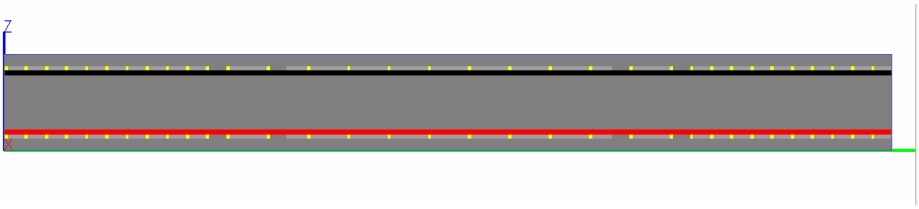
*Sectional view**	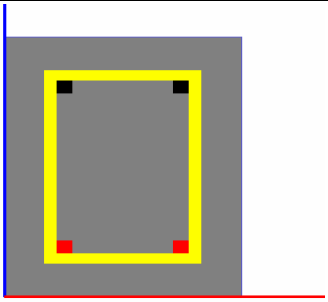

Figure 5-3- Sectional views for specimen DT50, 1 and DT100, 1

RED= diameter 10 reinforcement (Smeared) *BLACK= diameter 8 reinforcement (Smeared)*

YELLOW= diameter 8 transverse reinforcement (Smeared on the main beam and discrete on the overhung)

\+ *a) and b) Sections at the center* * *Section at mid-span*

DT50,2 and DT100,2	
Three-dimensional view	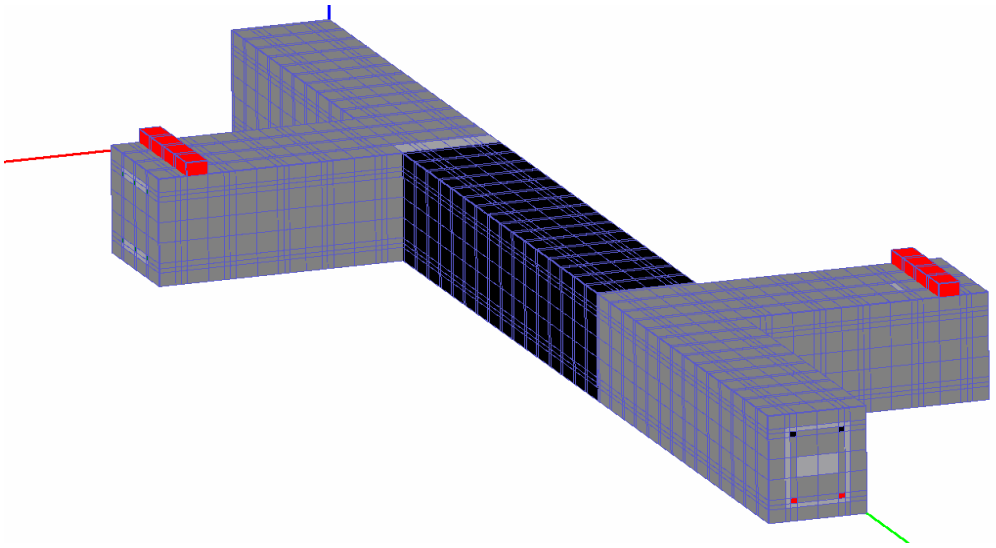
Longitudinal sections[+] *(DT50,2) (DT100,2)*	*a)* 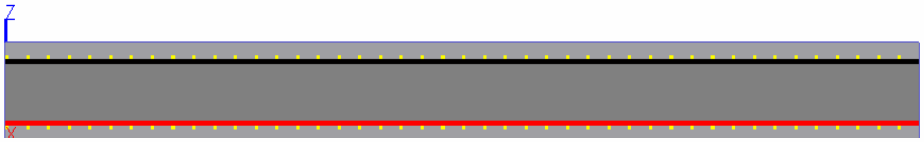 *b)* 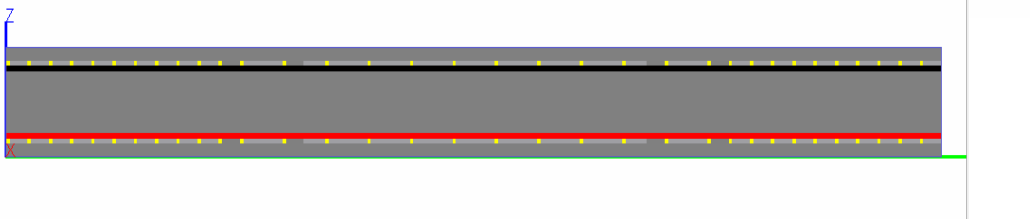
Sectional view[*]	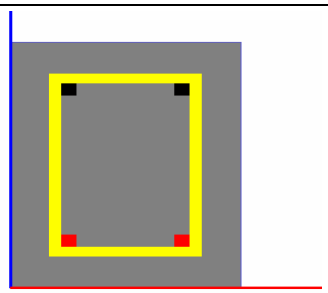

Figure 5-4-Sectional views for specimen DT50, 2 and DT100, 2

RED= diameter 10 reinforcement (Smeared) *BLACK= diameter 8 reinforcement (Smeared)*

YELLOW= diameter 8 transverse reinforcement (Smeared on the main beam and discrete on the overhung)

[+] *a) and b) Sections at the center* [*] *Section at mid-span*

6 RESULT AND DISCUSSION

6.1 Result of the Experiment

6.1.1 Specimen T50, 1

The experimental result for specimen T50, 1 is presented in Figure 6-1. A linear relationship between the torsional moment and the angle of twist is observed up to the cracking torque, and then the steep pre-crack torsional stiffness was softened after reaching the cracking torque around 3 KNm.

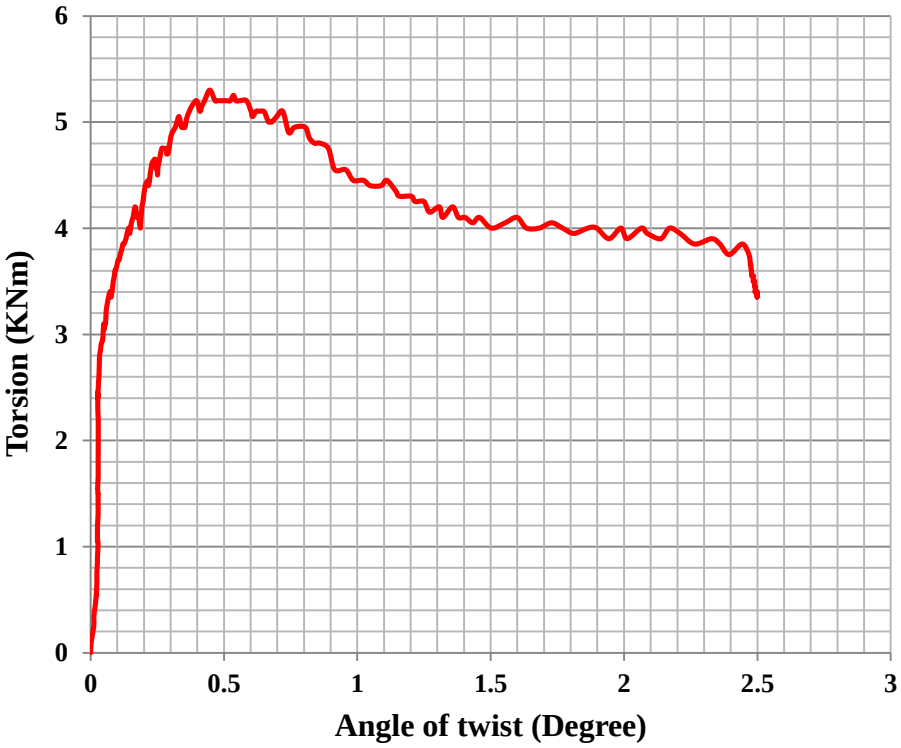

Figure 6-1- Torsion - Angle of twist for specimen T50, 2

When conducting the test, beginning at the cracking torque, a heavy sound was continuously heard. Post-experiment investigation of the specimen revealed that the sound was caused by the spalling of the concrete cover (see Figure 6-2). Additionally, further analysis of the experiment revealed that the peak strength of the specimen was controlled by the spalling of the concrete cover.

The peak torsional moment reached by the specimen was 5.2 KNm. At the ultimate strength of the specimen, the strain gauges attached to the transverse reinforcements showed the axial strain was well below the yield strain.

(a)

(b)

Figure 6-2- Spalled concrete cover (a) Top view (b) front view

The observed post-peak response of the specimen was ductile. This behavior may be attributed to the closely provided transverse reinforcement. A thorough observation of the end rotation of the

beams indicates a localized damage after the peak strength (see Figure 6-3); this phenomenon is also observed from the visual inspection of the final state of the specimen.

Prior to the peak strength, both ends of the beams were twisting with a similar rate. However, after reaching the peak strength, localized damage to the left part of specimens was responsible for the contribution of the majority of the total angle of twist. The final state of the test specimen exhibiting a substantial localized damage is shown in Figure 6-4.

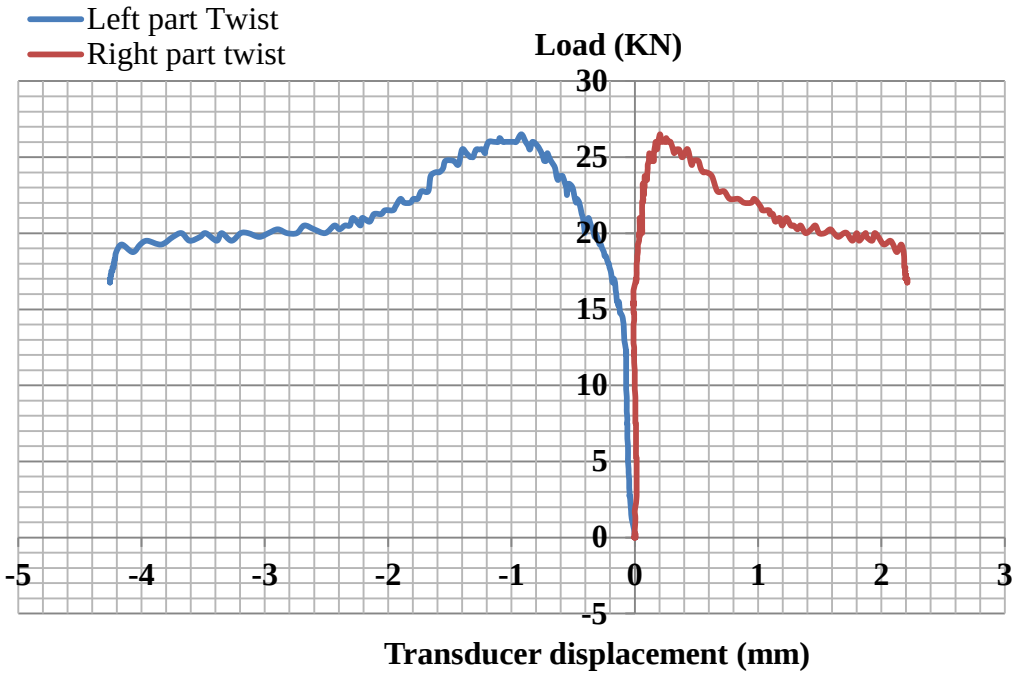

Figure 6-3- End member twist expressed in transducer displacement for T50, 1

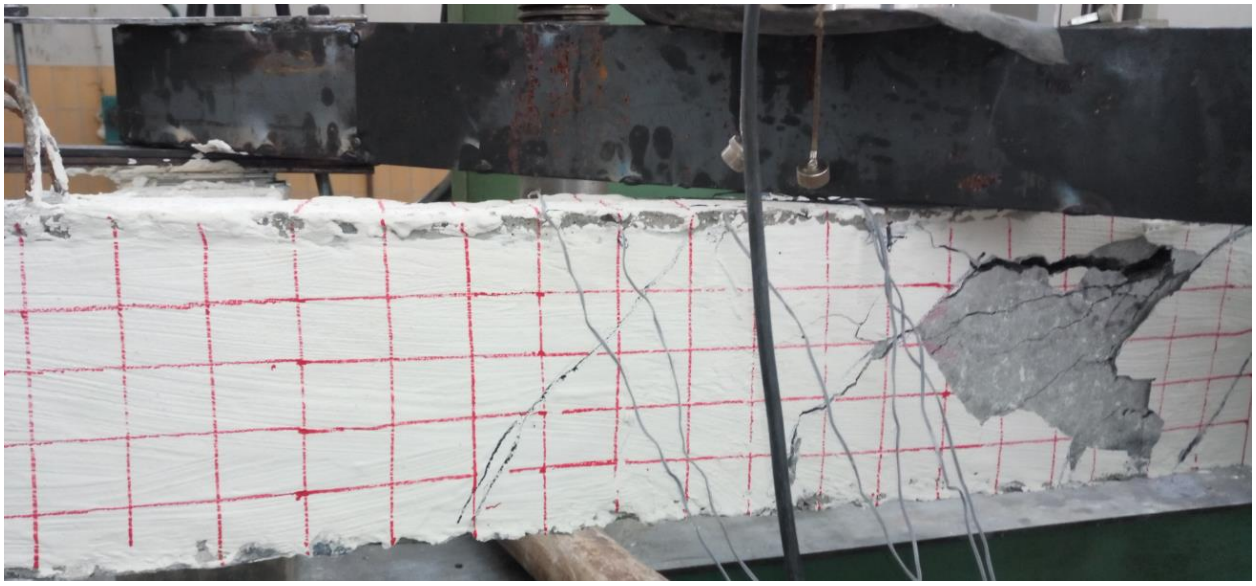

(a)

(b)

Figure 6-4- Final state of specimen T50, 1 (a) Front side (b) back side

6.1.2 Specimen T100, 1

The RC beam specimen T100, 1 was reinforced with transverse reinforcements set apart at 100 mm center to center. The general behavior of the specimen has three distinct components. The pre-peak response of the beam is observed to be dominated by two behaviors, a steep initial linear stiffness before cracking and a softened linear post cracking stiffness. The post-peak behavior of the specimen can be characterized by a steady loss of load carrying capacity (see Figure 6-5).

Figure 6-5- Torsion - Angle of twist for specimen T100, 1

Before cracking, the response of the specimen is similar to the behavior of specimen T50, 1. The cracking of the specimen was manifested with a loss of stiffness around 3KNm of the torsional moment. Similar to specimen T50, 1, a heavy sound was continuously heard from the onset of cracking. This sound is attributed to the concrete cover spalling phenomenon.

When the torsional moment reached 5.02 KNm, a sudden loss in carrying capacity of the specimen was observed, resulting in the maximum torsional carrying capacity of 5.02 KNm. Moreover, the ultimate capacity of the specimen was governed by the cover spalling phenomenon.

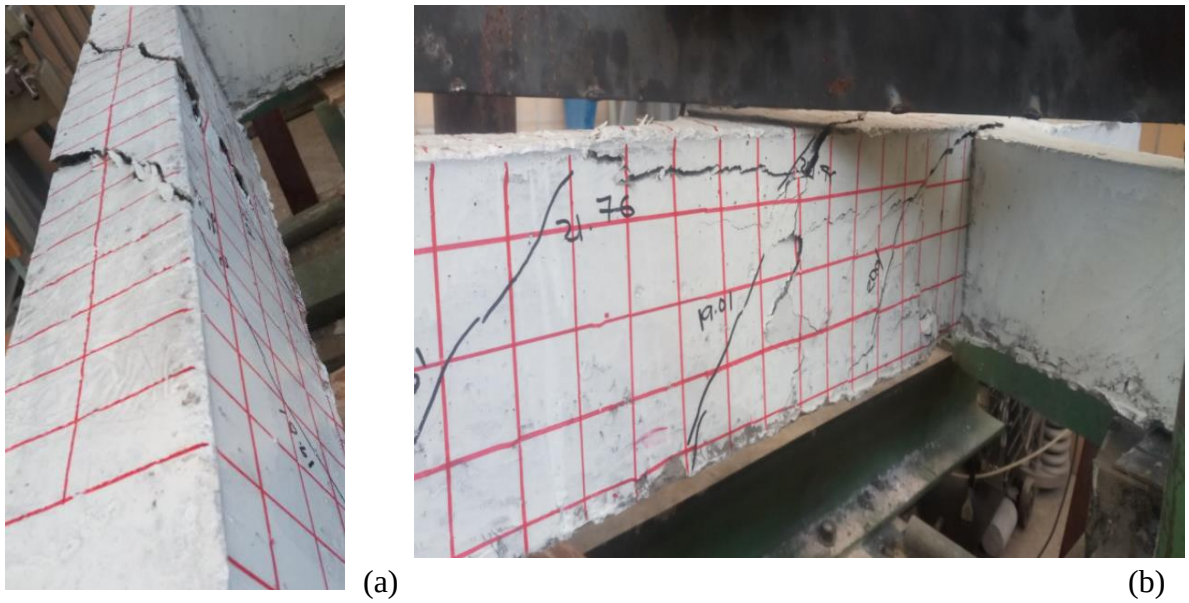

(a) (b)

Figure 6-6- Torsional Cracks (a) Top View (b) side view

The post-peak behavior of the specimen was essentially brittle. Comparing the post-peak behavior with that of T50, 1, one may observe that the spacing of transverse rebar has a great influence on the post-peak behavior of members subjected to torsion.

Post-experimental inquiry revealed that, due to the relatively wider spaced transverse reinforcements, the spiral cracks were penetrating deeply to the core of the member with a seemingly wider crack width (see Figure 6-7). These wide cracks might possibly be the cause of the brittle post-peak response.

Figure 6-7- Penetrating spiral cracks

Moreover, another key interest of investigation was the twist contribution of the segments along the length of the specimen. Starting from the beginning of loading to the peak strength, both ends of the beams were apparently twisting with a similar rate. During this phase of loading, a uniform distribution of the angle of twist per length can be assumed to take place throughout the length of the specimen. However, after reaching the peak strength, a localized damage to the right part of specimens was responsible for the contribution of the majority of the total angle of twist. This localization response can be observed from the load versus transducer displacement of end twist of the specimen shown in Figure 6-8.

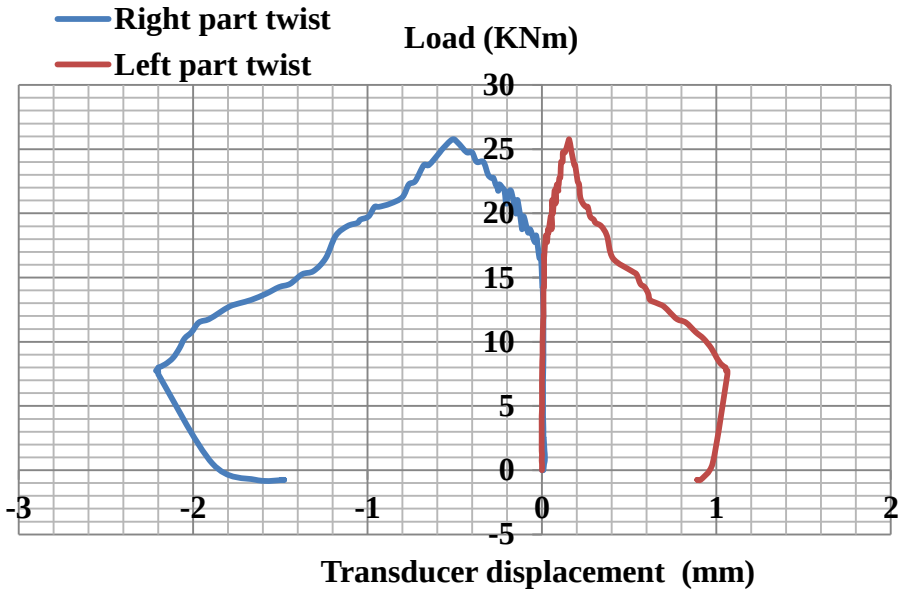

Figure 6-8- End member twist expressed in transducer displacement for T100, 1

6.1.3 Specimen T50, 2

The specimen T50, 2 was strengthened with two layers of externally bonded carbon fiber strips. The strengthened specimen was subjected to a similar monotonic loading as its companion control specimen, T50, 1. The response of the specimen is composed of three distinct behaviors in the ranges of pre-crack, between crack and peak strength, and post-peak region (see Figure 6-9).

Figure 6-9 Torsion - Angle of twist for specimen T50, 2 with two layers of carbon fiber

The pre-crack behavior of the specimen can be characterized by very high torsional stiffness. The provision of the carbon fiber strips increased the apparent cracking strength that was manifested around a torsional moment of 4.5 KNm. The cracking strength of the specimen was 50% greater than the control beams strength.

Starting around the cracking load, a continuous popping sound was heard. The sound was later attributed to the slipping between the fiber and the underlying concrete substrate. The region between the post-crack and the peak strength is observed to have a gradually changing torsional

stiffness. Unlike the control beam T50, 1, the torsional stiffness of the specimen in the region was constantly softening until it reached the peak strength.

A sudden loss in carrying capacity was observed after reaching a torsional moment of 8.2 KNm. The peak torsional strength reached by the specimen was 60% greater than the control beam. This additional strength is mainly attributed to the externally bonded carbon fiber strip.

Following the rupture of the carbon fiber strip near the right end of the critical region (see Figure 6-10), a sudden loss in load resistance occurred. This abrupt drop in strength supports the fact that most of the energy is stored elastically in the carbon fibers and the nature of the failure resembles that of brittle failure. Although part of the fibers near the right end was ruptured, the majority of the fiber strips and the concrete section remains effective and resulted in a constant post-peak response.

Figure 6-10- Carbon fiber rupture for specimen T50, 2

A post-experimental investigation shows that due to the provision of the externally bonded carbon fiber strips, the crack width of the spiral cracks was visibly narrower than that of the control beam. Additionally, the spiral cracks were distributed uniformly and the cracks were closely spaced, in which, it is believed to have enhanced the post-peak response (see Figure 6-11).

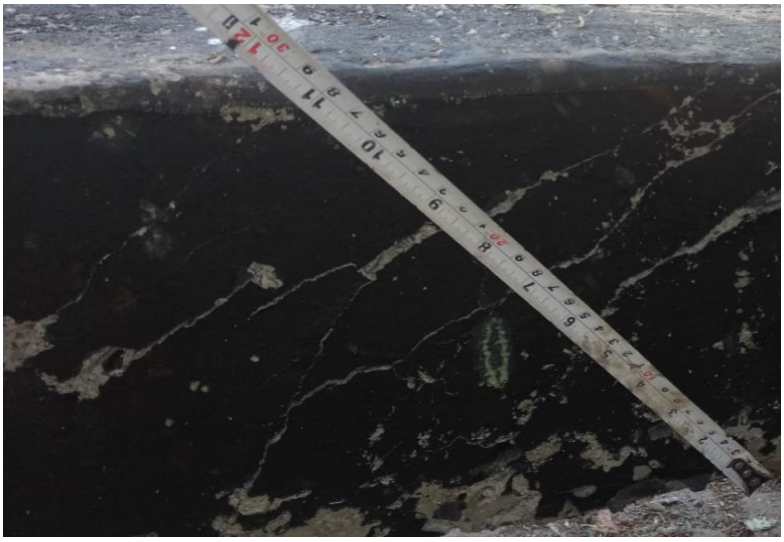

Figure 6-11- Spiral cracks for specimen T50, 2

A similar trend in member twisting was observed with that of the control beam. Similar to T50, 1, before the peak strength, a uniform angle of twist per length existed throughout the critical section. After reaching the peak strength, a localized damage resulted in larger twist demand of the right section of the specimen (see Figure 6-12).

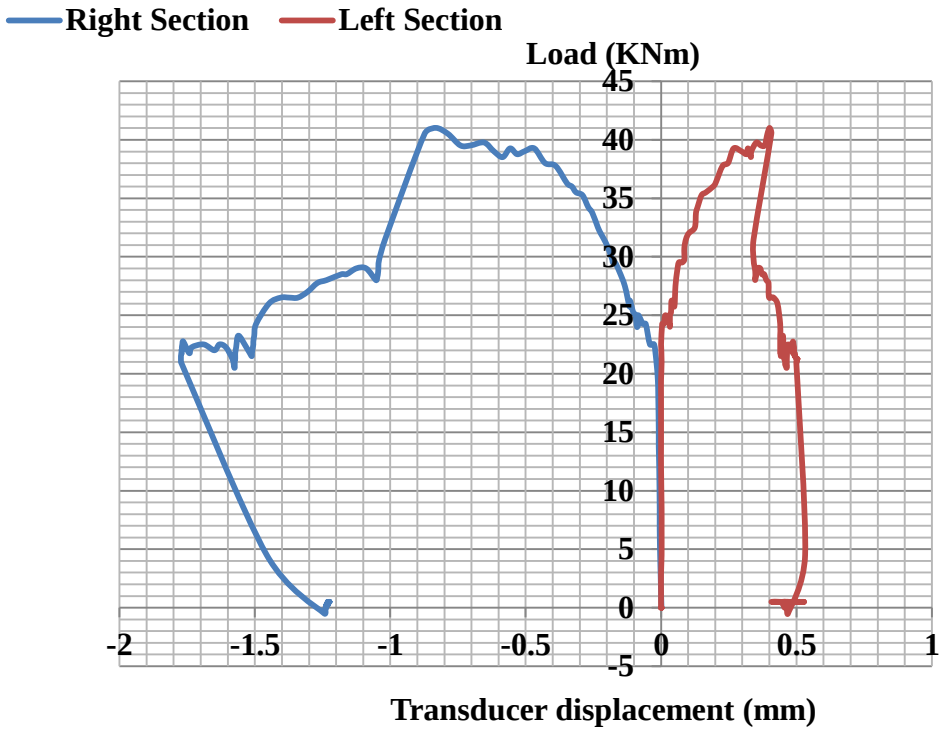

Figure 6-12- End member twist expressed in transducer displacement for T50, 2

6.1.4 Specimen T100, 2

The test specimen T100, 2 was provided with transverse reinforcement spaced 100 mm center to center. The sample was strengthened by two layers of carbon fiber layers. The Torsion Vs. the angle of twist behavior of the specimen is shown in Figure 6-13. Similar to the control beam T100, 1, the pre-crack response showed a very high torsional stiffness. The apparent cracking strength was manifested around a torsional moment of 5.6 KNm, which was 60% greater than the control beams cracking strength. The substantial increase in cracking strength partly attributed to the carbon fiber and partly to the relatively high tensile strength of the concrete used for the specimen.

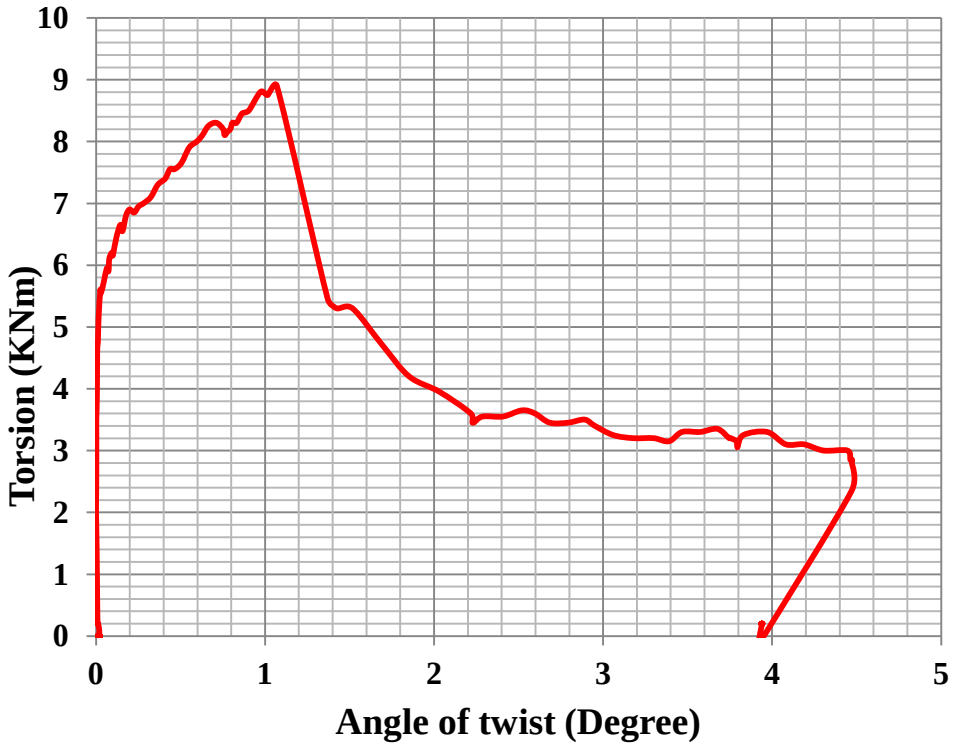

Figure 6-13 Torsion - Angle of twist for specimen T100, 2 with two layers of carbon fiber

Unlike specimen T50, 2, the post-peak behavior of the specimen is characterized by a single post cracking torsional stiffness. A popping sound was continually heard commencing near the cracking torque. Later examinations indicated that the debonding of the fibers was responsible for the popping sound that was heard during the test.

When the torsional moment reaches 8.9 KNm, a sudden dip in load carrying capacity was observed. The sudden drop results in a peak torsional strength of the specimen. This sudden drop in strength was due to the rupture of the carbon fibers at one end of the critical section (see Figure 6-14).The observed brittle failure was more pronounced than that of T50, 2. The reason for this higher brittle tendency might be the relatively wider spaced transverse reinforcement.

Figure 6-14- Rupture of the carbon fibers of specimen T100, 2

Although the dipping after the peak load was relatively higher, the post-peak behavior changed from brittle to ductile behavior. The torsional moment in the post-peak range even out to a torsional strength of 3.4 KNm. The observed post-peak behavior might be a result of combined action of the intact concrete section and the remaining integral carbon fiber strips.

Similar to the other tested specimens, a uniform angle of twist per length existed before localization commenced near the peak load. The total angle of twist after the peak strength was majorly contributed by the more damaged part of the specimen (see Figure 6-15).

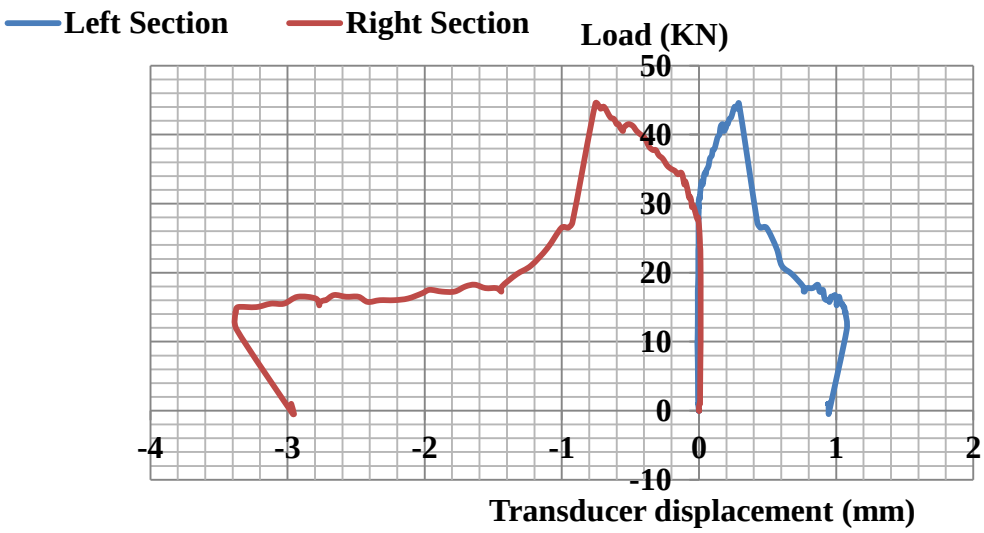

Figure 6-15- End member twist expressed in transducer displacement for T100, 2

Generally speaking, the provision of externally bonded carbon fiber strips enhances the cracking and the ultimate strength of the specimens. Referring to Figure 6-16, one may observe the effect of the carbon fibers in enhancing the energy absorption of the specimens.

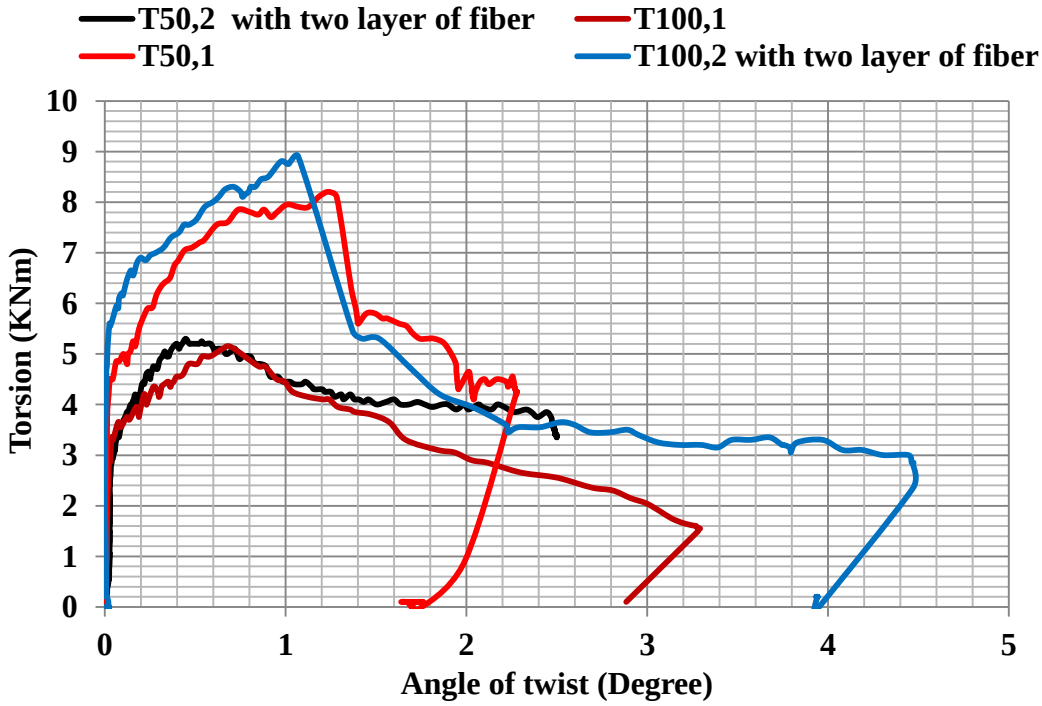

Figure 6-16 Comparisons of the experimental results

6.2 Result from NLFEA

6.2.1 Result from VecTor 3

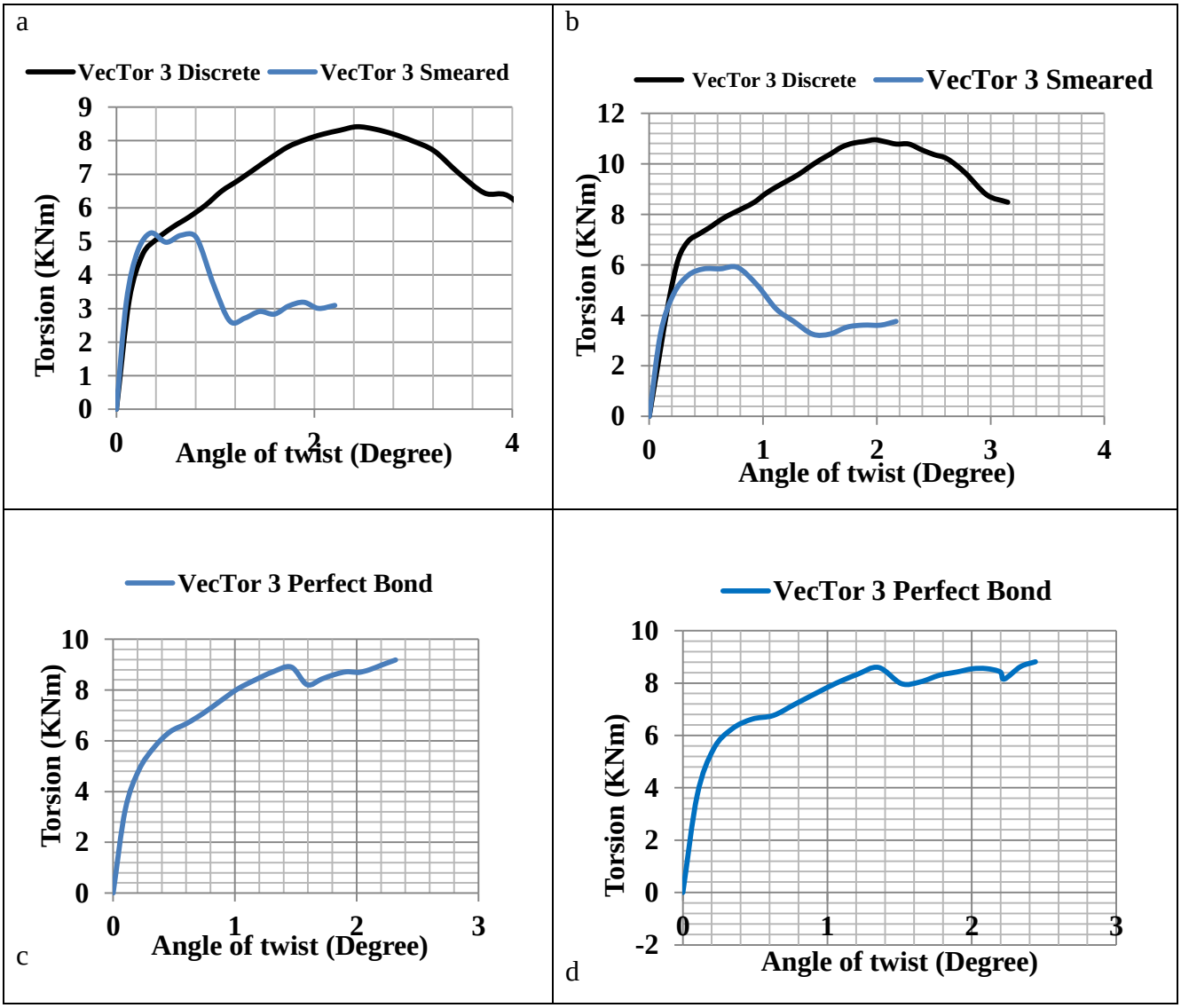

Figure 6-17-VecTor 3 Simulation results (a) VT100, 1 (b) VT50, 1 (c) VT50, 2 (d) VT100, 2

The results of the nonlinear finite element simulation conducted using VecTor 3 is presented in Figure 6-17. Modeling of the specimens was conducted using both smeared as well as discrete reinforcement approaches. For fiber wrapped elements VT50, 2 and VT100, 2, due to their similar response, only results of the smeared modeling are presented.

For models VT100, 1 and VT50, 1, the response from the discrete modeling of the reinforcements predicts a peak strength which was 90 to 100 % more than that of the smeared

modeling approach (see Figure 6-17 (a) and (b)). This behavior is distinctively observed for RC members under torsional loading. The highly varied response between this two modeling approaches is a consequence of the cover spalling phenomenon. It should be noted that the two modeling methods do not result in much difference for modeling of members subjected to actions other than torsional loadings, such as shear or flexural problems.

VecTor 3 responses for VT100, 1 predicts a brittle failure whereas, for VT50, 1, the post-peak response is ductile. The response for fiber-wrapped specimens VT50, 2 shows enhanced peak strength followed by a sudden drop in strength. Interestingly the simulation predicts a further strength enhancement in the post-peak region. Similar to VT50, 2, the response of VT100, 2 shows improved strength after the peak strength. This post-peak strength improvement may be attributed to the provision of the externally bonded fibers.

6.2.2 Result from DUCOM-COM3

a

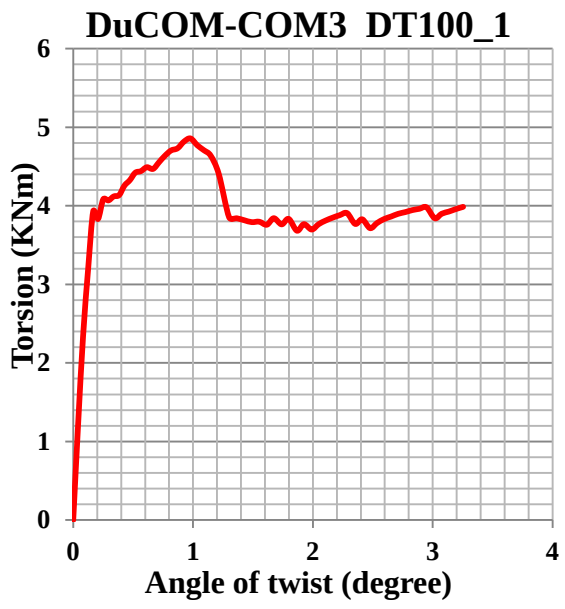

b

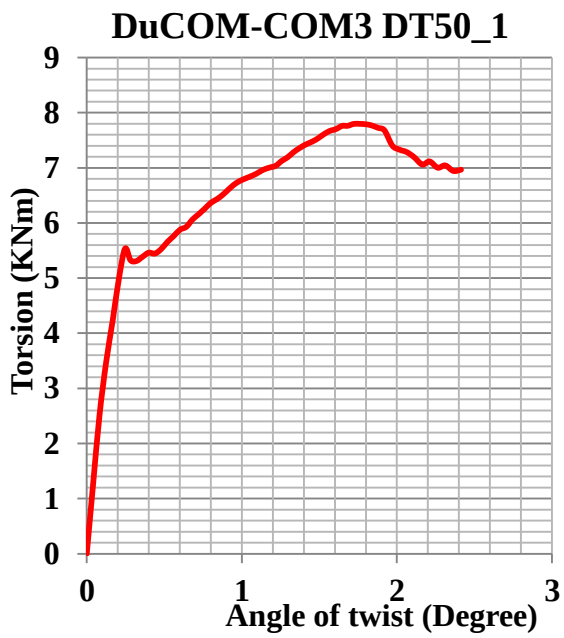

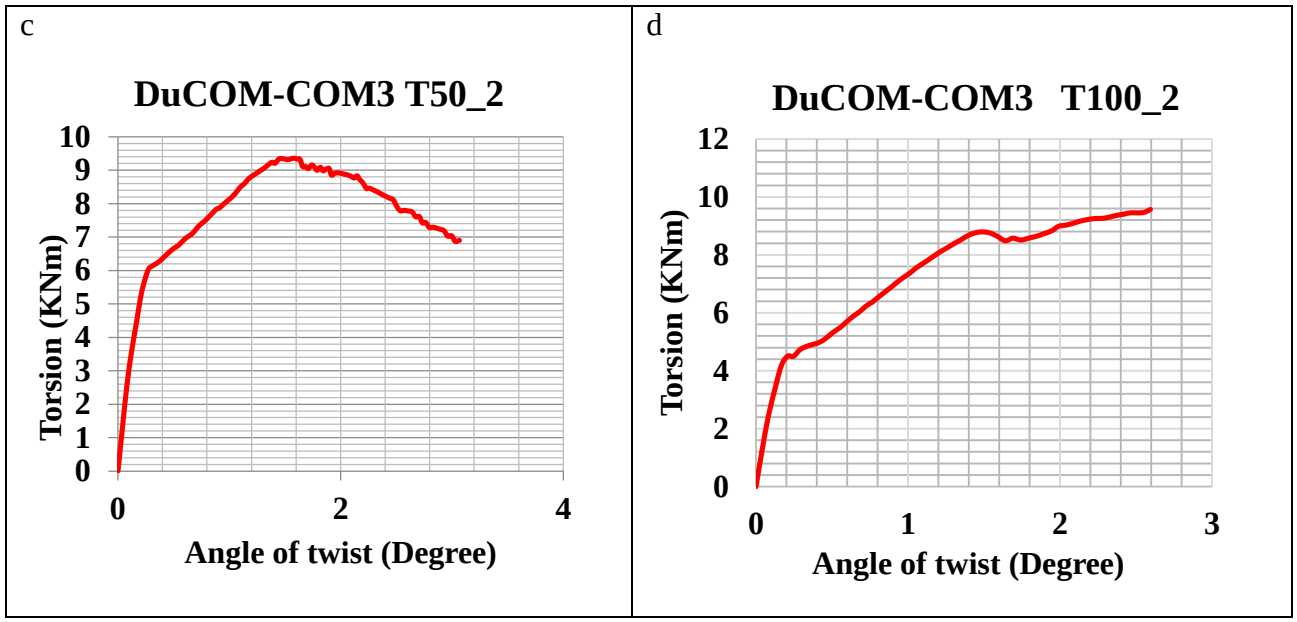

Figure 6-18- DuCOM-COM3 results (a) DT100, 1 (b) DT50, 1 (c) DT50, 2 (d) DT100, 2

The simulations from DuCOM-COM3 are presented in Figure 6-18.The modeling of the specimens was conducted using the smeared modeling approach. The concrete section within a range of seven times the diameter of the rebar was modeled with a tension stiffening behavior. Moreover, the concrete cover is modeled as plain concrete with tension softening behavior.

The response of specimen DT100, 1 shows a very high pre-crack torsional stiffness followed by a softened response. The change in stiffness was observed at the apparent cracking torque of 3.9KNm. After reaching a torsional moment of 4.9 KNm, a sudden brittle failure was observed. In the post-peak phase, the brittle and sudden drop in strength of the specimen was later stabilized to a torsional moment of 4KNm (see Figure 6-18a). The overall pre-peak behavior of DT50, 1 is similar to the response of DT100, 1. However, the post-peak behavior of DT50, 1 is slightly ductile and the observed cracking and ultimate strength of the specimen was somewhat higher than DT100, 1.

The simulation for the fiber wrapped specimens shows an enhanced cracking and ultimate strength than their respective control specimens (see Figure 6-18 c and d). Their pre-peak response can be characterized by a very high torsional stiffness before cracking and a softened linear post-crack stiffness. Unlike specimen T50_2, the post-peak response for specimen T100_2 shows a sudden drop in strength followed by strength recovery. The observed post-peak strength enhancement for T100_2 might be due to the positive effect of the fiber composite.

6.3 Result from the Combined Softened Membrane Model for Torsion and Flexure

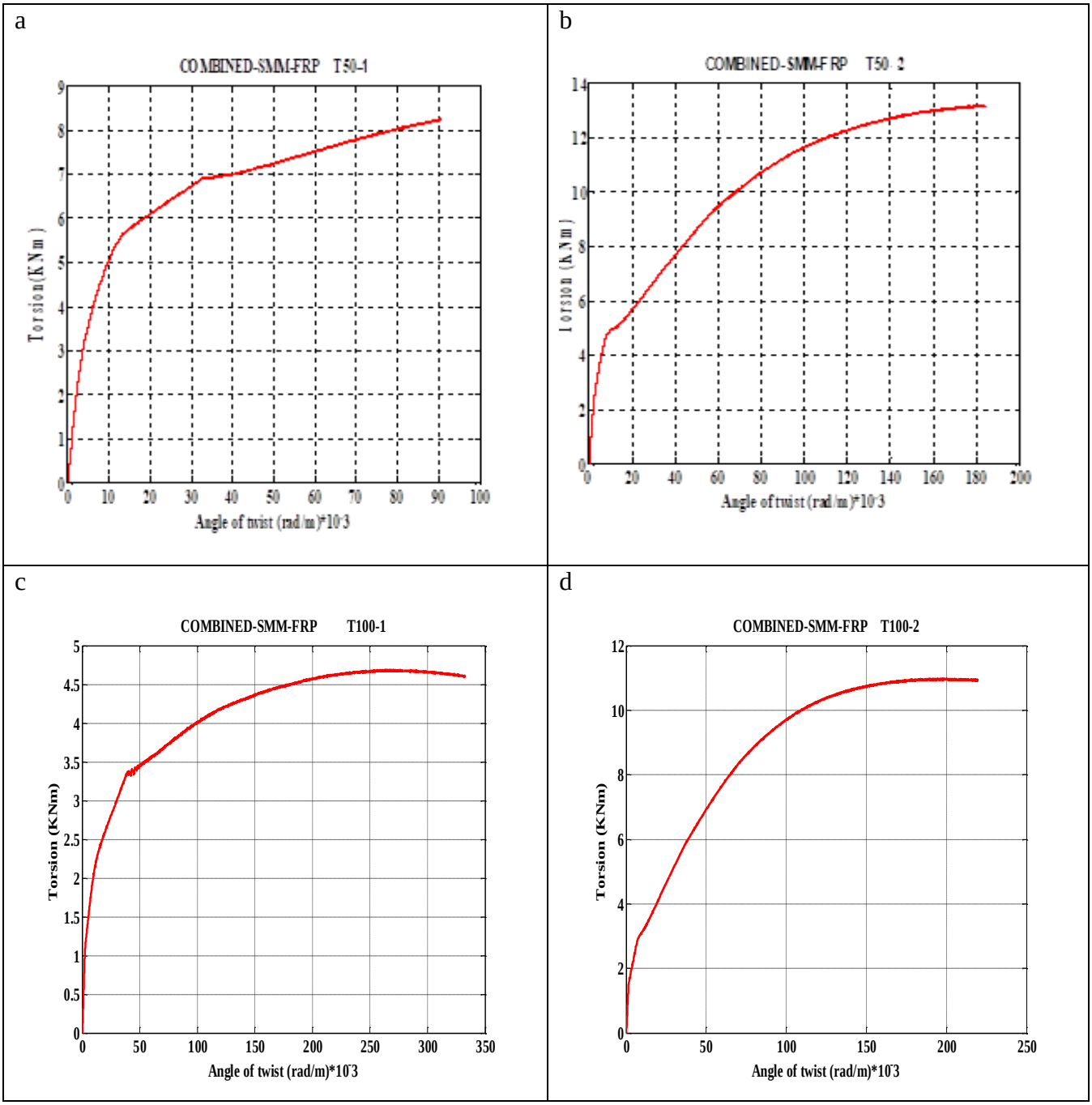

Figure 6-19- Combined-SMM-FRP results (a) T50, 1 (b) T50, 2 (c) T100, 1 (d) T100, 2

The results from the analytical model (COMBINED–SMM-FRP) are given in Figure 6-19. All four predictions show two distinct behaviors. A very high torsional stiffness was observed before the apparent cracking and then, a moderately softened response follows up to the peak strength of the specimens.

The carbon fiber strengthened specimens, T50, 2 and T100, 2, showed an enhanced cracking and ultimate strength than their respective control beams. An increase of more than 60 percent in ultimate strength is observed from the analysis.

The control beams, T50, 1 and T100, 1, were identical in all factors except in their transverse reinforcement spacing. The response of T50-1 is stiffer and the ultimate capacity of the specimen is 60 percent more than the specimen T100-1. The observed substantial increment in ultimate strength may be attributed to the closely spaced transverse reinforcements. Observing the above responses it may be safe to assume that, as the transverse reinforcement spacing is reduced, the ultimate strength can substantially increase. However, the prior statement only holds true as long as premature failures are avoided. Moreover, it should be noted that as the spacing of transverse reinforcement is reduced from some limit, the post-peak response will be brittle and failure might be controlled by concrete crushing.

6.4 Comparison between Results from the NLFEA Software's Simulation and the Experiment

6.4.1 Comparison between VecTor 3 and the Experiment

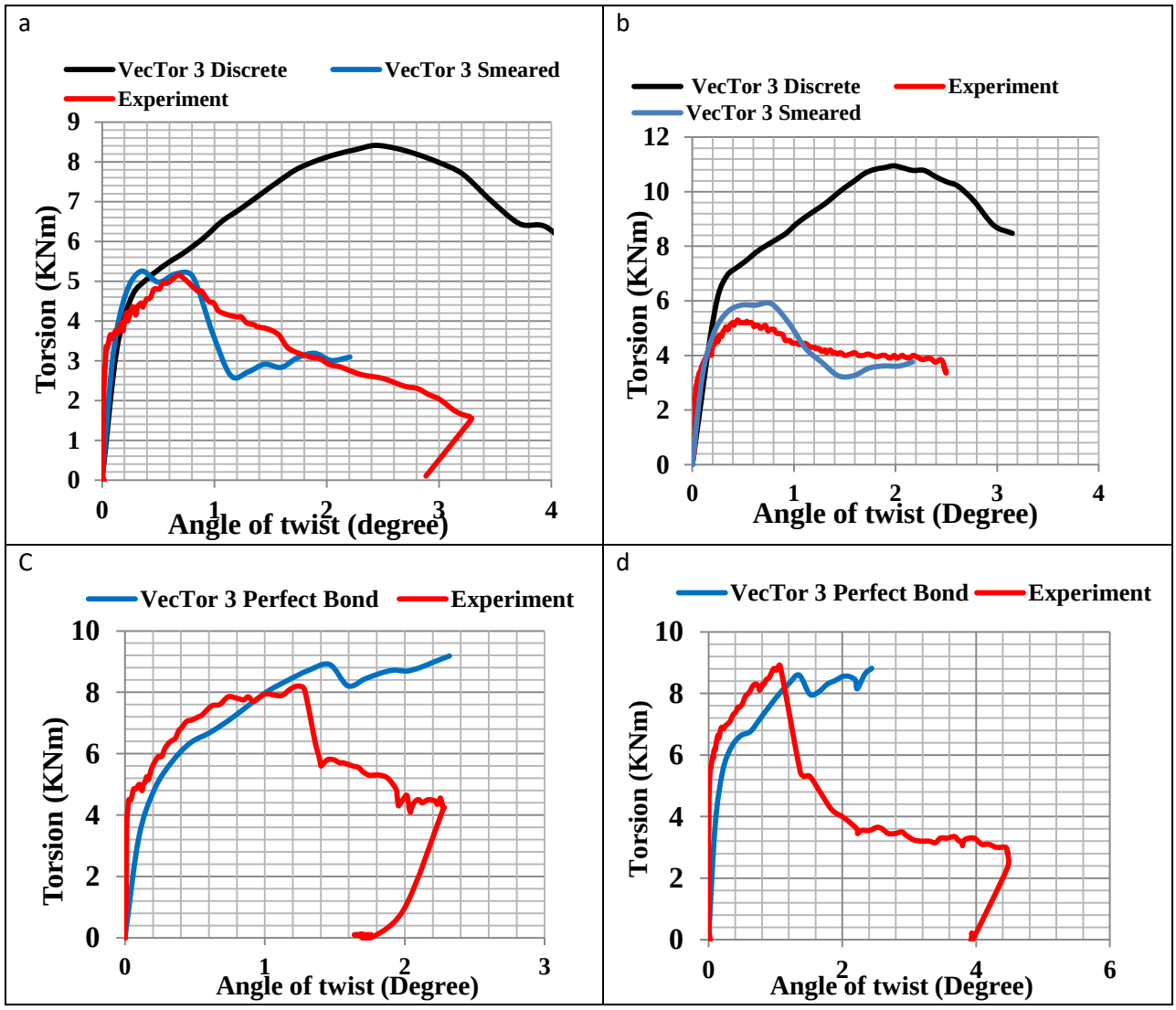

Figure 6-20-Comparison between VecTor 3 simulation and experiment results; (a) VT100, 1 (b) VT50, 1 (c) VT50, 2 (d) VT100, 2

In this section, the results from VecTor3 are compared with their representative samples from the experimental investigation. As it was mentioned in chapter 5, in VecTor modeling the RC beams were modeled using the smeared and discrete modeling approaches.

The discrete modeling approach for the control beams T100, 1 and T50, 1 seems to highly overestimate the peak torsional strength (see Figure 6-20 (a) and (b)). The post-peak response is also poorly predicted. While in the smeared modeling approach, for specimen T100, 1, the VecTor3 simulation shows an excellent prediction of the peak strength. Additionally, the post-peak behavior of the specimen is successfully captured by the model. The smeared modeling simulation for specimen T50, 1 has fairly predicted the peak as well as the ductile post-peak response.

From the above results, it may be stated that a smeared modeling approach is the appropriate modeling method for RC members subjected to torsional moment. The discrete modeling approach may result in unsafe prediction for torsional members by overlooking the cover spalling phenomenon.

The comparison between the responses of the carbon fiber strengthened experimental specimens (T50, 2 and T100,2) and their representative VecTor 3 models are given in Figure 6-20 (c) and (d). The overall behavior up to the peak torque strength is accurately predicted for both specimens. The peak torsional strength of the specimens was sufficiently estimated by the VecTor 3. However, in the post-peak region, there is a large difference between the predicted results of the model and the experimental result. Unfortunately, the post-peak response by the finite element model gives a highly ductile post-peak behavior. The reason for this erroneous post-peak prediction lies on the fact that, in the modeling of the fibers on the concrete substrate, it was assumed a perfect bond between the fiber and the concrete. In spite of that, during the experimental testing, a continuous debonding and slipping of fibers were observed.

Generally, VecTor 3 predicted the peak strength of both the control and strengthened specimens very well. Excluding the fiber wrapped elements; the package adequately predicted the overall loading behavior of the specimens. For three dimensional torsional problems, the post-peak modeling of the fiber wrapped members is expected to be greatly enhanced by the use of the appropriate bond-slip constitutive model.

6.4.2 Comparison between DuCOM-COM3 and the Experiment

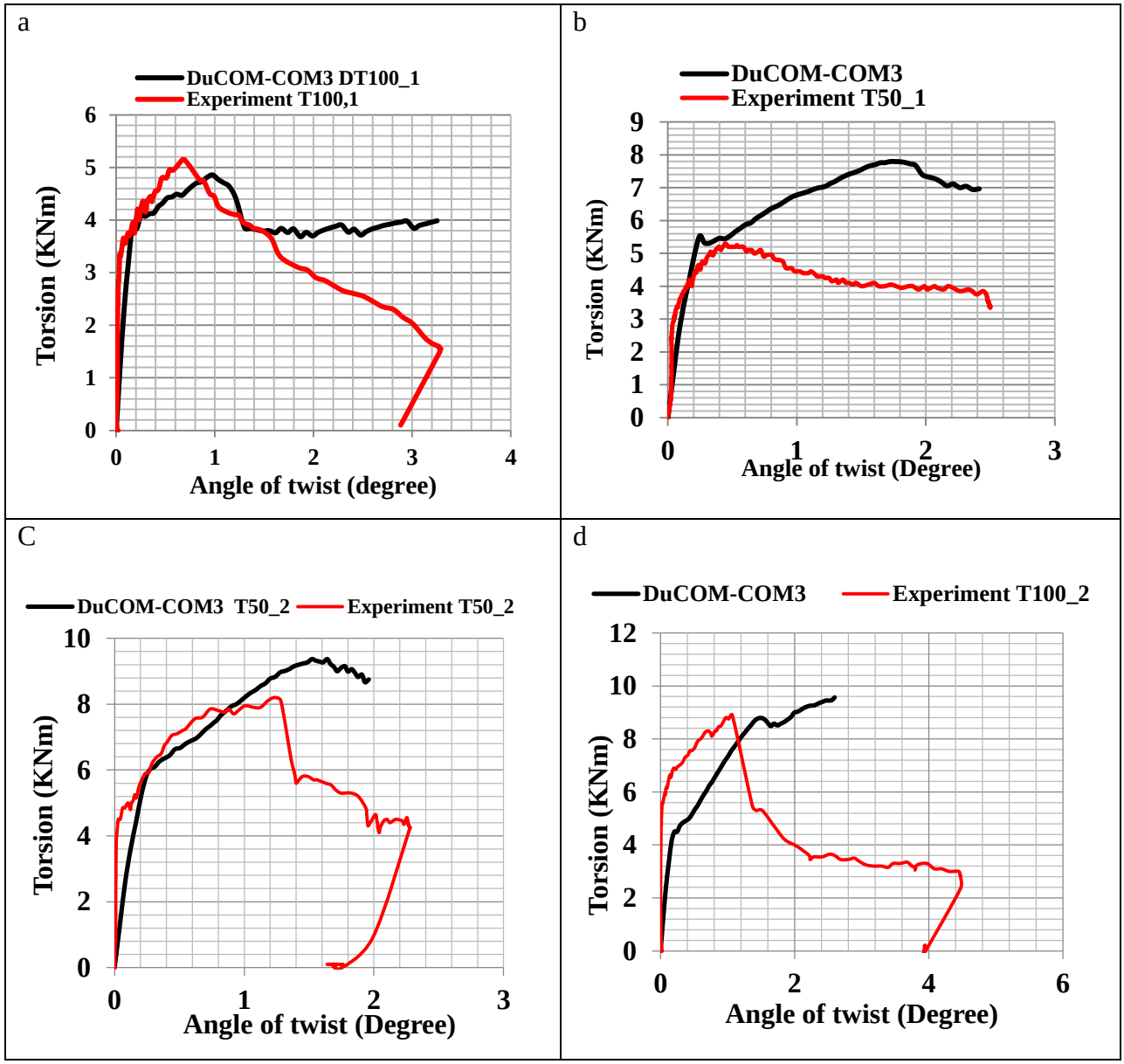

Figure 6-21- Comparison between DuCOM-COM3 simulation and experiment results; (a) DT100, 1 (b) DT50, 1 (c) DT50, 2 (d) DT100, 2

To evaluate the ability of DuCOM-COM3 in simulating torsional tests, the results of the experiment and the DuCOM-COM3 models are plotted together in Figure 6-21.

Generally, the DuCOM-COM3 prediction for specimen T100, 1 was fairly accurate. The major discontinuities such as cracking and peak strength were adequately captured.

Although the pre-crack torsional stiffness and cracking loads were adequately predicted, the post-crack stiffness was slightly underestimated. The reason for the relatively softened response is due to the modeling of the cover as plain concrete. In the post-peak region, the simulation predicts a brittle failure followed by a stabilized response, unfortunately, the experiment shows a drastic decline in the post-peak strength.

The comparison between the simulation and the experiment for specimen T50_1 is shown in Figure 6-21b. albeit the torsional stiffness predicted by the model was linear rather than the experimental observed nonlinear response; the simulation reasonably predicted the response up to the cracking strength. Contrary to the experiment, after the torsional moment of 5KNm, the simulation shows an enhanced strength. Although the concrete cover was modeled as plain concrete, it didn't prevent the concrete from resisting compression and it results in an overestimation of the ultimate capacity and post-peak response of the specimen.

The results of comparison between the prediction for fiber-wrapped specimens and the experiment is shown in Figure 6-21c and d. Considering the difficulty of modeling the cover spalling phenomenon, the overall response predicted by the model is within an acceptable range. For both specimens, the predicted pre-crack torsional stiffness is slightly softer than the experimental result. Following the cracking of the specimens, the predicted post-cracking stiffness is similar to the responses of the experimental specimens. The prediction of the peak strength for specimen T100, 2 was excellent. On the other hand, similar to the control specimen, the ultimate strength prediction of the specimen T50, 2 is overestimated by the package.

In the post-peak stage, initially, the simulation closely followed the behavior of the experimental specimens. However, due to inadequate modeling of the interface between the concrete and the fiber, an erroneous post-peak strength enhancement was predicted for specimen T100, 2.

Although the ultimate strength prediction for specimen T50, 2 was slightly overestimated, the brittle post-peak behavior was adequately captured by the package.

6.4.3 Comparison between Results from Analytical Model and the Experiment

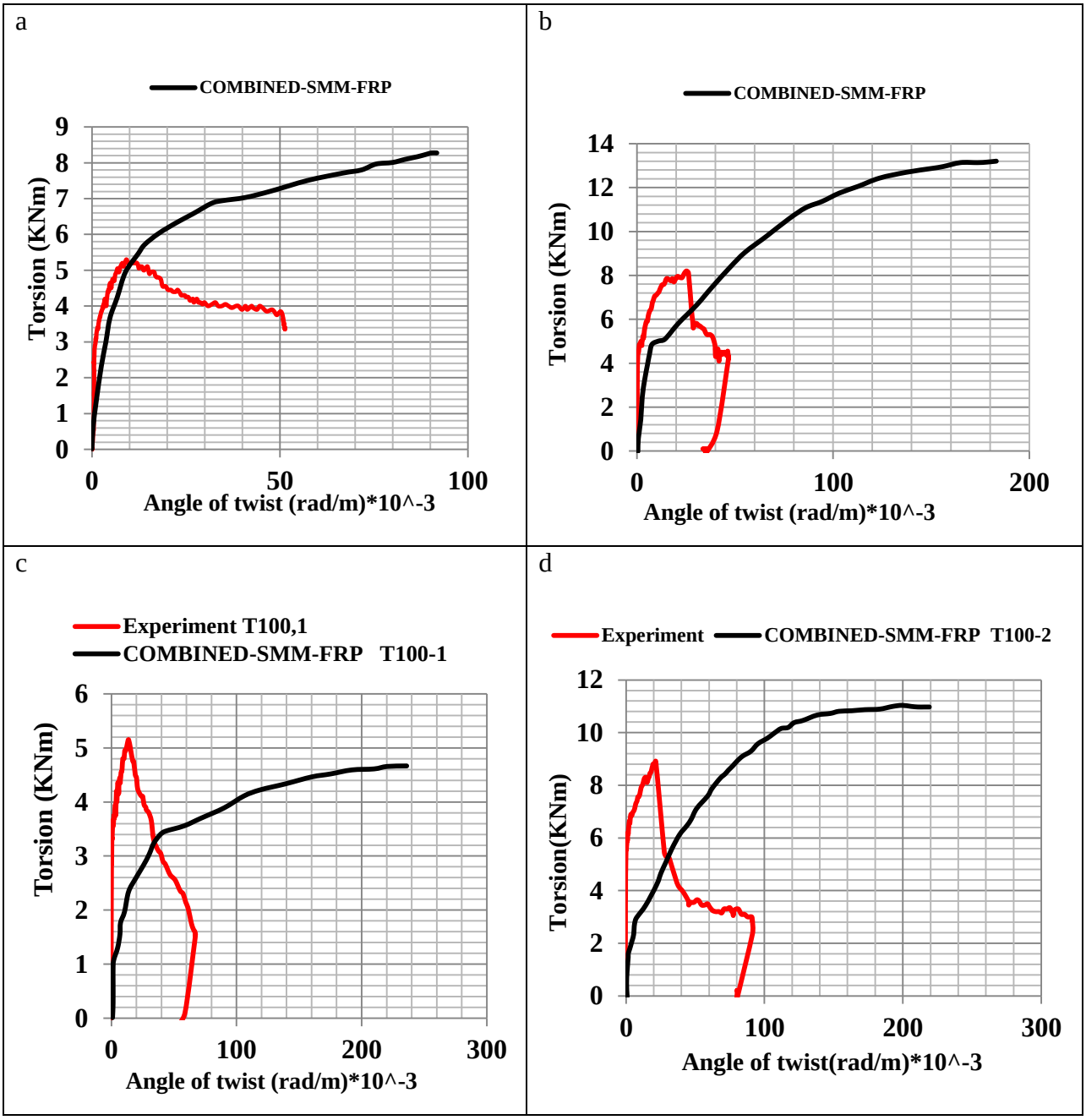

Figure 6-22- Comparison between COMBINED-SMM-FRP and experiment results; (a) T50, 1 (b) T50, 2 (c) T100, 1 (d) T100, 2

The results of the experiment and the analytical model are presented in Figure 6-22. Even though the analytical model (COMBINED-SMM-FRP) was shown to provide very good predictions for specimen tested by other researchers (see section 3.4.2), at first glance, the comparison between the proposed model and the experimental beams seemed slightly erratic.

However, those erratic predictions are not that surprising when considering all the test specimens failed prematurely due to the concrete cover spalling phenomenon. In the analytical modeling, the principal assumptions require the ultimate failure of the specimens to be associated with either concrete crushing or rebar rupture. Premature failures such as slipping of reinforcement and concrete cover spalling were not considered in the modeling.

The adverse effect of the concrete cover spalling on the ultimate strength might be observed from the result of T50-1 specimen's transverse reinforcement strain (Figure 6-23). A very good prediction of transverse reinforcement strain of the model is observed ranging from before crack through to post cracking. However, around strain level of 400 $\boldsymbol{\mu\varepsilon}$, the concrete cover spalling drastically changes the behavior. At the ultimate strength of the specimen, the strain level in the transverse reinforcements was well below yield strain.

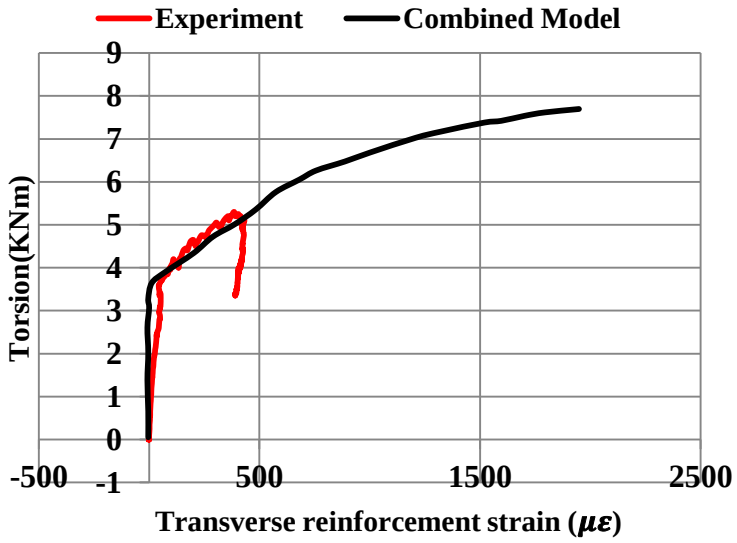

Figure 6-23-Transverse reinforcement strain

Analogous to the transverse strain comparison, the results between the model and the experiment for specimen T50-1 matched a very well up to the peak strength. When reaching a torsional moment of 5 KNm a substantial concrete cover spalling resulted in peak strength of the specimen. If the premature failure were to be avoided, the proposed model forecast an ultimate capacity of more than 60 percent that of T50-1.

Another interesting observation was the results of the strengthened specimens T50-2 and T100-2. The proposed model adequately predicted the behavior up to the cracking strength. However, after the cracking of the specimen, the model predicted a lower stiffness than the experiment. The post cracking stiffer response of the experiment might be attributed to the cover spalling.

As presented earlier (see section 6.1), cover spalling phenomena was commenced around the apparent cracking of the specimens. When the concrete cover starts spalling, there will be transverse movement or dilation which results in higher strain demand on the confining carbon fiber strips. In another word, the carbon fiber was activated earlier in the experiment than the case of the model and resulted in higher post-crack torsional stiffness. Ultimately, the higher strain demand in the fiber led to fiber rupture which resulted in the peak strength of the specimen. If the cover spalling were to be avoided, the proposed model forecast an ultimate capacity which is more than 60 percent that of the test specimens. The same mechanism might be the reason for the similar behavior for specimen T100-1. For specimen T100-1, the transverse reinforcement plays the role of the fibers. However, for the RC beam without fiber, the remaining smaller section of the spalled concrete results in strain demand rather than the dilation of the concrete cover.

6.4.4 Comparison of Results from the NLFEA Simulations and the Experiment

As explained in chapter 5, the nonlinear finite element tools used in the simulations are based on a different crack modeling approach. DuCOM-COM3 is based on the four-way fixed crack model whereas VecTor 3 is based on the Modified compression field theory (a rotating angle theory). Even though the underlying theories are on opposite ends of modeling cracks in RC structures, both tool previously showed their capability of predicting the complicated response of reinforced concrete structures. In the current simulations additional to the challenge of modeling of RC members, all of the tested specimens failed by concrete cover spalling; this results in additional modeling complication. The resulting plots of the finite element packages and the experiments are presented in Figure 6-24.

Both packages showed their excellent modeling capabilities for specimen T100, 1 (see Figure 6-24a). The post cracking and ultimate strength prediction by both tools are within a reasonable range.

For specimen T50_1, although the overall behavior was adequately captured by VecTor 3, the ultimate strength prediction was slightly on the unsafe side. The ultimate capacity and post-peak response of the specimen T50-1 was not adequately captured by DuCOM-COM3. The reason for this erroneous prediction lies on the difficulty of modeling of the complicated cover spalling phenomenon.

Similar to the control specimen, the prediction of T50_2 was overestimated by both packages. The peak strength prediction for specimen T100, 1 was accurately predicted by both tools. However, the post-peak response of the specimen T100, 2 was not adequately captured by both packages (see Figure 6-24 c and d).

During strengthening of structural members, it is vital to know the failure mechanism and post-peak ductility of the strengthened specimen. Although the packages adequately addressed the prediction of ultimate strength, the observed post-peak predictions points out a critical gap that must be addressed. To adequately capture the post-peak response of strengthened specimens, it is necessary to address the three-dimensional bond-slip behaviors between the fiber and the underlying concrete substrate.

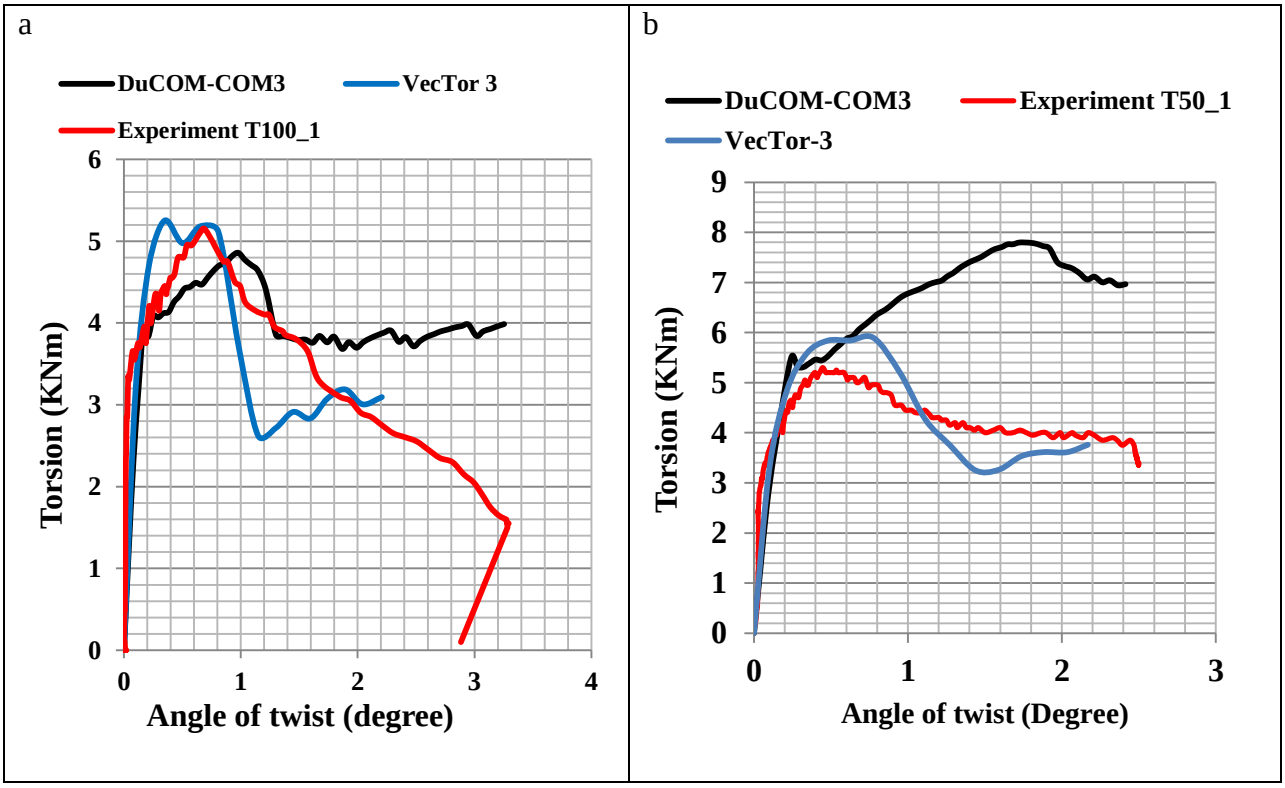

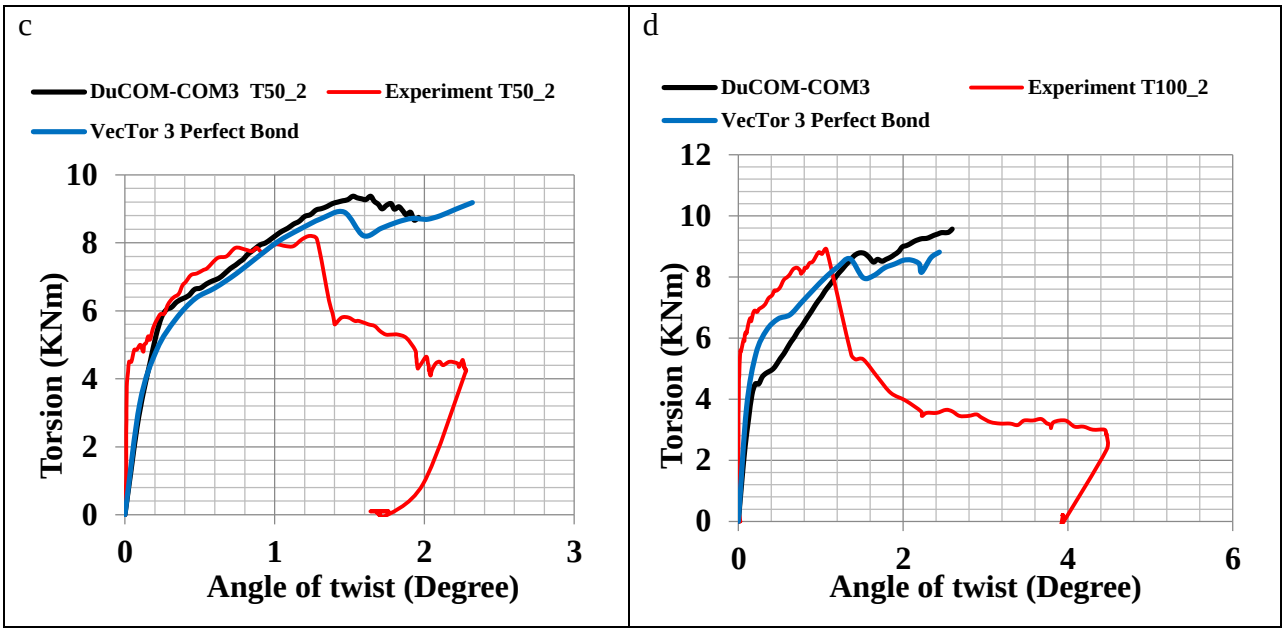

Figure 6-24-Comparison of results from the NLFEA simulations and the experiment (a) T100, 1 (b) T50, 1 (c) T50, 2 (d) T100, 2

6.5 Effect of Flexure on Torsional Capacity of RC Members

The proposed model is capable of computing the torsional capacity of RC beams subjected to combined loadings. In this section, by using the model and taking a simple case of RC beam section, the effect of flexure on the torsional capacity of the strengthened specimen will be investigated.

For demonstration, consider a reinforced concrete beam with parameters given in Table 6-1 and Figure 6-25. Moreover, the RC member is strengthened with three layers of CFRP wrapped in the transverse direction. The mechanical properties of the CFRP are given in Table 6-2.

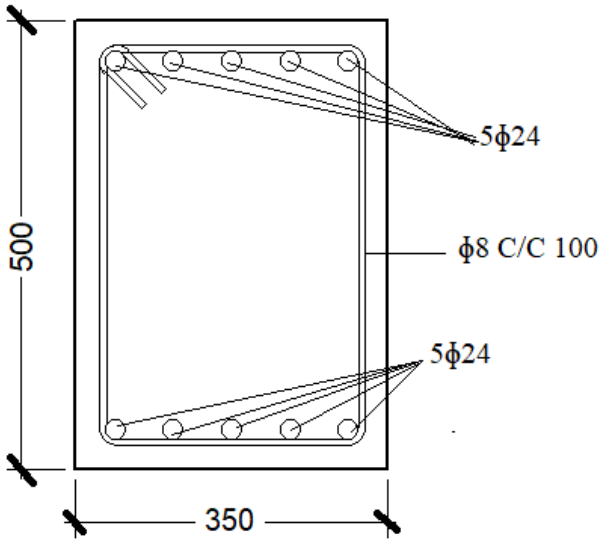

Figure 6-25-Geometric cross-section

Table 6-1- Details of the specimens

	Longitudinal rebar		Transverse rebar							
Case	Top	Bottom	Size (mm)	Spacing (mm)	Width (mm)	Height (mm)	fc (MPa)	fy*	fy#	T/M
1	5ϕ24	5ϕ24	8	100	350	500	30	400	500	∞
2	5ϕ24	5ϕ24	8	100	350	500	30	400	500	7
3	5ϕ24	5ϕ24	8	100	350	500	30	400	500	3
4	5ϕ24	5ϕ24	8	100	350	500	30	400	500	1

**Longitudinal rebar # Transverse rebars* T/M=*torsion to moment ratio*

Table 6-2- Mechanical Properties of the CFRP

Modulus	240,000 MPa
Design Thickness	0.111mm
Design Tensile Strength	3800 MPa
Ultimate Tensile Elongation	1.55%

To avoid failure of the specimen due to flexure, a sectional analysis is conducted using Response-2000. The resulting moment-curvature relationship is given in Figure 6-26. The strain in the concrete and in the rebar at first yielding of transverse rebar is shown on the diagram. The plot displays the ductile flexural behavior of the specimen.

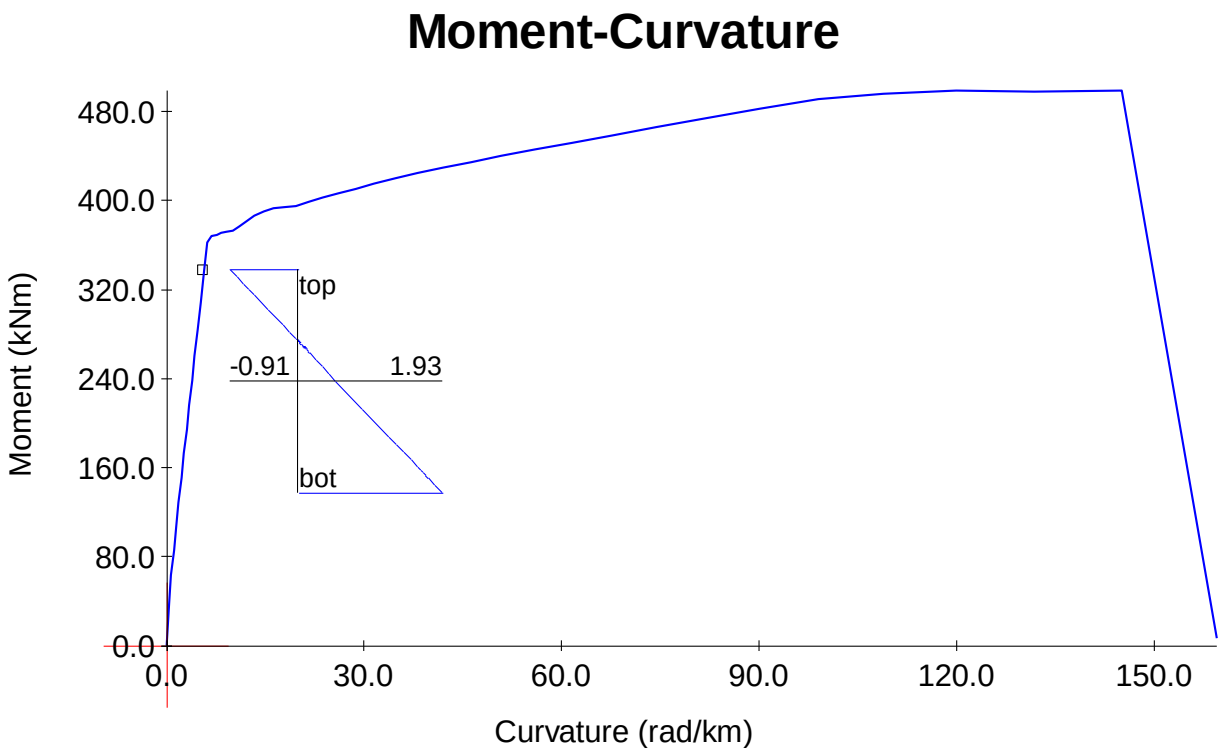

Figure 6-26-Moment-Curvature relationship

Although the demonstration is concerned with the effect of flexure on the strengthened specimen, it is imperative to observe the pure torsional capacity of the section without the fiber strengthening. Accordingly, the response of the bare RC specimen under pure torsion is provided in Figure 6-27.

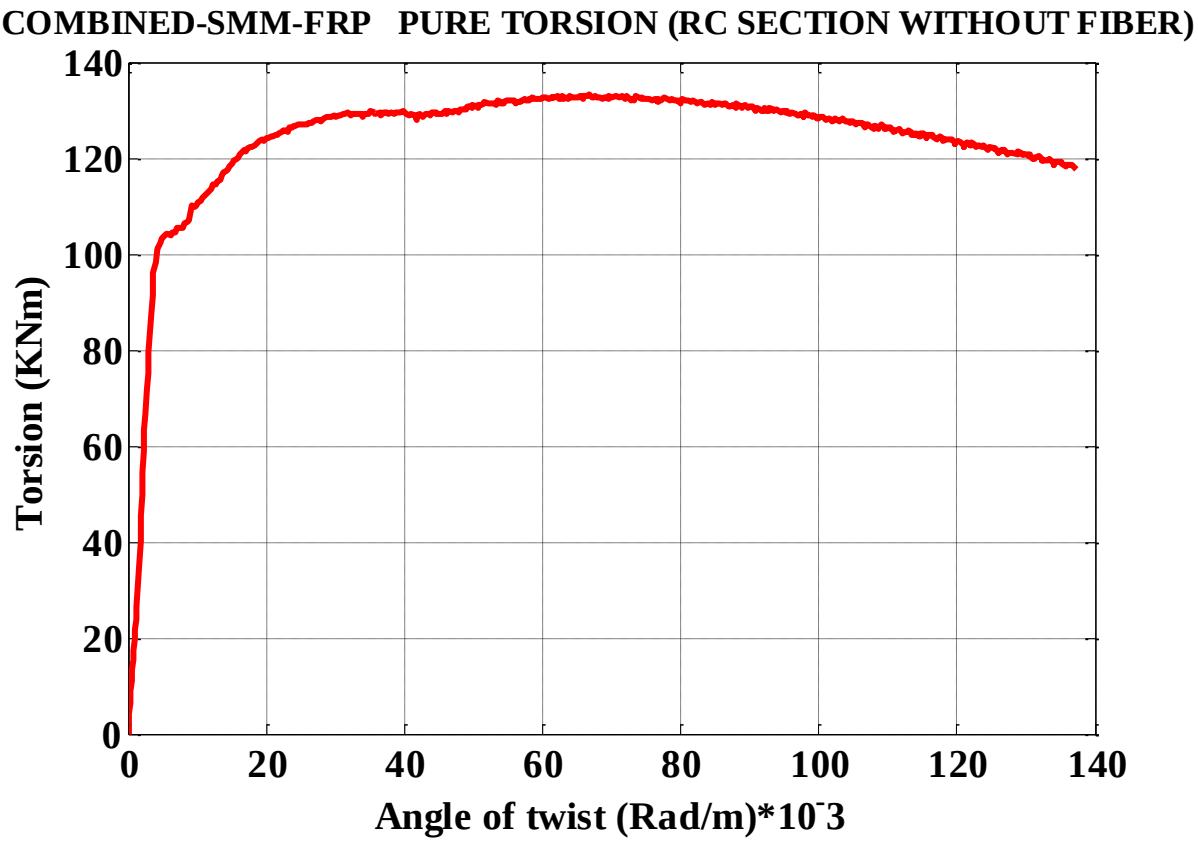

Figure 6-27- Pure torsional response before strengthening

The proposed model is used for plotting the response of the strengthened RC section under different ratios of torsion and flexure. The subsequent results are given in Figure 6-27. The first column shows the torsion–angle of twist response while the second column provides their respective torsion- longitudinal strains diagrams. Additionally, the overall response of all the specimens is plotted in Figure 6-28.

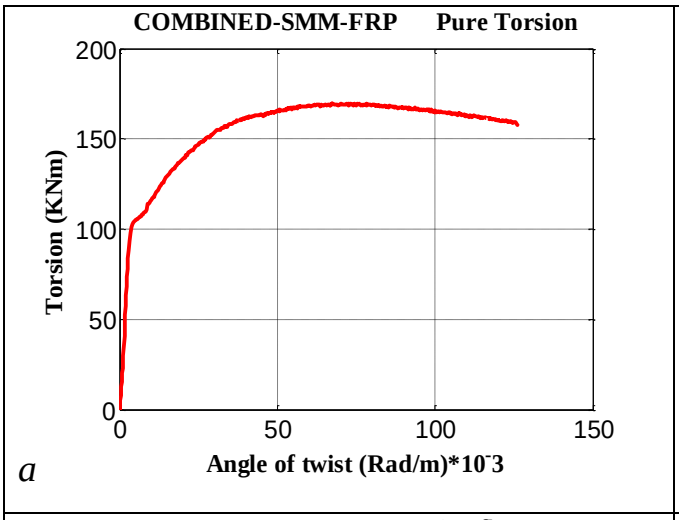
COMBINED-SMM-FRP Pure Torsion
Torsion (KNm)
Angle of twist (Rad/m)*10^-3
0
50
100
150
200

a

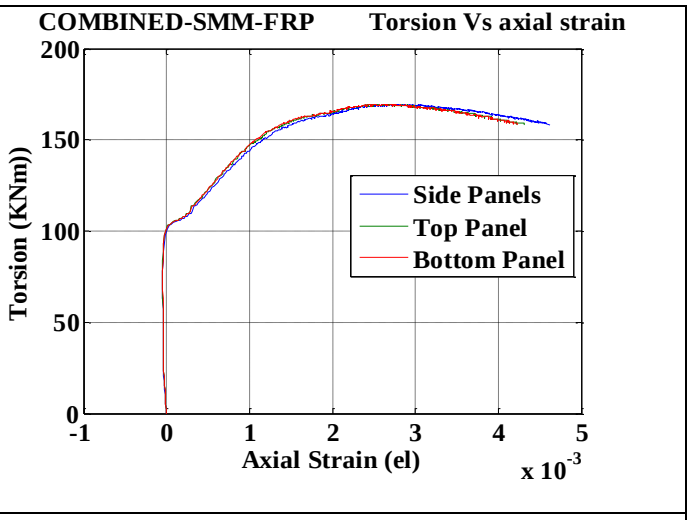
COMBINED-SMM-FRP Torsion Vs axial strain
Torsion (KNm))
Axial Strain (el)
x 10^-3
Side Panels
Top Panel
Bottom Panel

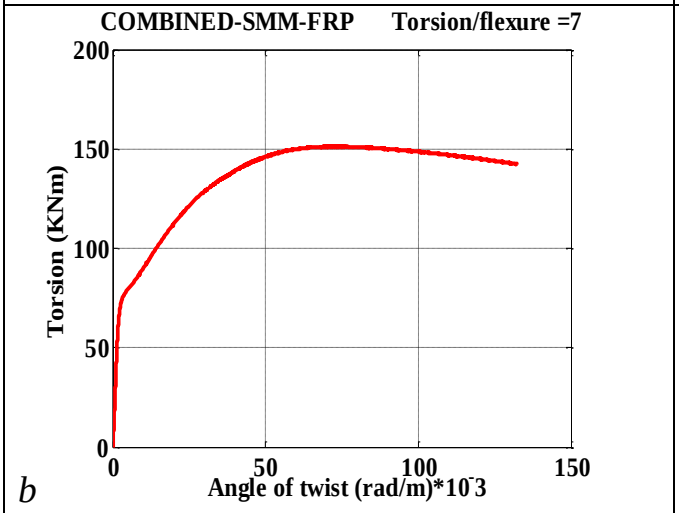
COMBINED-SMM-FRP Torsion/flexure =7
Torsion (KNm)
Angle of twist (rad/m)*10^-3

b

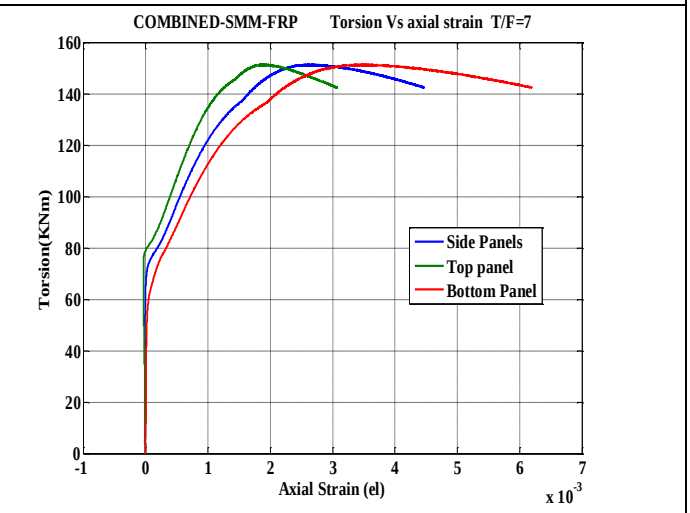
COMBINED-SMM-FRP Torsion Vs axial strain T/F=7
Torsion(KNm)
Axial Strain (el)
x 10^-3
Side Panels
Top panel
Bottom Panel

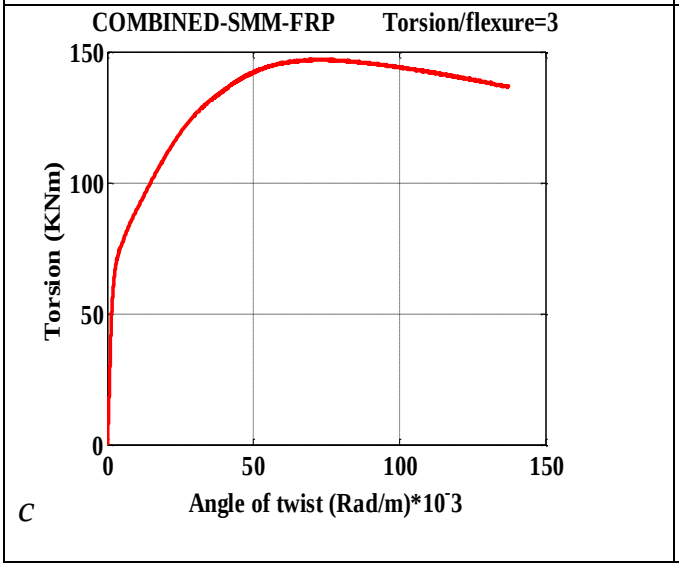
COMBINED-SMM-FRP Torsion/flexure=3
Torsion (KNm)
Angle of twist (Rad/m)*10^-3

c

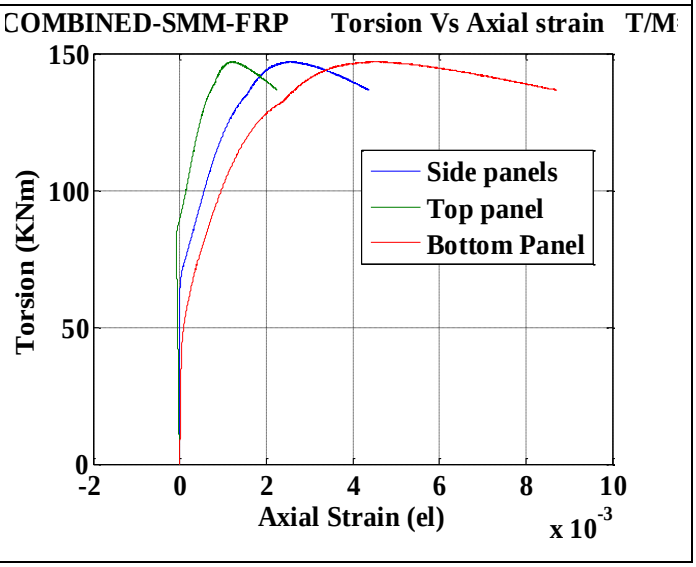
COMBINED-SMM-FRP Torsion Vs Axial strain
Torsion (KNm)
Axial Strain (el)
x 10^-3
Side panels
Top panel
Bottom Panel

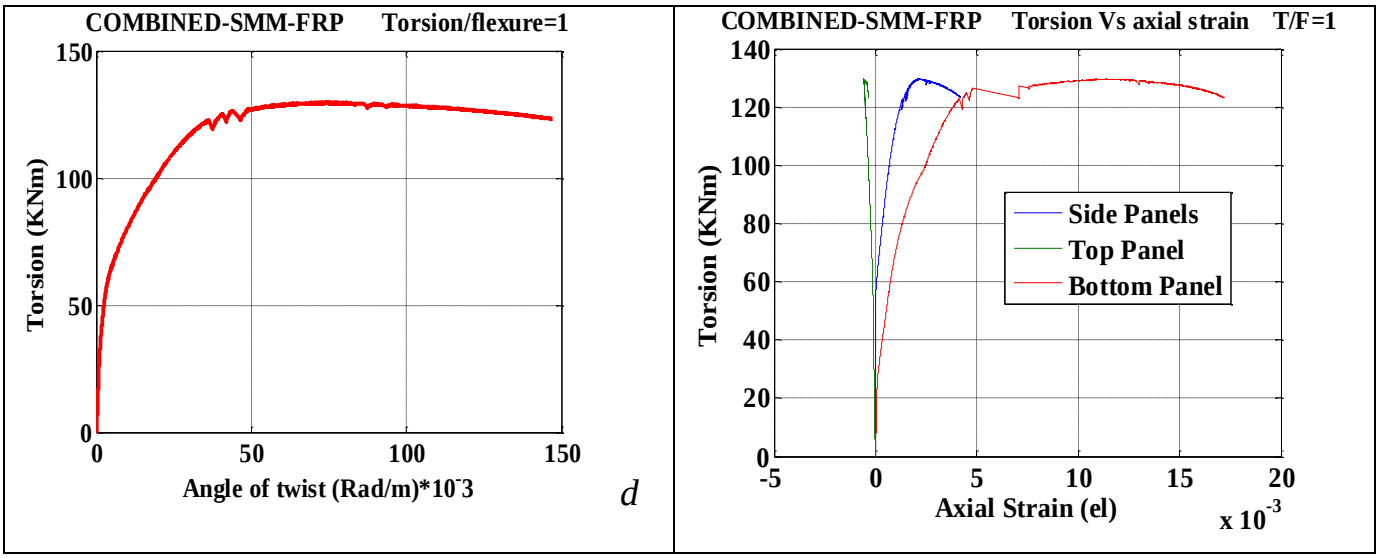

a-Case1 b-Case2 c-Case3 d-Case4

Figure 6-28- Torsional response for different ratios

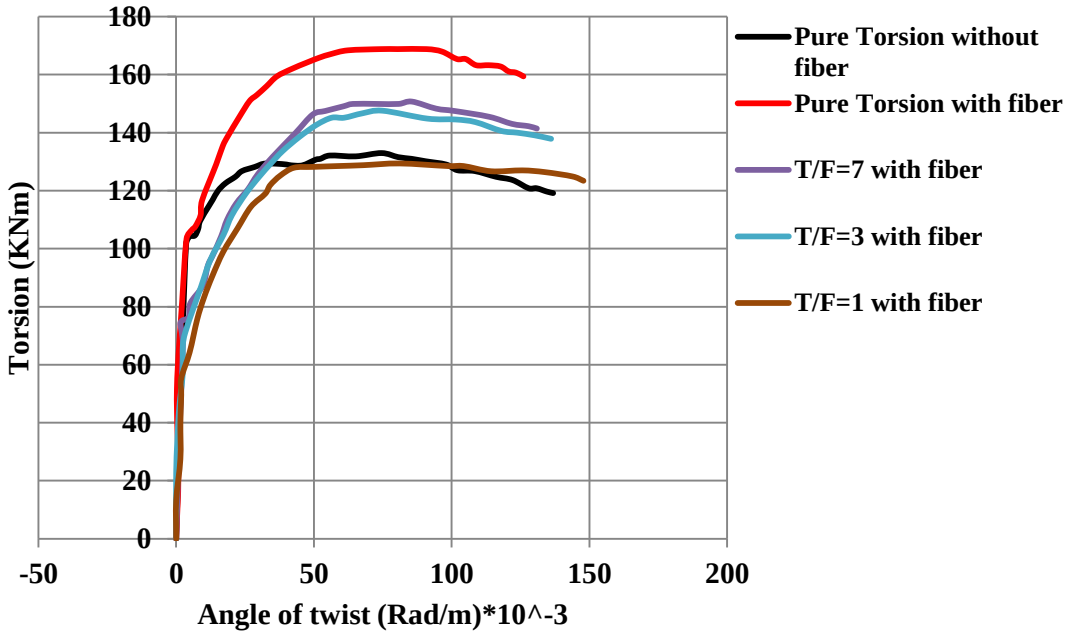

Figure 6-29- Comparison of the responses

As it can be seen from the above plots, as the presence of flexural moment grows, the anticipated torsional strength of the strengthened specimen decrease. The detrimental effect of flexure can clearly be observed from the comparison of the bare RC torsional capacity of the section with the torsional capacity of the strengthen specimens with flexure (see Figure 6-29).

A strength reduction of more than 25 percent is observed between the pure torsional strengthen specimen and that of the specimen with flexure to torsion moment of one. It should be noted that, in the current demonstration, this amount of reduction in strength occurs at flexure level of 25 percent of the flexural capacity of the section, which in a practical sense is a bending moment that takes place at the service load.

From the above comparison, one may safely conclude that, during strengthening of torsion critical members, the presence of associated flexural moment should be considered. Moreover, the combined action of torsion and flexure will be highly critical for members subjected to a large flexural moment such as curved beams and curved box girder bridges.

7 CONCLUSION AND RECOMMENDATION

7.1 Conclusions

The thesis presented experimental, nonlinear finite element and analytical investigation on the strengthening of torsion critical member using carbon fiber reinforced polymer. The proposed analytical model (COMBINED-SMM-FRP) is capable of predicting the response of fiber wrapped RC members subjected to combined torsion and flexure. COMBINED-SMM-FRP is also capable of predicting the behavior of RC beams without fibers ranging from the pre-crack state to post peak. Additionally, the applicability of the model is verified against numerous experimental tests conducted by other researchers.

The experimental, analytical and the nonlinear finite element studies showed the application of CFRP can substantially enhance the cracking and ultimate strength of torsion critical members. In the experimental study, an ultimate strength enhancement of more than 60 percent is observed for the strengthened specimen relative to their control specimens. Moreover, the study shows that during strengthening of torsion critical members, attention should be given to the associated bending moment as they greatly affect the torsional strength improvement.

In the thesis, the nonlinear finite element investigation was conducted using VecTor 3 and DUCOM-COM3. Both packages showed their excellent capability of modeling a torsion critical RC beam subjected to combined torsion and flexure. However, in the modeling of the carbon fiber strengthened specimen, the post-peak prediction was slightly erroneous. The inaccurate prediction in the post-peak region was due to the incapability of modeling the 3D bond-slip behavior between the concrete and the underlining concrete substrate. Additionally, during modeling of torsion critical members care should be given to cover spalling phenomenon. Improper modeling of cover spalling phenomena of torsional members results in unsafe and very erroneous prediction regarding strength and overall behavior.

7.2 Recommendations

The thesis presented the capability of modeling torsion critical members under combined action using the proposed model. Regarding the proposed model and the nonlinear finite element packages, the following recommendations are advanced for future works.

- The proposed model should be further developed to include biaxial bending, biaxial shear, and axial force.
- The model is capable of predicting the response of members failing either by concrete crushing or rebar/fiber rupture. Nevertheless, premature failures such as cover spalling are not addressed in the current model. Forthcoming studies should be directed in to rationally accounting the cover spalling phenomenon.
- Even though the proposed model works for wide range of parameters, it has been observed that there is a problem of stability during modeling of very congested transverse rebars. Although this problem is not usually encountered in practical applications, additional work is necessary to address this problem.
- Since the model uses rational constitutive laws for rebar and concrete, further study should be directed to model cyclic combined loadings.
- Regarding the nonlinear finite element packages, a more refined and easy to use bond-slip models are expected to provide a better prediction of the post-peak behavior of fiber wrapped RC members.

Regarding to the experimental investigation and verification, there is a lack of combined torsion-flexure and combined torsion-flexure-shear experimental tests on fiber strengthened RC members. For further application of the strengthening scheme, additional researches should focus on increasing the database of experimental tests of combined actions on the FRP strengthened specimens.

REFERENCES

ACI-440.2R-02, (2002), "Guide for the Design and Construction of Externally Bonded FRP Systems for strengthening Concrete Structures", American Concrete Institute, Farmington Hills, MI 48333-9094.

Allawi, A. A. (2006). "Nonlinear analysis of reinforced concrete beams strengthened by CFRP in torsion." Ph.D. thesis, Dept. of Civil Engineering,College of Engineering, Univ. of Baghdad, Baghdad, Iraq.

Ameli, M., Ronagh, H. R., & Dux, P. F. (2004, December). Experimental investigations on FRP strengthening of beams in torsion. In *Proc., 2nd International Conference on FRP composites in Civil Engineering, December, Adelaide, Australia* (pp. 587-592).

Belarbi, A., & Hsu, T. T. (1994). Constitutive laws of concrete in tension and reinforcing bars stiffened by concrete. *Structural Journal*, *91*(4), 465-474.

Belarbi, A., & Hsu, T. T. (1995). Constitutive laws of softened concrete in biaxial tension compression. *Structural Journal*, *92*(5), 562-573.

Bentz, E. C. (2000). *Sectional analysis of reinforced concrete members* (p. 310). Toronto: University of Toronto.

Blaschko, M., Niedermeier, R., & Zilch, K. (1998, January). Bond failure modes of flexural members strengthened with FRP. In *Second International Conference on Composites in InfrastructureNational Science Foundation* (Vol. 1).

Bredt R (1896) Kritische Bemerkungen zur Drehungselastizitat (Critical remarks on the elasticity rotation). Zeitschriftdes Vereines Deutscher Ingenieure 40(28):785–790 (in German)

Brena, S. F., Bramblett, R. M., Wood, S. L., & Kreger, M. E. (2003). Increasing flexural capacity of reinforced concrete beams using carbon fiber-reinforced polymer composites. *Structural Journal*, *100*(1), 36-46.

Colalillo, M. A., & Sheikh, S. A. (2014). Behavior of Shear-Critical Reinforced Concrete Beams Strengthened with Fiber-Reinforced Polymer-Experimentation. *ACI Structural Journal*, *111*(6), 1373.

Collins, M. P., Walsh, P. F., Archer, F. E., & Hall, A. S. (1968). Ultimate strength of reinforced concrete beams subjected to combined torsion and bending. *Special Publication*, *18*, 379-402.

Chajes, M. J., Januszka, T. F., Mertz, D. R., Thomson, T. A., & Finch, W. W. (1995). Shear strengthening of reinforced concrete beams using externally applied composite fabrics. *Structural Journal*, *92*(3), 295-303.

CSA-S806-02, (2002), "Design and Construction of Building Components with Fiber-Reinforced Polymers",Canadian Standards Association, Rexdale, Canada, 206 pp.

Elfgren, L., Karlsson, I., & Losberg, A. (1974). Torsion-bending-shear interaction for reinforced concrete beams. *Journal of the Structural division (1956-1982)*, *100*(ST 8, Proc. Paper 10749), 1657-1676.

FIB, (2001), "Externally Bonded FRP Reinforcement for RC Structures", (CEB-FIP) Technical Report, 14, pp.59-68.

GangaRao, H. V., & Vijay, P. V. (1998). Bending behavior of concrete beams wrapped with carbon fabric. *Journal of Structural Engineering*, *124*(1), 3-10.

Ghobarah, A., Ghorbel, M. N., & Chidiac, S. E. (2002). Upgrading torsional resistance of reinforced concrete beams using fiber-reinforced polymer. *Journal of composites for construction*, *6*(4), 257-263.

Hany, N. F., Hantouche, E. G., & Harajli, M. H. (2015). Axial stress-strain model of CFRP-confined concrete under monotonic and cyclic loading. *Journal of Composites for Construction*, *19*(6), 04015004.

Hii, A. K., & Al-Mahaidi, R. (2006). Experimental investigation on torsional behavior of solid and box-section RC beams strengthened with CFRP using photogrammetry. *Journal of Composites for Construction*, *10*(4), 321-329.

Hii, A. K., & Al-Mahaidi, R. (2007). Torsional capacity of CFRP strengthened reinforced concrete beams. *Journal of Composites for Construction*, *11*(1), 71-80.

Hsu, T. T., & Mo, Y. L. (1985, May). Softening of Concrete in Torsional Members-Theory and Tests. In *Journal Proceedings*(Vol. 82, No. 3, pp. 290-303).

Hsu, T. T., Belarbi, A., & Pang, X. (1995). A universal panel tester. *Journal of testing and evaluation*, *23*(1), 41-49.

Hsu, T. T., & Zhu, R. R. (2002). Softened membrane model for reinforced concrete elements in shear. *Structural Journal*, *99*(4), 460-469.

Jeng, C. H., & Hsu, T. T. (2009). A softened membrane model for torsion in reinforced concrete members. *Engineering Structures*, *31*(9), 1944-1954.

Japan Concrete Institute (JCI). (1998). ‘‘Technical report on continuous fiber reinforced concrete.’’ *TC 952*, Committee on Continuous Fiber Reinforced Concrete, Tokyo

Kachlakev, D., & McCurry, D. D. (2000). Behavior of full-scale reinforced concrete beams retrofitted for shear and flexural with FRP laminates. *Composites Part B: Engineering*, *31*(6-7), 445-452.

Khalifa, A., & Nanni, A. (2000). Improving shear capacity of existing RC T-section beams using CFRP composites. *Cement and Concrete Composites*, *22*(3), 165-174.

Lessig, N. N. (1959). Determination of load carrying capacity of rectangular reinforced concrete elements subjected to flexure and torsion. *Concrete and Reinforced Concrete Institute*, 5-28.

Maekawa, K., Okamura, H., & Pimanmas, A. (2003). *Non-linear mechanics of reinforced concrete*. CRC Press.

Malvar, L. J. (1995). Tensile and bond properties of GFRP reinforcing bars. *Materials Journal*, *92*(3), 276-285.

Matthys, S. (2000). *Structural behaviour and design of concrete members strengthened with externally bonded FRP reinforcement* (Doctoral dissertation, Ghent University).

McMullen, A. E., & Warwaruk, J. (1970). Concrete beams in bending, torsion and shear. *Journal of the Structural Division.*

Meier, U., and Kaiser, H. (1991). ‘‘Strengthening structures with CFRP laminates.’’ Proc., Advanced Compos. Mat. in Civ. Engrg. Struct., ASCE, New York, 224–232.

Mitchell, D., & Collins, M. P. (1974, August). Diagonal compression field theory-a rational model for structural concrete in pure torsion. In *Journal Proceedings* (Vol. 71, No. 8, pp. 396-408).

Mohammadizadeh, M. R., Fadaee, M. J., Ronagh, H. R., & Ahmadinezhad, A. (2008). Behavior of high-strength concrete beams strengthened with CFRP sheets in torsion. In *4th Intl Conf FRP Compo Civ Eng (CICE2008)*.

Mörsch, E. (1902). Der eisenbetonbau, seine anwendung und theorie. *Wayss and Freytag, AG, Im selbstverlag der Firma, Neustadt ad Haardt, May*.

Moslehy, Y., Labib, M., & Ayoub, A. (2010). Softening-Coefficient for FRP Shear-Strengthened Reinforced Concrete Elements. In *Earth and Space 2010: Engineering, Science, Construction, and Operations in Challenging Environments*(pp. 3034-3046).

Niedermeier, R. (2000). Zugkraftdeckung bei klebearmierten bauteilen (Envelope line of tensile forces while using externally bonded reinforcement). *TU Munchen (In German).*

Norris, T., Saadatmanesh, H., & Ehsani, M. R. (1997). Shear and flexural strengthening of R/C beams with carbon fiber sheets. *Journal of structural engineering*, *123*(7), 903-911.

Onsongo, W. M. (1978). Diagonal compression field theory for reinforced concrete beams subjected to combined torsion, flexure and axial load, Ph.D. dissertation, Dept. of Civil Engineering, Univ. of Toronto, Toronto.

Panchacharam, S., & Belarbi, A. (2002, October). Torsional behavior of reinforced concrete beams strengthened with FRP composites. In *First FIB Congress, Osaka, Japan* (Vol. 1, pp. 01-110).

Pang, X. B. D., & Hsu, T. T. (1995). Behavior of reinforced concrete membrane elements in shear. *Structural Journal*, *92*(6), 665-679.

Rahal, K. L., & Collins, M. P. (1995). Analysis of sections subjected to combined shear and torsion-a theoretical model. *ACI Structural Journal*, *92*, 459-459.

Rahal, K. N., & Collins, M. P. (2003). Combined torsion and bending in reinforced and prestressed concrete beams. *Structural Journal*, *100*(2), 157-165.

Rausch, E. (1929). Design of reinforced concrete in torsion (Berechnung des eisenbetons gegen verdrehung). *Technische Hochschule, Berlin, Germany (in German)*.

Ritchie, P. A., Thomas, D. A., Lu, L. W., & Connelly, G. M. (1990). External reinforcement of concrete beams using fiber-reinforced plastics.

Ritter, W. (1899). Die bauweise hennebique (hennebiques construction method).

Ronagh, H. R., & Dux, P. F. (2003, February). Full-scale torsion testing of concrete beams strengthened with CFRP. In *Proc., 1st Int. Conf. on the Performance of Construction Materials in the New Millennium* (pp. 735-743).

Salom, P. R., Gergely, J., & Young, D. T. (2004). Torsional strengthening of spandrel beams with fiber-reinforced polymer laminates. *Journal of Composites for Construction*, *8*(2), 157-162.

Sharif, A., Al-Sulaimani, G. J., Basunbul, I. A., Baluch, M. H., & Ghaleb, B. N. (1994). Strengthening of initially loaded reinforced concrete beams using FRP plates. *Structural Journal*, *91*(2), 160-168.

Shahawy, M. A., & Beitelman, T. (1996). *Flexural behavior of reinforced concrete beams strengthened with advanced composite materials* (No. CONF-960310--). Society for the Advancement of Material and Process Engineering, Covina, CA (United States).

Täljsten, B., & Elfgren, L. (2000). Strengthening concrete beams for shear using CFRP-materials: evaluation of different application methods. *Composites Part B: Engineering*, *31*(2), 87-96.

Triantafillou, T. C., & Antonopoulos, C. P. (2000). Design of concrete flexural members strengthened in shear with FRP. *Journal of composites for construction*, *4*(4), 198-205.

Vecchio, F. J., & Collins, M. P. (1986). The modified compression-field theory for reinforced concrete elements subjected to shear. *ACI J.*, *83*(2), 219-231.

Walsh PF, Collins MP, Archer FE, Hall AS (1966) The ultimate strength design of rectangular reinforced concrete beams subjected to combined torsion, bending and shear, vol CE8, No. 2. Civil Engineering Transactions, The Institution of Engineers, Australia, pp 143–157

Yang, G., Zomorodian, M., Belarbi, A., & Ayoub, A. (2015). Uniaxial tensile stress-strain relationships of RC elements strengthened with FRP sheets. *Journal of Composites for Construction*, *20*(3), 04015075.

Yang, G., Zomorodian, M., & Belarbi, A. (2017). Material laws of FRP-strengthened RC element in biaxial tension–compression. *Journal of Composites for Construction*, *21*(5), 04017030.

Zhang, Z., & Hsu, C. T. T. (2005). Shear strengthening of reinforced concrete beams using carbon-fiber-reinforced polymer laminates. *Journal of Composites for Construction*, *9*(2), 158-169.

Zhu, R. R., Hsu, T. T., & Lee, J. Y. (2001). Rational shear modulus for smeared-crack analysis of reinforced concrete. *Structural Journal*, *98*(4), 443-450.